International Journal of Polymer Science

Polymeric Membrane Science and Technology

Guest Editors: Hai-Yin Yu, Ling-Shu Wan, and Qian Yang

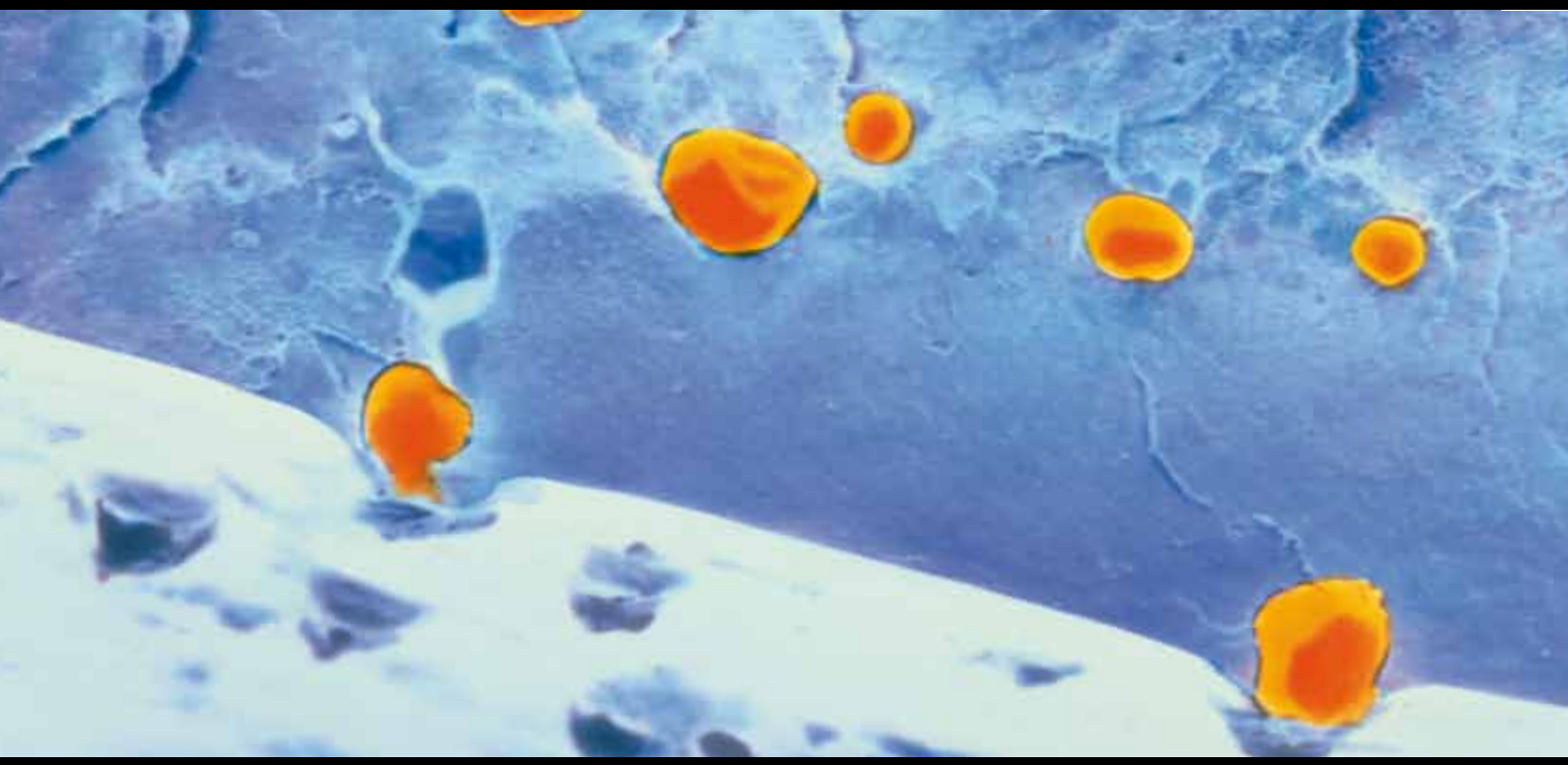

Polymeric Membrane Science and Technology

International Journal of Polymer Science

Polymeric Membrane Science and Technology

Guest Editors: Hai-Yin Yu, Ling-Shu Wan, and Qian Yang

Editorial Board

Contents

Hindawi Publishing Corporation
International Journal of Polymer Science
Volume 2013, Article ID 460898, 2 pages
http://dx.doi.org/10.1155/2013/460898

Editorial
Polymeric Membrane Science and Technology

Hai-Yin Yu,[1] Ling-Shu Wan,[2] and Qian Yang[3]

[1] *College of Chemistry and Materials Science, Anhui Normal University, 1 East Beijing Road, Wuhu, Anhui 241000, China*
[2] *MOE Key Laboratory of Macromolecular Synthesis and Functionalization, Department of Polymer Science and Engineering, Zhejiang University, Hangzhou 310027, China*
[3] *Department of Civil and Environmental Engineering, Clark School of Engineering, University of Maryland, College Park, MD 20742, USA*

Correspondence should be addressed to Hai-Yin Yu; yhy456@mail.ahnu.edu.cn

Received 19 September 2013; Accepted 19 September 2013

Membrane technology is becoming increasingly important due to high efficiency, low cost, and easy manipulation, and membranes are widely used in diverse fields including substance separation and purification, environment protection and remedy, and energy conversion and storage [1, 2]. Basic membrane research includes a number of scopes, including membrane surface modification [3] and its relation to membrane characterizations, membrane formation and structure on transport properties [4], theoretical analyses of membrane transport phenomena, experimental results on membrane permeation and selectivity, membrane fouling and its effect on membrane performance, membrane adsorber/membrane chromatography, membrane modules and their impact on device performance, and membrane processes/applications with a focus on the role of the membrane. In this special issue, we focus on the membrane formation and membrane surface modification and applications.

In "*the solubility of hydrocarbon gases in glassy polymers: fractal modeling,*" a fractal model was proposed to estimate the permeability and selectivity in gas transport through polymeric membranes; it was found that this model is very useful and it is found that the values of the solubility coefficient depend on the size of the gas penetrant molecules, their molecular interactions with the polymer, and the fractal dimensions of the polymer. The organic-inorganic hybrid membranes, including ZSM-5 filled polyether block amide membranes (PEBA) in *"ZSM-5 filled polyether block amide membranes for separating EA from aqueous solution by pervaporation*" vinyltriethoxysilane cross-linked polyacrylonitrile membrane and nano ZnO deposited polypropylene macroporous membrane in *"Decoloring methyl orange under sunlight by a photocatalytic membrane reactor based on ZnO nanoparticles and polypropylene macroporous membrane,"* can improve the desired properties of the membranes; the modified membranes possess both the advantages of the original membrane and the inorganic particles. The composite sponge of chitosan and gelatin at different proportions was prepared and the wound healing effect was evaluated; water uptake ability, antibacterial activity, and wound closure were enhanced at some extent in *"Curcumin-loaded chitosan/gelatin composite sponge for wound healing application."*

Last but not least, a careful modulation of polyurethane-keratin membrane structure by isocyanate and pH was performed and the removal of Cr(VI) from aqueous solution was performed; the results showed that the removal efficiency was significantly increased at low pH in *"Polyurethane-keratin membranes: structural changes by isocyanate and pH, and the repercussion on Cr(VI) removal."*

We hope that readers will find in this special issue not only accurate data but also important questions to be resolved such as preparation of hybrid membranes for decoloring organic dyes, effects of dye and nanoparticles loadings, and damages on the membranes due to long-time irradiation.

Hai-Yin Yu
Ling-Shu Wan
Qian Yang

References

[1] T. Vercellino, A. Morse, P. Tran et al., "Attachment of organo-selenium to polyamide composite reverse osmosis membranes to inhibit biofilm formation of *S. aureus* and *E. coli*," *Desalination*, vol. 309, pp. 291–295, 2013.

[2] B. Mi and M. Elimelech, "Organic fouling of forward osmosis membranes: fouling reversibility and cleaning without chemical reagents," *Journal of Membrane Science*, vol. 348, no. 1-2, pp. 337–345, 2010.

[3] X. M. Wu, L. L. Wang, Y. Wang, J. S. Gu, and H. Y. Yu, "Surface modification of polypropylene macroporous membrane by marrying RAFT polymerization with click chemistry," *Journal of Membrane Science*, vol. 421-422, pp. 60–68, 2012.

[4] L. S. Wan, J. W. Li, B. B. Ke, and Z. Xu, "Ordered microporous membranes templated by breath figures for size-selective separation," *Journal of the American Chemical Society*, vol. 134, no. 1, pp. 95–98, 2012.

Hindawi Publishing Corporation
International Journal of Polymer Science
Volume 2013, Article ID 892547, 12 pages
http://dx.doi.org/10.1155/2013/892547

Research Article

Polyurethane-Keratin Membranes: Structural Changes by Isocyanate and pH, and the Repercussion on Cr(VI) Removal

María D. Manrique-Juárez,[1,2] Ana L. Martínez-Hernández,[3,4] Oscar F. Olea-Mejía,[2] Jaime Flores-Estrada,[1] José L. Rivera-Armenta,[5] and Carlos Velasco-Santos[3,4]

[1] *Posgrado en Ciencia de Materiales, Facultad de Química, Universidad Autónoma del Estado de México, Paseo Colón Esquina, Paseo Tollocan, 50120 Toluca, MEX, Mexico*
[2] *Centro Conjunto de Investigación en Química Sustentable UAEM-UNAM, Facultad de Química, Universidad Autónoma del Estado de México, Km. 14.5 de la carretera Toluca-Atlacomulco, 50200 San Cayetano, MEX, Mexico*
[3] *División de Estudios de Posgrado e Investigación, Instituto Tecnológico de Querétaro, Avenida Tecnológico s/n, Esquina Gral. Mariano Escobedo, 76000 Colonia Centro Histórico, QRO, Mexico*
[4] *Centro de Física Aplicada y Tecnología Avanzada, UNAM, AP 1-10101, 76000 Juriquilla, QRO, Mexico*
[5] *División de Estudios de Posgrado e Investigación, Instituto Tecnológico de Cd. Madero, J. Rosas y J. Urueta s/n, Colonia Los Mangos, 89440 Ciudad Madero, TAMPS, Mexico*

Correspondence should be addressed to Ana L. Martínez-Hernández; almh72@gmail.com

Received 1 May 2013; Revised 1 August 2013; Accepted 20 August 2013

Academic Editor: Qian Yang

Keratin has the capacity to interact with metal ions. In order to take advantage of this potential, a novel membrane with polyurethane and keratin has been developed and studied for removal of Cr(VI) from aqueous solution. Physicochemical and morphological properties of these hybrid membranes were studied, varying synthesis parameters such as the type of isocyanate and pH in keratin solution. The effects of using diphenyl-methane-diisocyanate or toluene-diisocyanate and modifying the pH in keratin solutions were evaluated by scanning electron microscopy, Fourier transform infrared spectroscopy, and dynamical mechanical analysis. Results show that pH has a strong influence on morphology and on Cr(VI) removal efficiency. When pH in keratin solution is low (2.5), the protein separates from water, and a more closed cell in the membrane is obtained affecting its mechanical properties. The removal efficiency of Cr(VI) was also assessed at different pH values of chromium solutions. These results show that when pH of the Cr solution is acidic (at 1.5), the Cr(VI) removal percentages increase significantly, reaching up to a 58%. Thus this paper demonstrates the successful combination of synthetic and natural polymers depending on the process parameters to be applied in the critical purpose of remediation of Cr(VI) contamination.

1. Introduction

Polymeric membranes to remove high toxic contaminants have attracted highly the attention of a large sector of scientific community, since innovative materials with more potential are needed due to the increasing in pollution problems. New materials to remove pollution comprise polymer inclusion membranes and activated composites membranes, which have been developed using different active agents supported by diverse polymers as substrate. Thus, synthetic ion carriers such as tri-n-octylamine, dibenzo-21-crown-7, tertbutyl-dibenzo-21-crown-7 [1], methyltricaprylammonium chloride [2], and among others have been studied to remove anionic or cationic metal species. In spite of the successful results with this kind of membranes, other efforts including more ecofriendly materials must be developed. In this sense, natural materials have attracted also great attention as biosorbents due to their low cost and important efficiency as metallic ions receptors [3–5].

Recently, keratin from chicken feathers has been proposed as biosorbent, considering that it has abundant amino acid groups that have demonstrated good potential to attract

heavy metals [4, 6]. However, one limitation concerning the use of biosorbents is their handling; this is particularly true for feather keratin fibers, since one of their most important features is their low density [7–9]. Due to this inconvenience, new materials have been studied in order to improve the ability to support and obtain special physical characteristics that could give high interaction with pollutants, durability, and resistance to water flow [10–12]. Our research group has developed new polyurethane-keratin membranes with the aim of taking advantage of the natural affinity of keratin towards metals with the adequate porous support to act as membrane during separation processes [6, 7].

Polyurethane (PU) has been chosen due to the chemical compatible groups with keratin, because it is very important that the biosorbent could be strongly attached to the substrate and has the capacity to capture metal ions from the wastewater flow. In addition, different systems have used successfully polyurethane as membrane matrix or support foam [13–16].

Thus, in this work, we use keratin solutions extracted from chicken feathers as suitable biosorbents to remove Cr(VI); PU foams were synthesized with two types of isocyanates: diphenyl-methane-diisocyanate (MDI) and toluene-diisocyanate (TDI), which were mixed separately with polyol and keratin in order to study their effect on the membrane microstructure. The influence of pH is also evaluated, since it is one of the most important parameters as ionic charges on the biosorbent surface, responsible for metal ion attachment [7, 17, 18]. Besides, the isoelectric point of keratin (pH 4.0) [19] plays an important role, since water and amino hydrolysis depend on pH value, and isocyanates are very sensitive to their presence.

Chromium (VI) was chosen to be removed from water with these novel PU-keratin membranes due to the contaminant problems caused by this. Chromium is one of the most abundant hazardous metals on earth. As for Cr(VI), it is highly toxic and represents a threat for living organisms because it is a strong oxidant and soluble at all pH values. The ionic species of Cr(VI) depends strongly on the pH. When pH is from 1.0 to 6.0, $Cr_2O_7^{2-}$ and $HCrO_4^-$ coexist in equilibrium; if pH is higher than 8.0, CrO_4^{2-} is the predominant species. Different kinds of membranes have been probed to separate Cr(VI) from water; for instance, Alguacil et al. studied the transport of Cr(VI) from hydrochloric acid medium by pseudoemulsion membrane strip dispersion using a phosphonium salt as ionophore; with this system, a 95% extraction was obtained and by using NaOH solution, the system reaches 60% of removal [20]. Similar results removing Cr(VI) from hydrochloric acid aqueous solutions were reported using polymer inclusion membranes based on organic solvents: cellulose triacetate as the support, tri-n-octylamine as the ionic carrier, and o-nitrophenyl pentyl ether as plasticizer [21]. Alpaydin et al. studied the transport of Cr(VI) from aqueous solution by a bulk liquid membrane using p-tert-butylcalix[4]arene 3-diethylaminopropyl diamide derivative as a carrier; they observed the highest transport efficiency (around 96%) at pH 2.0 in the donor phase and at pH 5.0 in the acceptor phase [22]. These membranes reach high efficiency, but are completely based in synthetic supports and carriers. Efforts in using biosorbents to remove Cr(VI) were reported by several authors [17, 23–25], identifying as a key factor the pH of chromium solutions. This fact is an important parameter that has not been studied in the PU-keratin system. Thus, this paper is focused on both, the adsorption of Cr(VI) at different pH values and the improvement of the characteristics of new PU-keratin membranes through modification of their processing conditions, taking into account the behavior caused by keratin's isoelectric point.

2. Experimental

2.1. Materials. Keratin biofibers from chicken feathers were kindly supplied by Walter Schmidt and were obtained according to a patented process by Schmidt (US 5750030). Toluene diisocyanate (TDI) was provided by Poliformas Plasticas (Mexico), whereas diphenylmethane-diisocyanate (MDI) and poliol were purchased from Polioles (Mexico). Dehydrated (ethylenedinitrile) tetraacetic acid disodium salt (EDTA) was acquired from J. T. Baker. Urea, 2-mercaptoethanol, tris (hydroxymethyl) aminomethane (Tris), potassium dichromate ($K_2Cr_2O_7$), sulfuric acid (H_2SO_4), sodium hydroxide (NaOH), and 1,5-diphenylcarbazide were purchased from Sigma-Aldrich. All substances were of analytical grade. The dialysis membrane (Spectra/Por MWCO6-8000) was purchased from Cole Palmer.

2.2. Preparation of Keratin. In order to prepare membranes, keratin was used as solution, which was obtained by dissolving chicken feather biofibers according to the procedure described by Schrooyen et al. [26]. 30 g of keratin biofibers was solubilized in 750 cm^3 of water with 8 M urea, 3 mM EDTA, 125 mM 2-mercaptoethanol, and 200 mM tris, maintaining the pH at 9.0. After that, salt residues were separated from the keratin solution through a dialysis membrane. 10 cm^3 of keratin salt solution was dialyzed with 1 L of distillated water, which was replaced completely after 16 and 24 hrs. The dialysis process was stopped after 48 hrs. Dialyzed keratin solution was preserved at 4°C. The pH of the dialyzed keratin solution was adjusted by using H_2SO_4 or NaOH to 2.5, 6.0, and 9.5; these solutions were used in each PU-keratin membrane formulation as shown in Table 1.

2.3. Synthesis of Hybrid Polyurethane-Keratin Membranes. Polyurethane-keratin (PU-keratin) membranes were produced by *in situ* polymerization between isocyanate and polyol. Control membranes using distillated water (at pH 7.0) instead keratin solutions were produced using both TDI and MDI. The synthesis of PU-keratin membranes made with TDI includes dialyzed keratin solutions with a specific pH (2.5, 6.0, or 9.5) and polyol; they were mixed in a polypropylene flask for one minute. After that, TDI was poured in the mixture and stirred for 15 s. The mixture foams during the polymerization reaction producing the internal cells in membranes. For those membranes made with MDI, 2.3 cm^3 of dialyzed keratin solution was centrifuged at 2033 rpm; this produces 0.2 g of hydrated keratin that

Table 1: Nomenclature and components of polyurethane-keratin membranes.

Isocyanate type	Dialyzed keratin solution	Water	pH of keratin solution	Membrane nomenclature
TDI 3 g	—	2.3 cm^3	—	TPH
TDI 3 g	2.3 cm^3	—	6.0	TPKN
TDI 3 g	2.3 cm^3	—	2.5	TPKAc
TDI 3 g	2.3 cm^3	—	9.5	TPKAl
MDI 5.7 g	—	0.2 cm^3	—	MPH
MDI 5.7 g	2.3 cm^3	—	6.0	MPKN
MDI 5.7 g	2.3 cm^3	—	2.5	MPKAc
MDI 5.7 g	2.3 cm^3	—	9.5	MPKAl

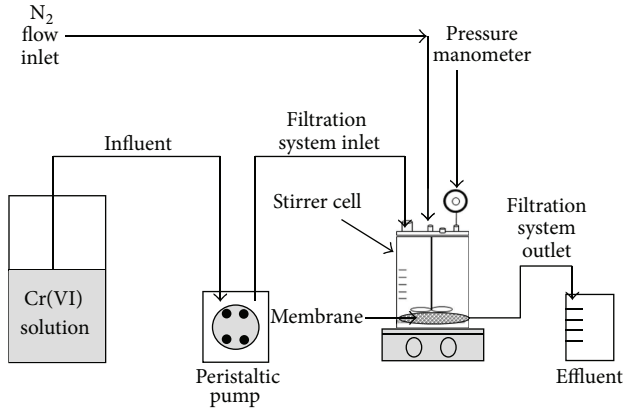

Figure 1: Filtration system by continuous flow.

was mixed with polyol and MDI in order to introduce the biopolymer during the polymerization process, analogous to TDI. Centrifugation of dialyzed keratin solution was realized in order to minimize the amount of water. This last procedure was carried out with systems using MDI. Table 1 shows the different conditions for the synthesized membranes, only 5.5 g of polyol remain constant in all membranes. When polymerization reaction was complete, the membranes were cut according to the filtration reactor geometry (diameter 47 mm, thickness 3 mm).

2.4. Preparation of Cr(VI) Solutions. Cr(VI) solutions were prepared by dissolving $K_2Cr_7O_2$ in distilled water; the influent concentration was 20 mg/L. The chromium solution was adjusted to 5.7, 2.5, and 1.5 by H_2SO_4 or NaOH solutions in order to study the effect of ionic species of Cr(VI) in the membrane efficiency.

2.5. Adsorption Experiments. The filtration experiments were performed in a Millipore filtration cell by continuous flow. The equipment, shown in Figure 1, consists in a solvent-resistant stirred cell, with the following characteristics: cell capacity 50 cm^3, stirred minimum volume 2.5 cm^3, membrane diameter 4.7 cm, effective membrane area 17.3 cm^2, and maximum operating pressure 6.2 bar. In order to equilibrate the system, first, deionized water was fed for 30 to 60 min. Once the filtration cell operated at equilibrium conditions, Cr(VI) aqueous solution was fed. This is considered the initial point of the continuous flow inlet. Feed solution (influent Cr(VI) aqueous solution at 20 mg/L) was injected with a peristaltic pump at 60 cm^3/min. The outlet flow (effluent of filtrated water) was maintained constant together with cell internal pressure (controlled between 0.7 and 2.8 bar) by a nitrogen gas flow injected into the cell. The cell is provided with an agitator system that operates at 150 rpm to maintain a homogenous solution. PU-keratin membranes were fixed at the bottom of the cell. Dimensions of the membranes were adjusted to 4.7 cm of diameter and 0.4 cm of thickness. The Cr(VI) aqueous solution is filtrated through PU-keratin membranes; the maximum feed velocity across the membrane surface was around 0.06 cm/s, maintaining contact between the influent and membranes for 36 s. The system was operated for 270 min, taking samples every 30 min.

The concentrations of Cr(VI) for the initial solution and the effluent were determined with UV-vis spectrophotometer equipment (Spectronic Genesis 2PC) at a wavelength of 540 nm using the 1,5-diphenylcarbazide complexation method, according to the Mexican Official Standard NMX-AA-044-SCFI-2001.

The removal percentage of Cr(VI) was determined by these simple equations:

$$P_t = \frac{C_t \cdot 100}{C_i},$$
$$\text{Removal percentage of Cr (VI)} = 100 - P_t, \quad (1)$$

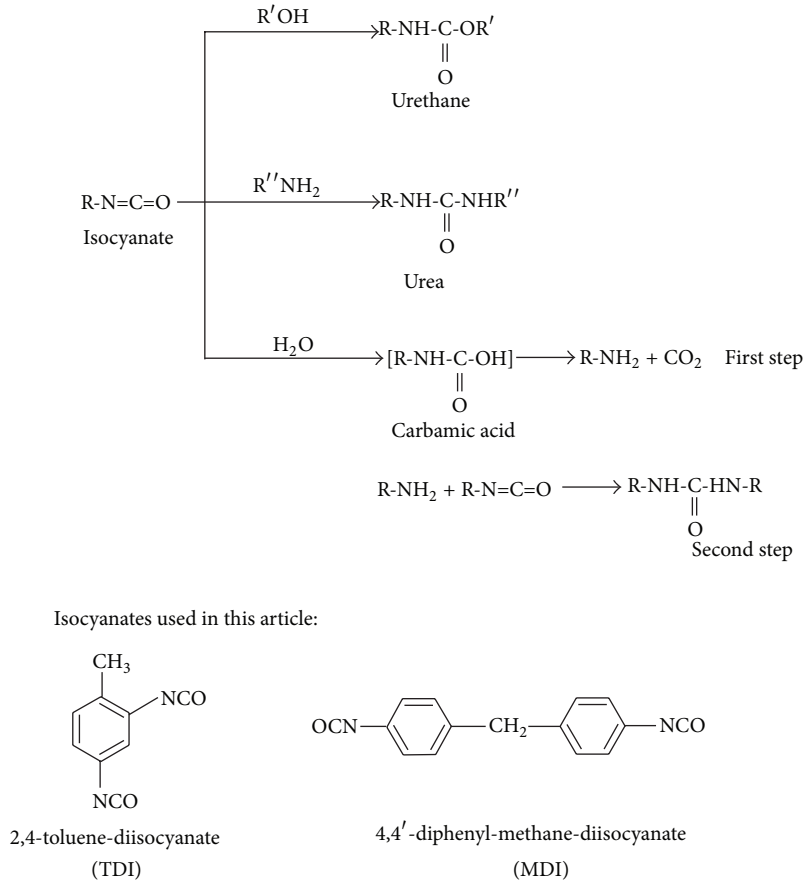

Figure 2: Scheme of possible reactions of isocyanates with moieties of polyethylene glycol-keratin-water system.

where C_i indicates the initial concentration of Cr(VI): 20 mg/L; C_t corresponds to the effluent concentration at predetermined time, the latter is obtained from a calibration curve according to the UV-Vis spectrophotometric method.

2.6. Membrane Characterization. The membrane morphology was studied before and after the filtration process by scanning electron microscopy (SEM) in a JEOL JSM 6510LV microscope at 20 kV and high vacuum. The membranes were characterized by SEM after filtration in order to observe any surface damage after flow. All the samples were gold-coated to prevent surface charging during SEM analysis. Functional groups of PU-keratin membrane and interactions between Cr(VI) and PU-keratin were studied by infrared spectroscopy using an IR Prestig-21 Shimadzu Corporation spectrometer on the attenuated total reflectance mode (ATR), in the range of 4000–500 cm^{-1}. In order to study the thermomechanical properties of the membranes, dynamic mechanical analysis was carried out in a DMA 2980 instruments equipment using a multifrequency model-dual cantilever; the heating rate used was 3°C/min using 1 Hz of frequency and a temperature range from 30 to 200°C.

3. Results and Discussion

3.1. SEM Characterization. One of the most important features of PU-keratin membranes is the cell conformation, since it influences the properties of flexible PU foams. The cell conformation is determined by the polymerization process in the first step of PU reaction. This involves the isocyanate group reacting with water to yield an unstable carbamic acid, which decomposes quickly in amine and carbon dioxide (Figure 2). The carbon dioxide production is proportional to the added water quantity and is related to the formation of cells and "foam" porous in PU. In order to observe some structural details and internal size cell, SEM images of TDI- and MDI- based PU-keratin membranes are shown in Figure 3. The nomenclature for each membrane is described in Table 1. There are some morphological differences mainly in the opening of the cells, where the TDI-based membranes (Figures 3(a)–3(d)) have a greater number of open cells compared to MDI-based membranes (Figures 3(e)–3(h)).

The TDI membranes have higher water content; this causes less homogeneity and greater amount of open cells, as can be observed in Figures 3(a)–3(d). Figure 3(e) shows the MDI membrane without keratin (MPH), where only 0.2 cm^3 of water was used instead of keratin solution. This membrane has nonuniform open cells similar to TPH and TPKAl (Figures 3(a) and 3(d), resp.). These three types of membranes have an irregular cell boundary, whereas TPKN, TPKAc, MPKN, and MPKAc (Figures 3(b), 3(c), 3(f), and 3(g)) have well-defined cell frames, no matter the diameter of the open cells. This fact indicates that keratin protein and pH on

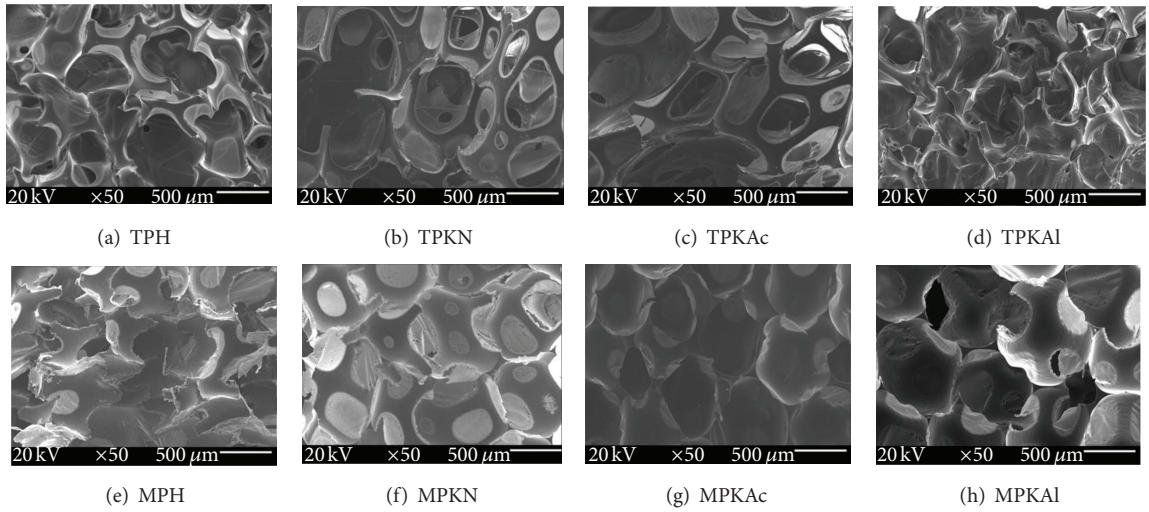

(a) TPH (b) TPKN (c) TPKAc (d) TPKAl

(e) MPH (f) MPKN (g) MPKAc (h) MPKAl

Figure 3: SEM images of PU-keratin membranes; ((a)–(d)) with TDI; ((e)–(h)) with MDI.

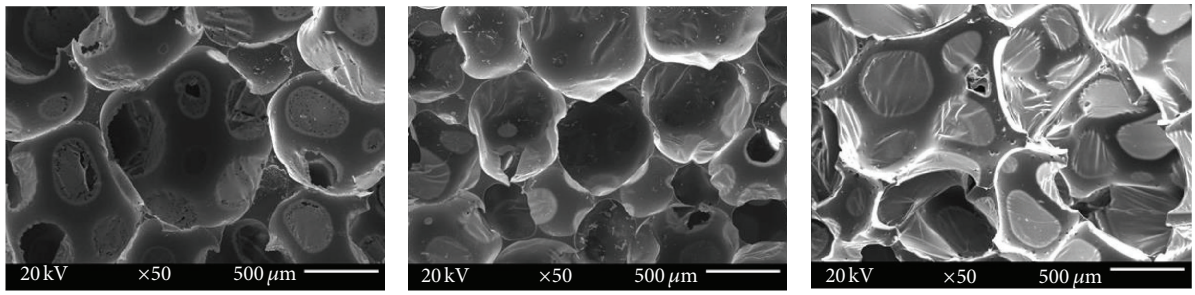

(a) MPKN (b) MPKAc (c) TPKAc

Figure 4: SEM images of PU-keratin membranes after the removal process.

keratin solution have an effective role in the polymerization process, since the morphological characteristics of PU have been affected. In addition, as MDI membranes contain lower levels of hydration, they have most of their cells closed because of the lower production of CO_2 as well as fewer urea microdomains which are partly responsible of the open cells [32]. As it can be observed the internal cells measure between 100 and 500 μm; with these open pore arrangements an easy accessibility of Cr(VI) ions is expected to interact with immobilized active sites of keratin.

Figure 4 shows SEM images of selected membranes after the removal process. As it can be observed, there are only few morphological changes that could reveal damage on the cell opening or over the surface throughout the membrane during the filtration process. The cells in tested MPKN membrane (Figure 4(a)) are almost unaltered, whereas those in tested MPKAc and TPKAc membranes (Figures 4(b) and 4(c), resp.) show only small ruptures in the cell borders compared to non-used MPKAc and TPKAc membranes (Figures 3(g) and 3(c), resp.). This demonstrates that the PU-keratin membranes remain almost unaltered after the removal process and cells do not undergo a severe collapse that could impede their use in additional cycles of removal. This structural integrity is due to open cells allowing water flux without high pressure conditions and preserving an effective contact between Cr(VI) ions and keratin amino acids.

3.2. Dynamic Mechanical Analysis. This analysis was used to determinate the viscoelastic properties: storage modulus (E') and loss factor (Tanδ) of flexible PU-keratin membranes. Figure 5 shows storage modulus versus temperature for the membranes synthesized with MDI and TDI, and Figure 6 shows the values of Tanδ for these membranes.

It is observed for the storage modulus curves, that there is a similar slope between 35 and 100°C for all MDI membranes (Figure 5(a)). The fall of these curves is related to thermal transitions of hard segments of PU [33], which have been modified according to the keratin solution. The higher E' (0.91 MPa at 40°C) for MPKAc indicates a more restricted mobility; therefore, this membrane has a more rigid behavior than the other MDI membranes.

On the other hand, E' for TDI membranes (Figure 5(b)) shows that TPH membrane (with E' of 0.59 MPa at 40°C) is more rigid than the other TDI membranes. However, this characteristic diminishes quickly as the temperature is increased around 100°C, whereas TPKAc and TPKN have a similar slope in E' decreasing. It is reported that the

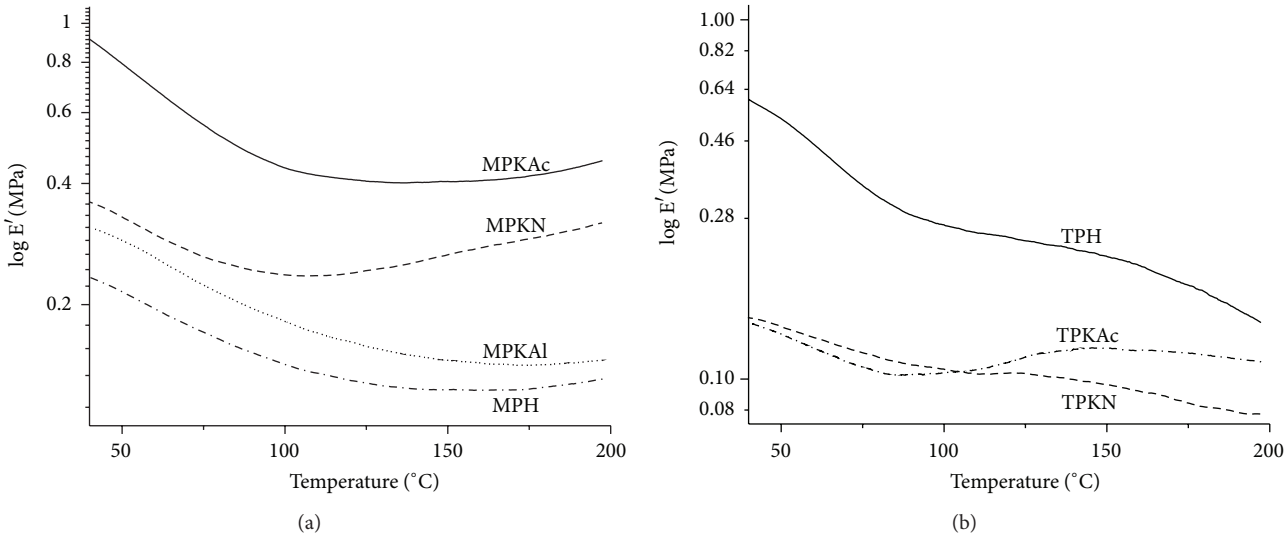

Figure 5: Storage modulus of PU-keratin membranes; (a) for MDI and (b) for TDI.

modulus in this region is proportional to either the number of crosslinks or the chain length between entanglements [34]. Thus, keratin, in this kind of PU membranes, produces more flexible membranes in the opposite behavior to MDI membranes. In addition, it is important to mention that E' values are in agreement with SEM results, where the most rigid membranes (with high values of E') show more closed cells than the membranes with less rigid behavior.

The transitions observed near 100°C are attributable to the presence of high concentration of hydrogen-bonded urethane groups and hard-segment domains which act as macroscopic crosslink. Hard and soft segments for MDI and TDI are shown in Figure 7. The segmented structure of PU explains the differences between storage modulus curves of MDI and TDI membranes, since MDI membranes show more rigid behavior than TDI membranes. This is related to the nature of isocyanate due to the number of aromatic rings. This polyurethane transition has been reported before by other authors [7, 35, 36].

In addition, Tanδ values show that MPH and MPKAl have the maximum values at around 80°C, whereas MPKAc and MPKN do not show this maximum (Figure 6(a)). This behavior, at elevated temperatures, implies that a high Tanδ value has a significant nonelastic strain component, while a low value means a more elastic material. Thus, these results in concordance with storage modulus give evidence that keratin produces more rigid membranes when MDI is used.

On the other hand, Tanδ for TDI membranes (Figure 6(b)) shows the maximum around 0.33 at 90°C to TPH. For TPKN and TPKAc, a maximum appears at around 112°C, indicating that keratin provides to TDI membranes high thermal stability, in spite of their flexibility.

This maximum signal in Tanδ, observed in both MDI and TDI membranes, is related to the thermal transition exposed before and detected at around 100°C. The analyzed viscoelastic behavior in these membranes strongly depends on the isocyanate and the pH of keratin solutions used in the polymerization reaction. So, it is important to consider that when the membrane is synthesized, the water of the keratin solution is involved in two competitive phenomena. One is the production of gaseous CO_2 that expands creating softer foam; the other phenomenon is when urea domains are generated by water and amino groups reacting with isocyanate; this produces hard segments and crosslinking, and therefore a rigid cell. Having in mind these considerations, when the pH of keratin solution is reduced to 2.5, keratin tends to separate from water and this is available to react freely with MDI producing a rigid MPKAc membrane. In the case of TDI, pure water reacts easily yielding the more rigid membrane: TPH; whereas pH of keratin solution loses its effect over hard segments production. At the same time, CO_2 production is facilitated with TDI producing a softer material in agreement E' results and SEM images, where TPH shows a higher number of opened cells compared to MPKAc with the highest quantity of closed cells.

3.3. Cr(VI) Removal Results. The highest Cr(VI) removal percentages for each PU-keratin membrane as a function of pH in chromium aqueous solution are summarized in Table 2. It is observed that with pH of 5.7, none of the seven membranes reached high removal percentages; only TPKAc achieved around 8% at 90 min of process; the rest of the membranes have lower values. In general, for this pH, TDI membranes have better performance than MDI, since only a 3% in removal percentage was reached by MPKAl at 30 min; the other MDI membranes adsorb below this value.

It is remarkable that when pH of Cr(VI) solution is diminished, better removal results are obtained. If pH is decreased at 2.5, both kinds of membranes show more affinity toward Cr(VI) ions. MPKAc achieves the most high removal percentage of these series: 22% at 30 min. TDI membranes removal is also controlled by pH, since with TPH membrane

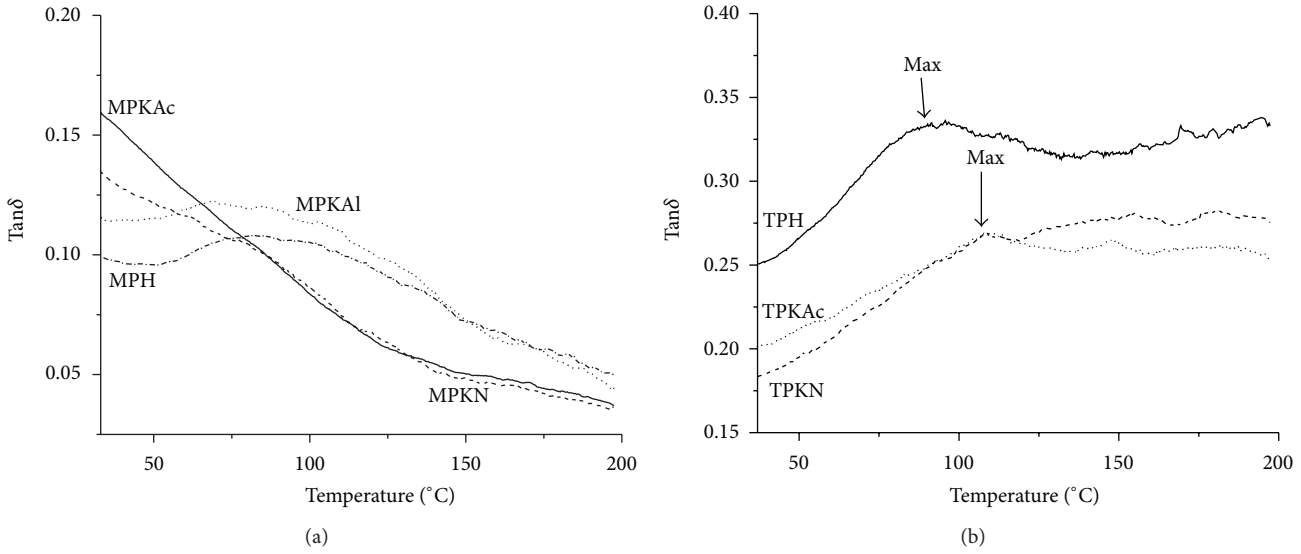

Figure 6: Tangent δ of PU-keratin membranes; (a) for MDI and (b) for TDI.

Table 2: Maximum values of Cr(VI) removal percentages through filtration process with PU-keratin membranes as function of pH.

Type of membrane	pH 5.7		pH 2.5		pH 1.5	
	Maximum value of Cr(VI) removal percentage	Time of removal (min)	Maximum value of Cr(VI) removal percentage	Time of removal (min)	Maximum value of Cr(VI) removal percentage	Time of removal (min)
MPH	0.81	90	6.44	240	25.24	90
MPKN	1.96	270	11.54	270	29.22	240
MPKAc	2.79	60	22.21	30	41.06	270
MPKAl	3.75	30	8.07	270	57.91	240
TPH	1.53	90	14.28	270	37.14	120
TPKN	4.19	30	13.06	30	38.16	180
TPKAc	8.14	90	5.77	270	26.47	60

a maximum removal percentage of 14% at 270 min was reached. TPKN reaches 13% of removal and TPKAc shows a minimum range for Cr(VI) removal: around 1 and 5%.

On the other hand, the highest removal percentages were achieved using Cr(VI) solution with pH of 1.5. MPKAl has the capacity to remove 57% of Cr(VI) with a regular tendency, which is observed also for the other membranes but with less removal ability. MPKAc reaches removal efficiency of 41%; for MPKN, the removal percentage was 29% and MPH shows 25%. The results with TDI membranes at pH of 1.5 are also higher than with the other pH values. The maximum removal percentage was achieved by TPKN (38%); TPH removal capacity was very similar, and its higher value was 37%. TPKAc shows a maximum removal value of 26%.

These results show that pH is the variable that most influences the removal of Cr(VI) in PU-keratin membranes. This can be explained because when pH is reduced, the membrane is charged positively due to protons presence, as was exposed by several authors [37–39]. In addition, pH below 4.0 (keratin isoelectric point) [19] produces that amino acids behave as cations increasing the electrostatic affinity. At the same time, the chemical species of chromium in water are negative ions for all pH values ($HCrO_4^-$, CrO_4^{2-}, and $Cr_2O_7^{2-}$). Therefore, when the pH is gradually reduced the PU-keratin membrane surface is more positively charged and the attraction between ions is stronger resulting in a more efficient Cr(VI) removal. In the other hand, when the pH of the Cr(VI) solution is increased, the negative charges on the polymer composite surface start appearing and the negative Cr ions are repelled [17, 38]. Figure 8 provides the chemical species of Cr(VI) as a function of pH and the variation of keratin charge according to its isoelectric point.

Figure 9 shows the behavior of removal process for MPKAl and TPKAc membranes using three different pH values (5.7, 2.5, and 1.5). The adequate morphology of these membranes (observed in Figures 3(c) and 3(h)), with their well integrated and uniform cells, is reflected in the regular tendency of the adsorption curves, which in addition to the pH influence (better adsorption at pH of 1.5) provide a good performance for these membranes. Specifically, the Cr(VI) removal percentage for the best membrane is from 30 to 57%. At the same time, it is worthy of mention that this

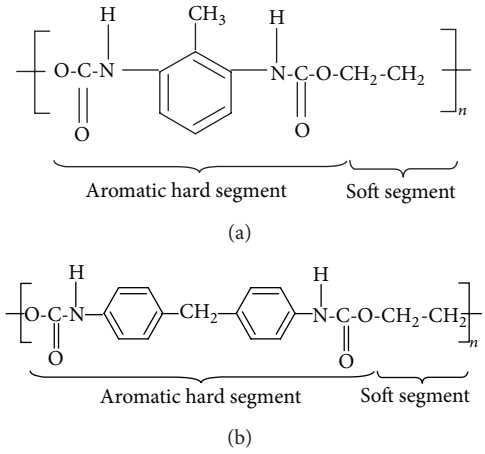

Figure 7: Chemical polyurethane zones, soft and hard segments: (a) TDI, (b) MDI.

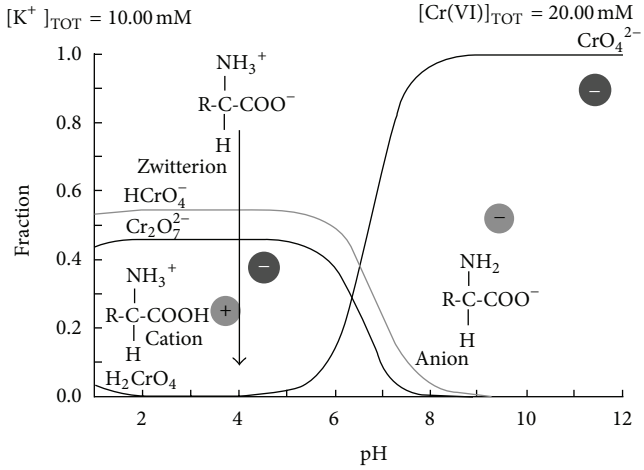

Figure 8: Distribution of Cr(VI) species as a function of pH.

is a continuous process, suitable of flux drops by fouling mechanisms, which are strongly influenced by the surface charge of the membrane [40]. Therefore, the membranes with the lowest adsorption values are also those with uneven process behavior as is observed in Figure 9.

Keratin is an important biopolymer that has begun a specific application in materials related to environmental remediation, based on its interesting characteristics to remove metal pollution. Table 3 shows the highest result obtained in this paper and some of the most relevant results obtained by other authors. It is clear that keratin removal efficiency varies amply, not only in processed and complex materials [6, 9, 27, 29] but also if it is used as a simple biosorbent [4, 8, 28, 30, 31]. Our results show the variations as a function of uptake time, pH of keratin solutions according to isoelectric point of this protein, pH of chromium solutions and structural characteristics of membrane. The performance of this membrane (57% of Cr(VI) removal) was superior compared with our previous results [6], the adsorption is significantly high due to presence of keratin, thus is demonstrated that a minimum quantity of

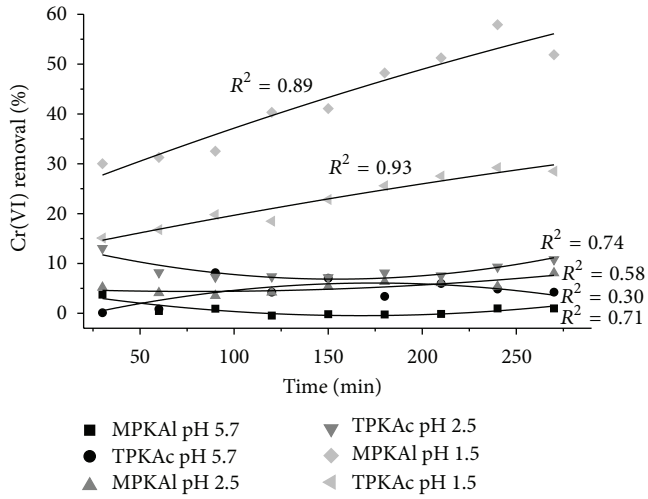

Figure 9: Cr(VI) removal percentages of MPKAl and TPKAc membranes as function of pH and time in the filtration system by continuous flow.

keratin (1.75%) with the adequate support could be as useful as feather fiber biosorbent (100% of keratin) [4, 8, 28, 30]. Some additional factors that affect the performance of keratin to remove metals are initial metal concentration, chemical treatment, and ionic charge of metal pollutants.

3.4. Infrared Spectroscopy. Figure 10 shows the normalized infrared spectra for MDI (10I) and TDI (10II) membranes, all before the removal process. The spectra have the same characteristic absorption bands identified for PU. The most important signals are v(N–H) band around 3313 cm^{-1} for secondary and primary amines [7, 41]; vibrations between 2980 and 2867 cm^{-1} characteristic of v(C–H) [7, 42]; the remaining isocyanate group appears nearby 2276 cm^{-1} for MDI and its absence in TDI evidences a complete reaction [7, 43]. Another characteristic band that can be observed in Figure 10 is the v(C=O) at different wavenumbers: the urethane carbonyl group at 1724 cm^{-1} and 1727 cm^{-1} for MDI and TDI spectra, respectively [7, 42, 43]; urea carbonyl group displays this band at 1712 cm^{-1} for MDI and by 1714 cm^{-1} for TDI [7, 41, 42]. It can be seen that the intensity of the urethane carbonyl band is higher for MDI, whereas for TDI urea, carbonyl signal is more intense than urethane carbonyl; this can be explained taking into account that water is highly responsible for urea domains and TDI membranes were formed with more water than MDI membranes. At the same time, MPH membrane was formed using more water compared to the rest of MDI membranes. At 1649 cm^{-1}, it is observed the v(C=O) for MDI, whereas for TDI it is found at 1662 cm^{-1}; this absorption corresponds to the amide carbonyl group and urea carbonyl [13, 42]. The band at 1594 cm^{-1} can be assigned as a vibration out of plane combination of in plane δ(N–H) and v(C–N) of amide II [44]. In the same region of amide II, the signals at 1538 cm^{-1} for MDI and at 1534 cm^{-1} for TDI, respectively, correspond to v(C–N) [41]. Aliphatic contributions are observed at 1457 cm^{-1}, 1415 cm^{-1}, 1373 cm^{-1}

Table 3: Keratin as biosorbent or functional component in materials applied in removal of metal pollution from water.

Material Description	Metallic species removed	Maximum removal	Keratin included	Reference
Polyurethane-feather keratin solution membrane	Cr(VI)	57%	0.2 g (1.75%)	This paper
Polyurethane-feather keratin biofiber membrane	Cr(VI)	38%	15%	[6]
Feather fibers	Pb(II)	81.6%	100%	[4]
Wool keratin/polyamide 6 nanofibres	Cu(II)	97%	90%	[27]
Feather fibers	Cu(II)	0.77 mmol/g	100%	[28]
	Zn(II)	0.95 mmol/g		
Membrane of wool keratose/silk fibroin blend	Cu(II)	2.88 μg/cm^3	50%	[29]
Algerian sheep hoof powder	Hg(II)	68 mg/g	100%	[30]
Chicken feather aminoacid solution immobilized on silica surfaces	Ca	93.88%	1 g	[9]
	Mg	72.55%		
	Fe	97.13%		
	Mn	95.66%		
Feather fibers	Pb	100%	100%	[8]
	Cu	48.8%		
	Zn	3.8%		
	Cd	17.0%		
	Ni	10.9%		
Chicken feather alkaline solution	Cu	0.14 mmol/g	5 mg/cm^3	[31]
	Zn	0.17 mmol/g		

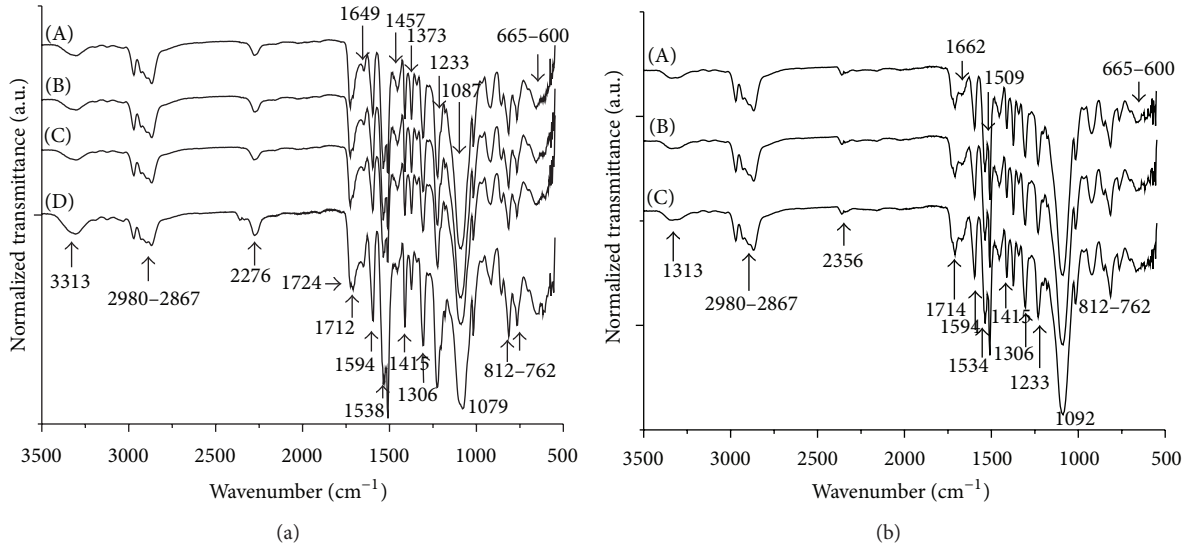

Figure 10: IR normalized spectra of PU-keratin membranes before removal process: (a) with MDI, (A) MPKAl, (B) MPKAc, (C) MPKN, and (D) MPH. (b) with TDI, (A) TPKAc, (B) TPKN, and (C) TPH.

and 1306 cm^{-1} [7]. The signal at 1233 cm^{-1} has been related to δ(N–H) and v(C–N) of amide III, both functional groups are present in PU and keratin [45]. The band for v(C–O–C) also provides evidence of keratin presence in Figure 10(a), since this signal undergoes a shift toward 1079 cm^{-1} in the case of the MPH membrane. This shift was induced in the absence of keratin for MPH synthesis. This effect is not significant in the case of TDI membranes (Figure 10(b)), where the peak at 1092 cm^{-1} remained constant for all spectra. The bands at 812–762 cm^{-1} correspond to the δ(C–H). The 762 cm^{-1} band is stronger for MDI than for TDI; this suggests a major contribution by MDI and this could be due to the double

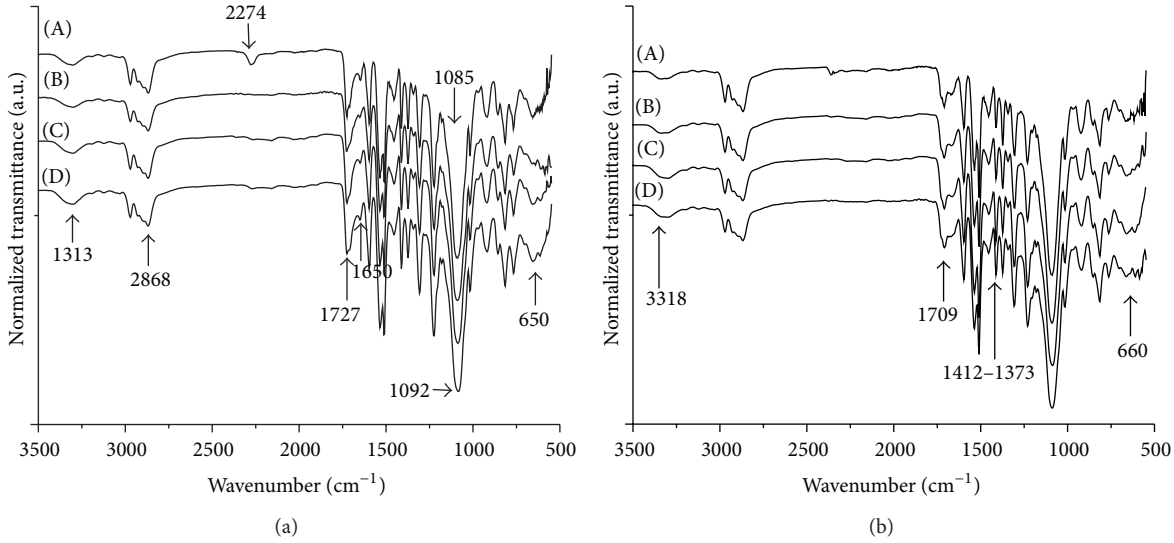

Figure 11: IR normalized spectra of membranes after the removal process; (a) for MPKAl membranes: (A) before removal process, (B) pH 5.7, (C) pH 2.5, and (D) pH 1.5. (b) for TPKAc membranes: (A) before removal process, (B) at pH 5.7, (C) at pH 2.5, and (D) at pH 1.5.

aromatic ring present in this type of polymer in comparison with TDI membranes. The bands between 665 and 600 cm^{-1} are attributed to the NH wagging and v(C–S) [6, 7, 45].

Figure 11 shows the infrared normalized spectra for membranes MPKAl and TPKAc after the removal process at different pH values in the removal medium. In the MPKAl spectra (Figure 11(a)), several changes in the intensity of the bands are observed under chromium solution, but these changes are more representative when the pH is lower (spectrum d). This phenomenon is more perceptible on the v(N–H) at 3313 cm^{-1}, v(C=O) at 1724 cm^{-1}, and v(C–S) bands at 665–600 cm^{-1}. At 2276 cm^{-1}, the vibration corresponding to the remaining isocyanate disappears in all cases under chromium contact, which indicates the dissociation of the isocyanate molecule and its interaction with metal ions. This statement is supported by the increase of the v(N–H) band at 3313 cm^{-1}. Besides, when the pH is decreased to 1.5, the v(C–O–C) signal at 1087 cm^{-1} shows a shift to 1092 cm^{-1}; this functional group is formed by the isocyanate and alcohol group or could be formed by an isocyanate and the acid side of the amino acid keratin chain. It is suggested that the electrostatic attractions between the membrane and the metallic species are strong enough to modify the vibrational mode in this moiety.

In addition, TPKAc membranes (Figure 11(b)) also have some changes in their spectra when Cr(VI) solutions pass through. The described signals at 3313 cm^{-1} and 1714 cm^{-1} for v(C=O) and between 665 and 600 cm^{-1} were modified in their intensities. Besides, the intensities in the range from 1415 to 1272 cm^{-1} change; while the 1415 cm^{-1} peak increases, the 1373 cm^{-1} decreases, so the chromium membrane interactions affect directly the δ(C–H) vibration [14, 17].

4. Conclusions

Polyurethane-keratin membranes, using two types of isocyanates, were successfully synthesized and applied as separation membranes to remove Cr(VI) in aqueous solution. The polyurethane-keratin foam microstructure was directly affected by the type of isocyanate (MDI or TDI) and the pH on keratin solution (acid keratin 2.5, neutral keratin 6.0, or alkaline keratin 9.5). The microstructural study by SEM allows establishing a correlation between the keratin pH and the cell opening, which is also reflected in the adsorption behavior. Additionally, morphologic changes in the membranes were not detected after the removal process, which indicates an adequate structural resistance useful for several cycles of water treatment processing. DMA results show that the storage modulus is higher for MDI membranes and the highest value corresponds to MPKAc due to less formation of gaseous CO_2 and therefore the formation of more rigid foam. In the case of TDI membranes, the absence of keratin in urea microdomains plays an important role that overtakes the CO_2 production, since contrary to expectations, TPH (with more CO_2 formation) is the most rigid membrane in this set. The Cr(VI) removal results show that pH in the removal system directs the efficiency of the process. When pH is reduced, the surface is more positively charged and attracts the negative Cr(VI) ions. The functional groups affected by the removal process according to the IR analysis were C=O, C–O–C, and C–S; these were mainly observed when the pH was lower. Finally, the most efficient system was MPKAl with a Cr(VI) solution of pH 1.5, removing up to 57% of the initial chromium concentration.

Conflict of Interests

The authors do not have potential conflict of interests.

Acknowledgments

Ana L. Martínez-Hernández is grateful to the financial support from L'oreal-Mexico, Mexican Academy of Science,

and UNESCO under the program "For Women in Science" and to DGEST Mexico for the financial support obtained in the project 2778.09P. Financial support from CONACYT-México (Master Degree Scholarship to M. Dolores Manrique-Juárez) is gratefully acknowledged. The authors would like to thank Mr. Guillermo Vazquez for his computer technical assistance.

References

[1] C. A. Kozlowski, W. Walkowiak, W. Pellowski, and J. Koziol, "Competitive transport of toxic metal ions by polymer inclusion membranes," *Journal of Radioanalytical and Nuclear Chemistry*, vol. 253, no. 3, pp. 389–394, 2002.

[2] L. Melita and M. Popescu, "Removal of Cr(VI) from industrial water effluents and surface waters using activated composite membranes," *Journal of Membrane Science*, vol. 312, no. 1-2, pp. 157–162, 2008.

[3] J. Wang and C. Chen, "Biosorbents for heavy metals removal and their future," *Biotechnology Advances*, vol. 27, no. 2, pp. 195–226, 2009.

[4] G. de la Rosa, H. E. Reynel-Avila, A. Bonilla-Petriciolet, I. Cano-Rodríguez, C. Velasco-Santos, and A. L. Martínez-Hernández, "Recycling poultry feathers for Pb removal from wastewater: kinetic and equilibrium studies," *World Academy of Science, Engineering and Technology*, vol. 23, pp. 394–402, 2008.

[5] C. R. Jácome-Pilco, E. Cristiani-Urbina, L. B. Flores-Cotera, R. Velasco-García, T. Ponce-Noyola, and R. O. Cañizares-Villanueva, "Continuous Cr(VI) removal by Scenedesmus incrassatulus in an airlift photobioreactor," *Bioresource Technology*, vol. 100, no. 8, pp. 2388–2391, 2008.

[6] V. Saucedo-Rivalcoba, A. L. Martínez-Hernández, G. Martínez-Barrera, C. Velasco-Santos, J. L. Rivera-Armenta, and V. M. Castaño, "Removal of hexavalent chromium from water by polyurethane-keratin hybrid membranes," *Water, Air, and Soil Pollution*, vol. 218, no. 1–4, pp. 557–571, 2011.

[7] V. Saucedo-Rivalcoba, A. L. Martínez-Hernández, G. Martínez-Barrera, C. Velasco-Santos, and V. M. Castaño, "(Chicken feathers keratin)/polyurethane membranes," *Applied Physics A*, vol. 104, pp. 219–228, 2011.

[8] P. Kar and M. Misra, "Use of keratin fiber for separation of heavy metals from water," *Journal of Chemical Technology and Biotechnology*, vol. 79, no. 11, pp. 1313–1319, 2004.

[9] S. A. Sayed, S. M. Saleh, and E. E. Hasan, "Removal of some polluting metals from industrial water using chicken feathers," *Desalination*, vol. 181, no. 1–3, pp. 243–255, 2005.

[10] M. Y. Arica and G. Bayramoğlu, "Cr(VI) biosorption from aqueous solutions using free and immobilized biomass of *Lentinussajor-caju*: preparation and kinetic characterization," *Colloids and Surfaces A*, vol. 253, no. 1–3, pp. 203–211, 2005.

[11] X. J. Hu, J. S. Wang, Y. G. Liu et al., "Adsorption of chromium(VI) by ethylenediamine-modified cross-linked magnetic chitosan resin: isotherms, kinetics and thermodynamics," *Journal of Hazardous Materials*, vol. 185, no. 1, pp. 306–314, 2011.

[12] R. S. Vieira, M. L. M. Oliveira, E. Guibal, E. Rodríguez-Castellón, and M. M. Beppu, "Copper, mercury and chromium adsorption on natural and crosslinked chitosan films: an XPS investigation of mechanism," *Colloids and Surfaces A*, vol. 374, no. 1–3, pp. 108–114, 2011.

[13] G. Ciobanu, G. Carja, and O. Ciobanu, "Use of SAPO-5 zeolite-filled polyurethane membranes in wastewater treatment," *Desalination*, vol. 222, no. 1–3, pp. 197–201, 2008.

[14] S. Das, A. K. Banthia, and B. Adhikari, "Porous polyurethane urea membranes for pervaporation separation of phenol and chlorophenols from water," *Chemical Engineering Journal*, vol. 138, no. 1–3, pp. 215–223, 2008.

[15] K. Pyrzynska, "Sorbent materials for separation and preconcentration of gold in environmental and geological samples—a review," *Analytica Chimica Acta*, vol. 741, pp. 9–14, 2012.

[16] S. H. Jang, B. G. Min, Y. G. Jeong, W. S. Lyoo, and S. C. Lee, "Removal of lead ions in aqueous solution by hydroxyapatite/polyurethane composite foams," *Journal of Hazardous Materials*, vol. 152, no. 3, pp. 1285–1292, 2008.

[17] G. Blázquez, F. Hernáinz, M. Calero, M. A. Martín-Lara, and G. Tenorio, "The effect of pH on the biosorption of Cr(III) and Cr(VI) with olive stone," *Chemical Engineering Journal*, vol. 148, pp. 473–479, 2009.

[18] Z. Aksu, F. Gönen, and Z. Demircan, "Biosorption of chromium(VI) ions by Mowital B30H resin immobilized activated sludge in a packed bed: comparison with granular activated carbon," *Process Biochemistry*, vol. 38, no. 2, pp. 175–186, 2002.

[19] G. Özdemir and Ö. E. Sezgin, "Keratin-rhamnolipids and keratin-sodium dodecyl sulfate interactions at the air/water interface," *Colloids and Surfaces B*, vol. 52, no. 1, pp. 1–7, 2006.

[20] F. J. Alguacil, M. Alonso, F. A. Lopez, and A. Lopez-Delgado, "Pseudo-emulsion membrane strip dispersion (PEMSD) pertraction of chromium(VI) using CYPHOS IL101 ionic liquid as carrier," *Environmental Science and Technology*, vol. 44, no. 19, pp. 7504–7508, 2010.

[21] C. A. Kozlowski and W. Walkowiak, "Removal of chromium(VI) from aqueous solutions by polymer inclusion membranes," *Water Research*, vol. 36, no. 19, pp. 4870–4876, 2002.

[22] S. Alpaydin, A. Ö. Saf, S. Bozkurt, and A. Sirit, "Kinetic study on removal of toxic metal Cr(VI) through a bulk liquid membrane containing p-tert-butylcalix[4]arene derivative," *Desalination*, vol. 275, no. 1–3, pp. 166–171, 2011.

[23] A. B. Albadarin, A. H. Al-Muhtaseb, N. A. Al-laqtah, G. M. Walker, S. J. Allen, and M. N. M. Ahmad, "Biosorption of toxic chromium from aqueous phase by lignin: mechanism, effect of other metal ions and salts," *Chemical Engineering Journal*, vol. 169, no. 1–3, pp. 20–30, 2011.

[24] F. Gode, E. D. Atalay, and E. Pehlivan, "Removal of Cr(VI) from aqueous solutions using modified red pine sawdust," *Journal of Hazardous Materials*, vol. 152, no. 3, pp. 1201–1207, 2008.

[25] M. R. Hadjmohammadi, M. Salary, and P. Biparva, "Removal of Cr(VI) from aqueous solution using pine needles powder as a biosorbent," *Journal of Applied Sciences in Environmental Sanitation*, vol. 6, pp. 1–13, 2011.

[26] P. M. M. Schrooyen, P. J. Dijkstra, R. C. Oberthür, A. Bantjes, and J. Feijen, "Partially carboxymethylated feather keratins. 2. Thermal and mechanical properties of films," *Journal of Agricultural and Food Chemistry*, vol. 49, no. 1, pp. 221–230, 2001.

[27] A. Aluigi, C. Tonetti, C. Vineis, C. Tonin, and G. Mazzuchetti, "Adsorption of copper(II) ions by keratin/PA6 blend nanofibres," *European Polymer Journal*, vol. 47, no. 9, pp. 1756–1764, 2011.

[28] C. Yang, L. Guan, Y. Zhao, and Y. Yan, "Sorption of Cu^{2+} and Zn^{2+} by natural biomaterial: duck feather," *Applied Biochemistry and Biotechnology*, vol. 142, no. 2, pp. 168–178, 2007.

[29] C. S. Ki, E. H. Gang, I. C. Um, and Y. H. Park, "Nanofibrous membrane of wool keratose/silk fibroin blend for heavy metal ion adsorption," *Journal of Membrane Science*, vol. 302, no. 1-2, pp. 20–26, 2007.

[30] D. Touaibia and B. Benayada, "Removal of mercury(II) from aqueous solution by adsorption on keratin powder prepared from Algerian sheep hooves," *Desalination*, vol. 186, no. 1–3, pp. 75–80, 2005.

[31] S. Al-Asheh, F. Banat, and D. Al-Rousan, "Beneficial reuse of chicken feathers in removal of heavy metals from wastewater," *Journal of Cleaner Production*, vol. 11, no. 3, pp. 321–326, 2003.

[32] A. Aneja and G. L. Wilkes, "Exploring macro—and microlevel connectivity of the urea phase in slabstock flexible polyurethane foam formulations using lithium chloride as a probe," *Polymer*, vol. 43, no. 20, pp. 5551–5561, 2002.

[33] Y. Xu, Z. Petrovic, S. Das, and G. L. Wilkes, "Morphology and properties of thermoplastic polyurethanes with dangling chains in ricinoleate-based soft segments," *Polymer*, vol. 49, no. 19, pp. 4248–4258, 2008.

[34] K. P. Menard, *Dynamic Mechanical Analysis, A Practical Introduction*, CRC Press, Boca Raton, Fla, USA, 2008.

[35] L. Zhang, H. K. Jeon, J. Malsam, R. Herrington, and C. W. Macosko, "Substituting soybean oil-based polyol into polyurethane flexible foams," *Polymer*, vol. 48, no. 22, pp. 6656–6667, 2007.

[36] J. L. Rivera-Armenta, T. Heinze, and A. M. Mendoza-Martínez, "New polyurethane foams modified with cellulose derivatives," *European Polymer Journal*, vol. 40, no. 12, pp. 2803–2812, 2004.

[37] Y. C. Sharma, B. Singh, A. Agrawal, and C. H. Weng, "Removal of chromium by riverbed sand from water and wastewater: effect of important parameters," *Journal of Hazardous Materials*, vol. 151, no. 2-3, pp. 789–793, 2008.

[38] V. K. Gupta, A. Rastogi, and A. Nayak, "Adsorption studies on the removal of hexavalent chromium from aqueous solution using a low cost fertilizer industry waste material," *Journal of Colloid and Interface Science*, vol. 342, no. 1, pp. 135–141, 2010.

[39] Y. C. Sharma, "Cr(VI) removal from industrial effluents by adsorption on an indigenous low-cost material," *Colloids and Surfaces A*, vol. 215, no. 1–3, pp. 155–162, 2003.

[40] T. Moritz, S. Benfer, P. Árki, and G. Tomandl, "Influence of the surface charge on the permeate flux in the dead-end filtration with ceramic membranes," *Separation and Purification Technology*, vol. 25, no. 1–3, pp. 501–508, 2001.

[41] G. Mendikute, L. Irusta, and M. J. Fernández-Berridi, "Infrared study of the photochemical behaviour of aromatic poly(ether urethanes): effect of various stabilizers," *E-Polymers*, article 125, 2009.

[42] L. C. Ciobanu and C. Ciobanu, "Characterization of the surface and mechanical behavior of polyurethane microporous films doped with silver nanoparticles," *E-Polymers*, article 091, 2009.

[43] C. Merlini, V. Soldi, and G. M. O. Barra, "Influence of fiber surface treatment and length on physico-chemical properties of short random banana fiber-reinforced castor oil polyurethane composites," *Polymer Testing*, vol. 30, no. 8, pp. 833–840, 2011.

[44] K. B. Gireesh, K. K. Jena, S. Allauddin, K. R. Radhika, R. Narayan, and K. V. S. N. Raju, "Structure and thermo-mechanical properties study of polyurethane-urea/glycidoxypropyltrimethoxysilane hybrid coatings," *Progress in Organic Coatings*, vol. 68, no. 3, pp. 165–172, 2010.

[45] S. Zhang, Z. Ren, S. He, Y. Zhu, and C. Zhu, "FTIR spectroscopic characterization of polyurethane-urea model hard segments (PUUMHS) based on three diamine chain extenders," *Spectrochimica Acta*, vol. 66, no. 1, pp. 188–193, 2007.

Hindawi Publishing Corporation
International Journal of Polymer Science
Volume 2013, Article ID 529021, 4 pages
http://dx.doi.org/10.1155/2013/529021

Research Article

The Solubility of Hydrocarbon Gases in Glassy Polymers: Fractal Modeling

Georgii V. Kozlov,[1] Jorge A. Cruz-Morales,[2] Joel Vargas,[2] and Mikhail A. Tlenkopatchev[2]

[1] *Kabardino-Balkarian State University, Chernishevsky Street 173, Nalchik 360004, Russia*
[2] *Instituto de Investigaciones en Materiales, Universidad Nacional Autónoma de México, Apartado Postal 70-360, CU, Coyoacán, 04510 México, DF, Mexico*

Correspondence should be addressed to Mikhail A. Tlenkopatchev; tma@unam.mx

Received 26 April 2013; Revised 11 August 2013; Accepted 12 August 2013

Academic Editor: Ling-Shu Wan

This work describes the fractal modeling of the solubility of *n*-alkanes, *n*-alkenes, methylacetylene, allene, ethylacetylene, and butadiene hydrocarbon gases in glassy poly(vinyltrimethylsilane) (PVTMS). The proposed equation represents satisfactorily the solubility coefficients of the hydrocarbon gases in glassy PVTMS as a function of the fractal dimension of the polymer and the effective diameter of a gas penetrant molecule. It is found that the calculated solubility coefficients have a good correlation with the experimental data. The proposed model can predict the solubility of hydrocarbon gases in glassy polymers.

1. Introduction

The separation of oxygen and nitrogen from air for the industrial combustion is carried out using membranes technology [1]. This technology is also used for the removal of hydrogen from mixtures with nitrogen or hydrocarbons in petrochemical processes [1]. Frozenness of polymer chains in the glassy state hinders chains fluctuations that give rise to the formation of channels through which the diffusant can migrate to a neighbor cavity. Here both solubility and diffusion may control gas separation of similar size; however, when the size of the diffusants largely differs, diffusion may be the controlling step. Furthermore glassy polymers with bulky side groups in their structure contain anomalous large cavities; such fact facilitates the gas permeability without adversely affecting the permselectivity. These polymers have in general high glass transition temperatures, and therefore aging processes that might affect the gas transport are not important at the temperatures of work. Polycarbonates, polysulfones, polyimides, and substituted polynorbornenes have attracted much attention for the gas separation [1–6].

It is important to devise methods that permit the prediction of the membrane performance for the gas separation as a function of the chemical structure. In this sense, the fractal modeling is an important tool for this purpose. Recently, authors proposed the fractal analysis of the gas permeability in semicrystalline polyethylene [7, 8].

Membranes prepared from PVTMS were industrially produced and used in the former Soviet Union and France. Furthermore, this material is known for more than 40 years as a polymer that exhibits a good O_2 permeability and O_2/N_2 selectivity. In this regard, the aim of this study consists in applying fractal analysis to describe the solubility coefficients of the hydrocarbon gases in glassy PVTMS membranes.

2. Materials and Methods

In the framework of the fractal model, it is assumed that the solubility of simple gases which are not interacting with polymers proceeds by deposition of gas penetrant molecules on the walls of free volume microvoids (true sorption) [12]. In this case, the general solubility model of a gas in a polymer can be written as [7, 13]

$$S \sim {F_g}^{D_f/2}, \tag{1}$$

where F_g is the cross-sectional area for the gas penetrant molecules and D_f is the dimension of extra energy localization domains for the polymer structure (D_f is related to the

fractal dimension of the polymer layer) [13]. The value of D_f can be calculated in the following way.

The relative fraction of the closely packed segments in clusters (φ_{cl}) is a parameter of order in strict physical sense, and it is related to the glass transition temperature of the polymer (T_g) through the following percolation correlation [14, 15]:

$$\varphi_{cl} = 0.03\left(T_g - T\right)^{0.55}, \tag{2}$$

where T is the temperature at which the parameter is measured ($T = 293$ K).

The fractal dimension of the polymer structure d_f can be calculated using [15]

$$d_f = 3 - 6\left(\frac{\varphi_{cl}}{\mathrm{Cs}\cdot S_{cr}}\right)^{1/2}, \tag{3}$$

where d_f is the fractal dimension of the supermolecular (supersegmental) structure of the polymer, S_{cr} is the cross-sectional area of a macromolecule in Å^2, and Cs is a characteristic ratio which is the index of chain flexibility [16, 17]. The values of Cs and S_{cr} can be estimated according to the literature [13, 17, 18]. Finally, the dimension of D_f can be estimated from [19]

$$D_f = 1 + \frac{1}{\left(3 - d_f\right)}. \tag{4}$$

The calculated value of D_f for the glassy PVTMS is $D_f = 4.33$.

For the PVTMS, we have $T_g = 440$ K, $T = 293$ K, $\varphi_{cl} = 0.467$, $d_f = 2.70$, Cs = 6.7, and $S_{cr} = 22.7$.

In order to construct an effective model for the solubility coefficient (related to the permeability model of gas transport in polymer membranes [4, 13]), we include the Lennard-Jones characteristic constant force potential (ε/k) which describes the interactions between gas-gas molecules as a function of the distance [11]. Thus, the fractal model of the solubility coefficient can be written as

$$S = S_0\left(F_g^{\mathrm{ef}}\right)^{D_f/2}\left(\frac{\varepsilon}{k}\right), \tag{5}$$

where S is the solubility coefficient of a gas in the polymer (cm^3 of gas (STP)/cm^3 of polymer cmHg), S_0 is a constant, and (F_g^{ef}) is the effective square of a cross sectional-area of a gas penetrant molecule. It is worth noting that the values of the solubility coefficients of the hydrocarbon gases are not described by (5) using the known values of maximum (d_{max}) and minimum (d_{min}) gas diameters [9, 10]. Here we have estimated for the C_1–C_4 hydrocarbon gases the effective diameter values (d_{ef}) taking into account the orientation of a gas molecule inside the microvoids in the polymer. The backcalculation of the effective diameter using the values of gas solubility shows the systematic increase of d_{ef}/d_{min} ratio as the Lennard-Jones characteristic constant force potential (ε/k) increases (Figure 1). This correlation can be expressed by

$$\frac{d_{\mathrm{ef}}}{d_{\mathrm{min}}} = 1 + 1.15\times 10^{-3}\left(\frac{\varepsilon}{k}\right). \tag{6}$$

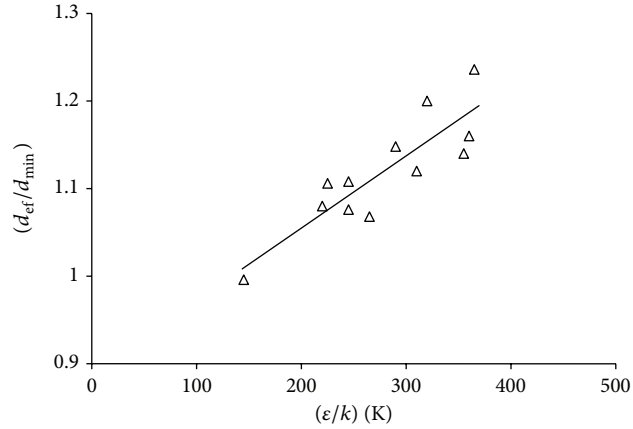

Figure 1: Plot of effective diameter and minimum diameter ratio (d_{ef}/d_{min}) of C_1–C_4 hydrocarbon gases against the Lennard-Jones characteristic constant force potential (ε/k).

The values of (F_g^{ef}) in (5) are estimated from the effective diameter values (d_{ef}) of gas penetrant molecules calculated using (6).

3. Results and Discussion

The glassy membranes contain microvoids, which account for the excess volume in the glassy state. The presence of microvoids in glassy polymers is confirmed by numerous experiments [20, 21]. The diameters of these microvoids have the value of several Angstroms and their walls are represented as vibrating centers around equilibrium positions of chain fragments. In other words, microvoids are a consequence of a critical displacement of kinetic units from an equilibrium position [22]. According to this model, solubility of a gas occurs in the continuous phase, whereas the microvoids act as sites where the gas is adsorbed. Successful gas adsorption requires not only an appropriate orientation of the molecules in microvoids but also the radius of the channel to be larger than the radii of the gas penetrant molecules.

The values of the effective diameter and minimum diameter ratio d_{ef}/d_{min} of a gas penetrant against the Lennard-Jones characteristic constant force potential (ε/k) (6) are shown in Figure 1. It is seen that the values of (d_{ef}/d_{min}) ratio increase as the Lennard-Jones characteristic constant force potential (ε/k) increases. This phenomenon can be explained by the orientation of gas penetrants during the sorption process. The orientation of a gas molecule inside the polymer means the increase of the effective diameter of a gas penetrant molecule. Consequently, the gas solubility coefficient increases as the effective diameter increases according to (5). The physical meaning of a constant S_0 in (5) can be determined from the following condition:

$$\left(F_g^{\mathrm{ef}}\right)^{D_f/2}\left(\frac{\varepsilon}{k}\right) = 1. \tag{7}$$

Here we discuss the conditions for the realization of (7). The value of minimum diameter for the gas He is 1.8 Å, which

Table 1: Values of diameters and force constants (ε/k) of C_1–C_4 hydrocarbon gases for the calculation of a solubility coefficient in PVTMS.

Hydrocarbon	d, Å [9, 10]	d_{ef}, Å [11]	d_{ef}, Å, from (6)	(ε/k), K [11]
CH_4	3.3–4.2	3.18 ± 0.14	3.30	154 ± 15.6
C_2H_6	3.7–5.2	3.69 ± 0.08	4.06	250 ± 22
C_3H_8	4.1–5.8	4.09 ± 0.08	4.76	305 ± 28
C_4H_{10}	4.6–6.9	4.40 ± 0.08	5.66	364 ± 35
C_2H_4	3.6–5.5	3.57 ± 0.08	3.82	225 ± 15
C_3H_6	4.1–5.4	3.86 ± 0.13	4.63	294 ± 32
C_4H_8	4.5–5.2	4.18	5.36	356
C_2H_2	3.5–5.7	3.38 ± 0.06	3.70	223 ± 23
C_3H_4 (m)[a]	4.0–4.8	3.62 ± 0.07	4.62	321 ± 25
C_4H_6 (e)[b]	4.4–5.0	3.81	5.26	360
C_3H_4 (a)[c]	4.6–4.9	3.64 ± 0.07	5.38	335 ± 14
C_4H_6 (b)[d]	5.0	3.85	5.45	327

[a]m is methylacetylene.
[b]e is ethylacetylene.
[c]a is allene.
[d]b is butadiene.

Table 2: Comparison of calculated (S_{cal}) and experimental (S_{exp}) values of solubility coefficient of hydrocarbon gases in PVTMS.

Hydrocarbon	d_{ef}, Å, from (6)	$S_{exp} \times 10^{-3}$[a] [11]	$S_{cal} \times 10^{-3}$[a], from (6)
CH_4	3.30	10	15
C_2H_6	4.06	70	109
C_3H_8	4.76	400	421
C_4H_{10}	5.66	1660	1766
C_2H_4	3.82	47	63
C_3H_6	4.63	310	332
C_4H_8	5.36	—	1163
C_2H_2	3.70	33	49
C_3H_4 (m)[b]	4.62	300	357
C_4H_6 (e)[c]	5.26	—	1022
C_3H_4 (a)[d]	5.38	315	403
C_4H_6 (b)[e]	5.45	—	981

[a]Units of S: cm^3 of gas (STP)/(cm^3 of polymer cmHg).
[b]m is methylacetylene.
[c]e is ethylacetylene.
[d]a is allene.
[e]b is butane.

corresponds to $F_g^{ef} = 2.54$ Å [23]. The value of D_f can be alternatively estimated using

$$D_f = 2\frac{(1-\upsilon)}{(1-2\nu)}, \tag{8}$$

where υ is Poisson's coefficient.

The minimum value of υ ($\upsilon = -1$) in (8) corresponds to $D_f = 1.33$. In this case, the criterion for (7) has the condition $(\varepsilon/k) = 0.583$ K. This value about 3 orders of magnitude is lower than the values of ε/k for the hydrocarbons of C_1–C_4 [19]. This means that the value of S_0 in (5) corresponds to a minimum solubility of a gas molecule where a gas molecular interaction does not count. Thus, the estimated values of S_0 for PVTMS are equal to 4.0×10^{-8}. Table 1 shows the values of diameters and force constants (ε/k) of C_1–C_4 hydrocarbons.

As shown in Table 1, the d_{ef} values of hydrocarbons, calculated by (6), are higher than the d_{min} values according to [9, 10]. The latter could be attributed to the orientation of the gas penetrant molecules during sorption inside the microvoids in the polymer.

Table 2 shows the experimental S_{exp} [11] and calculated S_{cal} results of the solubility coefficients for the hydrocarbon gases in PVTMS. The results indicate that a good concordance between the calculated S_{cal}, using (5), and experimental S_{exp} values of the solubility coefficient is observed. A reasonable agreement is also observed for the larger molecules of C_4H_6 and C_4H_8. The values of the solubility coefficient follow the trend $S(CH_4) < S(C_2H_2) < S(C_2H_4) < S(C_3H_4) < S(C_2H_6) < S(C_3H_6) < S(C_4H_{10})$.

As a powerful tool, the fractal model can also be used to estimate other variables such as permeability and selectivity

in gas transport through polymeric membranes. In this regard, we are trying to obtain the experimental parameters of the fractal model to achieve the theoretical values of the permeability and solubility coefficients in amorphous polymers such as polynorbornene dicarboximides with different pendant groups (phenyl, adamantyl, and cyclohexyl), reported in previous work [24].

4. Conclusions

Equation (5) represents satisfactorily the solubility coefficients for the C_1–C_4 hydrocarbon gases in a glassy PVTMS. According to this equation, the values of the solubility coefficient depend on the size of the gas penetrant molecules, their molecular interactions with the polymer, and fractal dimensions of the polymer. The solubility coefficients increase as the effective diameters of the gases also increase. In all cases, the calculated results are in good agreement with experimental data. The fractal modeling proposed in this study should be useful for the prediction of the gas solubility in glassy polymer membranes.

Conflict of Interests

The authors declare that there is no conflict of interests regarding the publication of this paper.

Acknowledgments

The authors thank CONACYT-SEMARNAT (Contract 23432) for generous support for this research.

References

[1] R. E. Kesting and A. K. Fritzche, *Polymeric Gas Separation Membranes*, chapter 6, John Wiley & Sons, New York, NY, USA, 2nd edition, 1993.

[2] H. Ohya, V. V. Kudryavtsev, and S. I. Semenova, *Polyimide Membranes: Applications, Fabrication and Properties*, Kondansha, Tokyo, Japan, 1996.

[3] W. J. Koros and G. K. Fleming, "Membrane-based gas separation," *Journal of Membrane Science*, vol. 83, no. 1, pp. 1–80, 1993.

[4] D. R. Paul and Y. P. Yampolskii, *Polymeric Gas Separation Membranes*, chapter 4, CRC Press, Boca Raton, Fla, USA, 1994.

[5] A. Pineda Contreras, M. A. Tlenkopatchev, M. Del Mar López-González, and E. Riande, "Synthesis and gas transport properties of new high glass transition temperature ring-opened polynorbornenes," *Macromolecules*, vol. 35, no. 12, pp. 4677–4684, 2002.

[6] J. Vargas, A. A. Santiago, M. A. Tlenkopatchev, M. López-González, and E. Riande, "Gas transport in membranes based on polynorbornenes with fluorinated dicarboximide side moieties," *Journal of Membrane Science*, vol. 361, no. 1-2, pp. 78–88, 2010.

[7] G. V. Kozlov, V. V. Afaunov, N. I. Mashukov, and Y. S. Lipatov, *Fractal and Local Order in Polymeric Materials*, Nova Science, New York, NY, USA, 2001.

[8] G. V. Kozlov and G. E. Zaikov, "The diffusion of gases in semicrystalline polyethylene and its melt," *Vysokomolekularnye Soedineniya B*, vol. 45, no. 7, pp. 1197–1201, 2003 (Russian), English translation *Polymer Science Series B* , vol. 45, pp. 181–187, 2003.

[9] A. S. Michaels and H. J. Bixler, "Solubility of gases in polyethylene," *Journal of Polymer Science*, vol. 50, pp. 393–412, 1961.

[10] A. R. Berens and H. B. Hopfenberg, "Diffusion of organic vapors at low concentrations in glassy PVC, polystyrene, and PMMA," *Journal of Membrane Science*, vol. 10, no. 2-3, pp. 283–303, 1982.

[11] V. V. Teplyakov and S. G. Durgaryan, "On the relation between the parameters of permeability of gases and hydrocarbons in polymers," *Vysokomolekulyarnye Soedineniya A*, vol. 28, pp. 564–572, 1986 (Russian).

[12] E. Baer, *Engineering Design For Plastic*, chapter 2, Reinhold Publishing, New York, NY, USA, 1963, Khimiya, Moscow, Russia, 1967.

[13] G. V. Kozlov and G. E. Zaikov, *Fractals Analysis of Gas Transport in Polymers*, chapters 2, 3 and 5, Nova Science, New York, NY, USA, 2008.

[14] V. I. Novikov and G. V. Kozlov, "Fractal analysis of macromolecules," *Uspekhi Khimii*, vol. 69, pp. 378–397, 2000, English translation *Russian Chemical Reviews*, vol. 69, pp.347–366, 2000.

[15] G. V. Kozlov, L. K. Nafadzokova, and G. E. Zaikov, "Fractal model of the free volume of vitreous poly(vinyltrimethylsilane) from data on gas diffusion," *Glass Physics and Chemistry*, vol. 33, no. 5, pp. 481–485, 2007.

[16] V. P. Budtov, *Physical Chemistry of Polymer Solutions*, Khimiya, Saint-Petersburg, Russia, 1992, (Russian).

[17] S. M. Aharoni, "On entanglements of flexible and rodlike polymers," *Macromolecules*, vol. 16, no. 11, pp. 1722–1728, 1983.

[18] S. Wu, "Chain structure and entanglement," *Journal of Polymer Science B*, vol. 27, no. 4, pp. 723–741, 1989.

[19] A. S. Balankin, *Synergetics of Deformed Solids*, vol. 1, Publishing House of the Ministry of Defense of the USSR Press, Moscow, Russia, 1991, (Russian).

[20] B. D. Malhotra and R. A. Pethrick, "Positronium annihilation studies of polycarbonate, polyethersulphone and polysulphone," *European Polymer Journal*, vol. 19, no. 6, pp. 457–459, 1983.

[21] Q. Deng, F. Zandiehnadem, and Y. C. Jean, "Free-volume distributions of an epoxy polymer probed by positron annihilation: temperature dependence," *Macromolecules*, vol. 25, no. 3, pp. 1090–1095, 1992.

[22] D. S. Sanditov and G. V. Kozlov, "On the nature of fluctuation holes in a simplest model of relaxation in amorphous polymers," *Vysokomolekulyarnye Soedineniya A*, vol. 38, pp. 1389–1398, 1996 (Russian), English translation *Polymer Science A*, vol 38, pp. 919–923, 1996.

[23] N. I. Nikolaev, *Diffusion in Membranes*, Khimiya, Moscow, Russia, 1980, (Russian).

[24] M. A. Tlenkopatchev, J. Vargas, M. D. M. López-González, and E. Riande, "Gas transport in polymers prepared via metathesis copolymerization of exo-N-phenyl-7-oxanorbornene-5,6-dicarboximide and norbornene," *Macromolecules*, vol. 36, no. 22, pp. 8483–8488, 2003.

Hindawi Publishing Corporation
International Journal of Polymer Science
Volume 2013, Article ID 106570, 7 pages
http://dx.doi.org/10.1155/2013/106570

Research Article

Curcumin-Loaded Chitosan/Gelatin Composite Sponge for Wound Healing Application

Van Cuong Nguyen,[1] Van Boi Nguyen,[1] and Ming-Fa Hsieh[2]

[1] *Department of Chemical Engineering, Industrial University of Ho Chi Minh City, 12 Nguyen Van Bao Street, Go Vap, Ho Chi Minh City 70000, Vietnam*
[2] *Department of Biomedical Engineering, Center for Nanotechnology and Institute of Biomedical Technology, Chung Yuan Christian University, 200 Chung Pei Road, Chungli, 32023 Taoyuan, Taiwan*

Correspondence should be addressed to Van Cuong Nguyen; nvc@hui.edu.vn

Received 8 June 2013; Revised 4 July 2013; Accepted 4 July 2013

Academic Editor: Hai-Yin Yu

Three composite sponges were made with 10% of curcumin and by using polymers, namely, chitosan and gelatin with various ratios. The chemical structure and morphology were evaluated by FTIR and SEM. These sponges were evaluated for water absorption capacity, antibacterial activity, *in vitro* drug release, and *in vivo* wound healing studies by excision wound model using rabbits. The *in vivo* study presented a greater wound closure in wounds treated with curcumin-composite sponge than those with composite sponge without curcumin and untreated group. These obtained results showed that combination of curcumin, chitosan and gelatin could improve the wound healing activity in comparison to chitosan, and gelatin without curcumin.

1. Introduction

Medicines derived from plants play an important role in the healthcare of many cultures, both ancient and modern. Curcumin (diferuloylmethane, a polyphenol) is an active agent of the perennial herb *Curcuma longa* (commonly known as turmeric). Curcumin is a naturally occurring polyphenolic phytoconstituent which presents anticancer, antioxidant, anti-inflammatory, hyperlipidemic, antibacterial, wound healing, and hepatoprotective activities [1, 2]. The therapeutic efficacy of curcumin is limited due to its poor aqueous solubility and extensive first pass metabolism [3–5]. Topical formulation of curcumin (curcumin incorporated collagen matrix) was a feasible and productive approach to support dermal wound healing [1]. Therefore, development of novel curcumin formulation and delivery systems is required. The topical delivery of naturally occurring compounds, such as curcumin or catechins, is able to increase its solubility, stability, and pharmacological activities, resulting in improvement of therapeutic effects [6].

Additionally, chitosan, a polysaccharide biopolymer derived from naturally occurring chitin, displays unique polycationic, chelating, and film-forming properties due to the presence of active amino and hydroxyl functional groups. Chitosan also exhibits a number of interesting biological activities, including antimicrobial activity, induced disease resistance in plants, and diverse stimulating or inhibiting activities toward a number of human cell types [7, 8]. Moreover, chitosan can be used to prevent or treat wound and burn infections due to its intrinsic antimicrobial properties and its ability to deliver extrinsic antimicrobial agents to wounds and burns [9]. Additionally, it can accelerate the functions of inflammatory cells, macrophages, and fibroblasts [10, 11]. Chitosan and its derivatives are also used to increase the stability of the drug in which the drugs are loaded in chitosan film or chitosan nanoparticles, resulting in enhancement of drug accumulation [12] and toxicity to cancer cells [13, 14]. Gelatin is also a natural polymer derived from collagen of animal skin and bones. It is biocompatible, hydrophilic, and biodegradable under normal physiological conditions.

Gelatin is known to prevent fluid loss due to exudation, resulting in enhancement of its wound healing properties [15, 16]. Thus, the present study focused on the preparation and evaluation of composite sponge made with two natural polymers: chitosan and gelatin at different proportions. Moreover, curcumin was loaded into the chitosan and gelatin sponge for wound healing application.

2. Materials and Methods

2.1. Materials. Chitosan is extracted from crab shells which was prepared from our lab. The degree of deacetylation of the chitosan was approximately 85%. Curcumin was purchased from Vietnam Institute of Dietary Supplement (Hanoi, Vietnam) and acetic acid and gelatin were purchased from Sigma-Aldrich Chemical Co (USA). All chemicals used in this study were of reagent grade.

2.2. Preparation of Composite Sponge. Chitosan (1.0 g) was dissolved in 1% aqueous acetic acid (100 mL) to form a 1% chitosan solution (w/v) at room temperature. Gelatin (10%) solution was prepared by dissolving gelatin powder (10 g) in 100 mL of deionized water at room temperature. The composite sponges were prepared by dissolving chitosan solution into the gelatin solution with different portions (3 : 1, 1 : 1, and 1 : 3) of chitosan and gelatin, named as SP3, SP2 and SP1, respectively. The resulting solution was vigorously mixed under magnetic stirrer until the opaque aqueous solution was obtained. The solution was sonicated for 5 min for the removal of entrapped air bubbles. Then the air bubble-free solution was poured into separated petridishes and frozen at −40°C for 24 h followed by lyophilization to obtain composite sponge. For curcumin encapsulated in composite sponge, 1 mL of curcumin solution (0.5% w/v in absolute ethanol) was added to opaque aqueous solution. Then the solution was poured into separated petridishes, frozen at −40°C for 24 h, and followed by lyophilization to obtain curcumin composite sponge.

2.3. Characterization of Composite Sponge. The chemical structure and morphology of chitosan/gelatin composite sponges were evaluated using FT-IR (PerkinElmer) and SEM (JSM-5500).

2.4. Water Absorption Test. The water absorption capacity of the composite sponge was determined by incubating the composite sponge in phosphate-buffered saline (PBS) at pH 7.4 at 37°C for 2 h. The wet weight of the swollen sponge was measured immediately after gently blotting with filter paper to remove absorbed water on surface, followed by lyophilization and reweighing. The water content of the sponge was calculated as follows:

$$E_{\text{ad}} = \left[\frac{W_e - W_0}{W_0}\right] \times 100, \quad (1)$$

where E_{ad} is the percentage water adsorption of chitosan-gelatin sponge at equilibrium. W_e and W_0 represent the weight of the chitosan-gelatin sponge at equilibrium and initial weight of the chitosan-gelatin sponge, respectively.

2.5. Weight Loss of Prepared Sponges. The prepared sponges were immersed in PBS buffer solution at 37°C. After 24 h, the sponges were taken out, washed with deionized water, frozen, and lyophilized. The weights of sponges were measured after lyophilization. Weight loss of sponges was calculated through the following equation: $\%W = (W_0 - We)/W_0 \times 100$, where W_0 and W_e are the initial weight of sponge (g) and weight of sponge after lyophilization (g), respectively.

2.6. In Vitro Drug Release. The composite sponges (3 × 3 cm) were dispersed in 20 mL phosphate buffer solution, pH 7.4 at 37°C. All the supernatants were pipetted out periodically and replaced with equivalent volume of fresh phosphate buffer solution. The concentration of released drug was then determined by UV-Vis spectrometer at 420 nm using a standard curve of curcumin in ethanol. The percentage of curcumin released was determined as curcumin release (%) = curcumin released at time t/total curcumin loaded in sponge × 100.

2.7. Evaluation of Antimicrobial Activity. The measurements of the antimicrobial activities of individual chitosan and composite sponge were conducted by agar diffusion method using *Pseudomonas aeruginosa*. The zone of inhibition was determined by placing a definite size of sponge in inoculated solidified nutrient agar medium in a petriplate. Petriplates were incubated for 24 h at 37°C. This was done in triplicate with each film for each organism, and an average diameter of zone of inhibition was noted.

2.8. Cytotoxicity. The cytotoxicity of curcumin sponge was conducted on mouse fibroblast cells (L929) indirect MTT method [17]. The cells were seeded into 96-well microplates at a density of 10^3 cells/well at 37°C under humidified atmosphere containing 5% CO_2. Triplicates of sterilized sample were taken and then incubated in serum containing media for 24 h at 37°C. 100 μL of the media from each sample was taken and transferred into each well then incubated for another 24 h. After that, MTT solution was added to each well followed by 4 hours of incubation at 37°C. Subsequently, the medium was removed and violet crystals formed were solubilized with DMSO. After shaking slowly twice for 5 seconds, the absorbance of each well was determined using Eliza reader at 570 nm. The cell viability was expressed as a percentage of the control.

2.9. Evaluation of Wound Healing Activity. The wound healing activity was evaluated by excision wound model in albino rabbits (1.7 to 2.0 kg). All *in vivo* experiments were carried out in accordance with the ethical guidelines for Animal Care and Use Committee of Medical and Pharmaceutical University (Ho Chi Minh City). The animals were anesthetized by using lidocaine 25% prior to the test. The dorsal hair of the rabbit was removed. Full thickness wound of 2.5 × 2.5 cm^2 was excised from the back of the rabbit. The wound was covered

with an equal size of drug-loaded sponge or blank sponge. The cotton gauge was used for control. The sponge was removed and replaced by fresh sponge every three days. The wound closure was observed at different periods of treatment using a digital camera. Wound area was calculated on the 0th, 3rd, 12nd, 15th and 21st days. On day 21st, histological examinations of skin wound tissue were carried out. The skin wound tissue of animal was excised, fixed with 10% formalin, and stained with hematoxylin-eosin (H&E) reagent for histological observations.

3. Results and Discussion

The composite sponges were prepared in different ratios of chitosan and gelatin (3 : 1, 1 : 1, and 1 : 3) (Figure 1). The results indicated that increasing of gelatin concentration leads to increase of folding endurance. The composite sponge SP1 showed the highest folding endurance among all composite sponges (data not shown). To examine the chemical structures of various sponges prepared under different feeding ratios, the prepared sponges were examined by FTIR spectra. The –CH– stretching vibration of the chitosan and gelatin is at 2936–2969 cm^{-1}, while peaks of chitosan at 1650 and 1560 cm^{-1} correspond to the amide carbonyl group (amide I) and the bending frequency of the amide N–H group (amide II), respectively (Figure 2). The FT-IR of composite sponge exhibited a mixture of characteristic absorptions because of amine groups of chitosan and the carboxylic acid groups of gelatin. The peaks of C = O of amide I for chitosan at 1650 cm^{-1} was shifted to 1669 cm^{-1} in composite sponges. The intensity of C = O peaks increased with the decline ratio of gelatin in composite sponge from 1 : 3 to 3 : 1 (chitosan/gelatin). These results can be attributed to the interaction of $-NH^{3+}$ of chitosan and the COO^{-} of gelatin in three composites [18, 19].

Figure 3 shows the cross-section morphology of chitosan/gelatin composite sponges. According to the figure, the sponges appeared as a very porous structure. Additionally, the roughness of chitosan/gelatin sponge surface was decreased with increasing of gelatin content (Figures 3(a)–3(c)). It was found that the large pores were observed in cross-section morphology of chitosan/gelatin sponges (Figures 3(d)–3(f)). The pore sizes were 43.06, 35.6, and 29.9 μm for SP3, SP2, and SP1, respectively. The sponges with low gelatin level represent regular pore size. On the other hand, the irregular pore size was observed in cross-section morphology of sponge with high gelatin content. The irregular pore size appearing in the sponge with high gelatin level may be deduced from the incompatibility between chitosan and gelatin molecules.

Water absorption capacity is an important parameter for biological applications and wound healing. It presents the capacity of sponge to absorb wound exudates. As the gelatin contents of prepared sponges were increased, the water adsorption capacities were significantly decreased. This is because lower water content led to smaller pore size during the preparation of the sponges. As a result, the water uptake was relatively lower. The water uptake capacity was 227%, 351%, and 2352% for ratio of chitosan/gelatin 1 : 3, 1 : 1, and 3 : 1, respectively. The high water content in prepared sponges was explained by the hydrophilic and swelling properties of gelatin [20]. The SP3 presented maximum water absorption capacity among all prepared sponges; the sponge can retain water in porous pore surrounding by cell walls. Additionally, it decreased about 10-fold for SP1 and SP2 which may attribute to the swelling and dissolving of gelatin that could decrease the pore size leading to less water absorption and therefore could not retain much water within their network structure. Furthermore, the water absorption capacity of drug-loaded sponge was not significantly different from blank sponge. The similar results were also reported in previous study [18]. These results were further confirmed by weight loss of sponges. Table 1 presents that the weight losses were 81.5, 66.5 and 16% for SP1, SP2, and SP3, respectively. The weight loss is reasonable as more gelatin can resist the dissolution in water. The water uptake may be related to the pore. The more gelatin, the smaller pores, and pore volume were observed.

The *in vitro* release profile of curcumin-sponge was conducted in phosphate buffer solution. The average percent release of curcumin was approximately 91%, 55%, and 37% for

(a) (b)

Figure 1: Prepared composite sponge with ratio of chitosan and gelatin (3 : 1) (a) curcumin-sponge and (b) blank sponge.

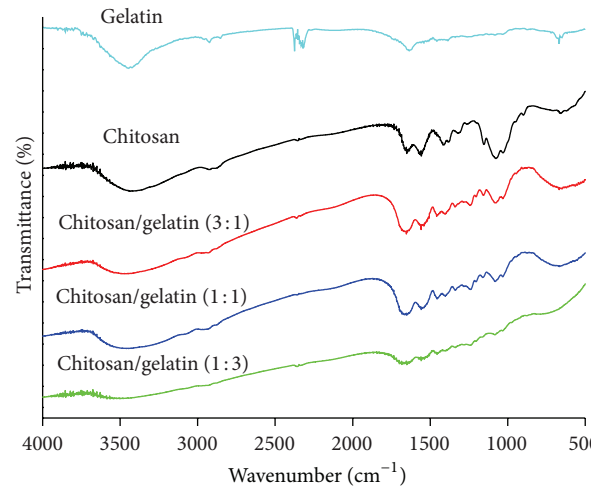

Figure 2: FT-IR spectra of prepared composite sponge with various ratios of chitosan and gelatin.

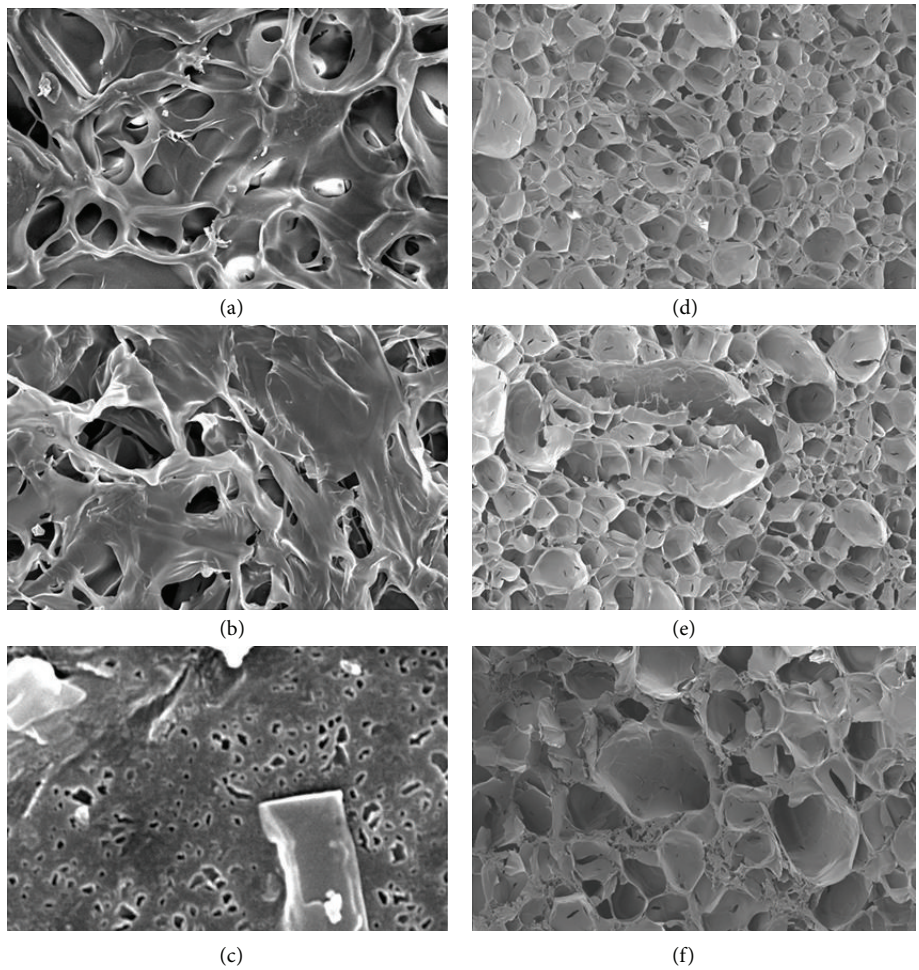

Figure 3: SEM images of surface morphology of chitosan/gelatin sponges (a) SP3, (b) SP2, and (c) SP1. Cross-section morphology of chitosan/gelatin sponges (d) SP3, (e) SP2, and (f) SP1 (scale bar at 100 μm).

Table 1: Composition and physical parameter of prepared sponges.

Sample no.	Feeding ratio		Average water uptake (%)	Weight loss (%)
	Chitosan	Gelatin		
SP1	1	3	227	81.5
SP2	1	1	351	66.5
SP3	3	1	2352	16

Table 2: The curcumin release profile of prepared sponges.

Time (h)	Drug release (%)		
	SP1	SP2	SP3
0	0.00	0.00	0.00
1	16.35	1.38	0.53
6	30.85	4.47	1.62
24	43.53	10.21	7.38
30	49.44	13.59	8.15
48	59.44	29.73	9.21
54	63.41	33.97	14.26
72	78.12	43.26	23.09
96	90.97	54.71	36.91

SP1, SP2, and SP3, respectively, in 96 h. The curcumin release increased with increase of gelatin content in prepared sponge (Table 2). This is because the hydrophilicity of curcumin was relatively lower. According to the partition ratio between sponge phase and water phase, the drug in the sponge having a higher gelatin content is preferred to be released, instead of being dissolved by the sponge.

From the results of antibacterial activity studies of prepared sponges against *P. aeruginosa*, it can be seen that the inhibition zone is larger in curcumin composite sponge than that of chitosan sponge without curcumin. It can be also seen that the SP3 sponge exhibited a higher inhibition zone than those of SP1 and SP2 sponges (Figure 4). The inhibition zones were 21 mm and 17.5 mm for curcumin-loaded SP3 and SP3 without curcumin, respectively.

The cytotoxicity of prepared sponges to L929 cells was evaluated using MTT assay method. The results demonstrate the cell viability after 24 h incubation with medium released

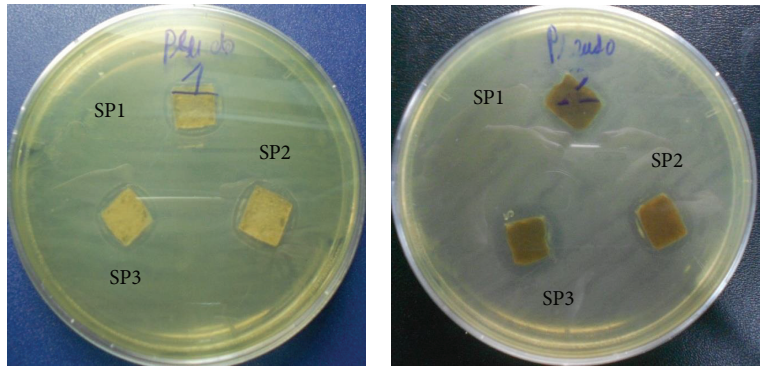

(a) (b)

Figure 4: Antibacterial activity of prepared sponges against *Pseudomonas aeruginosa:* (a) sponges without curcumin and (b) curcumin-sponges.

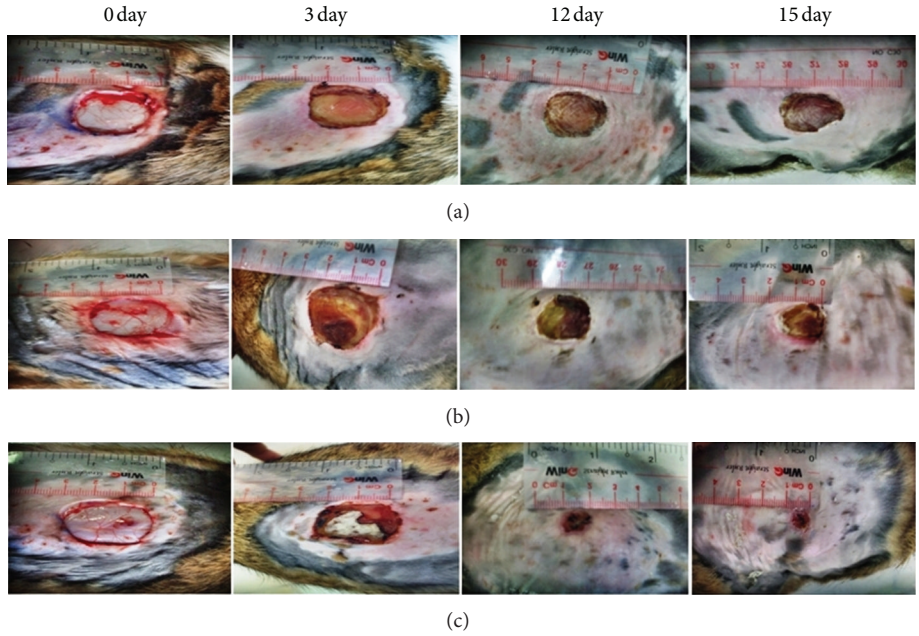

(a)

(b)

(c)

Figure 5: Photographs of macroscopic appearance of wound repair covered with (a) control, (b) blank sponge, and (c) curcumin sponge, at day 0, day 3, day 12, and day 15, respectively.

from sponges. The results present that cell viability decreased to approximately 90% in the presence of medium containing sponge without curcumin and curcumin sponge. The cell viability suggests that these sponges have generally low cytotoxicity to the L929 fibroblast cells (data not shown).

The SP3 sponge was selected for wound healing test. The percentage of wound closure in untreated and treated groups was measured on 3rd, 12nd, 15th, and 21st post wound day and the results are presented in Table 3. The wound closure was similar in three groups on 21st post wound day. The wound closure was 99.49%, 97.63%, and 94.30% for curcumin-SP3, blank SP3 and control group, respectively. It was found that the wounds treated with curcumin composite and composite without curcumin have shown faster wound healing than wound untreated group. Moreover, the wound closure on the 12nd and 15th day was significantly increased in curcumin SP3 in comparison with SP3 without curcumin (Figure 5). These results enhance the wound healing activity and could be a good material to be employed as wound dressing.

Histological Examination. The histological examination of three different kinds of wound dressing applied on skin wound of rabbit is presented in Figure 6. As can be seen in Figure 6, the tissue is in the acute stage of wound healing for control (Figure 6(a)). The tissue is under subacute stage of wound healing due to that there are many eosinophil, allergic reactions may be considered (Figure 6(b)). The

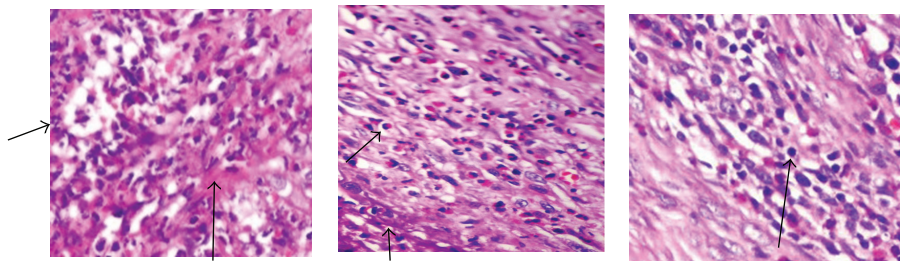

(a) (b) (c)

Figure 6: The H&E stained sections of twelve-day postsurgery of wound treated with (a) control: Short arrow—polymorphonuclear neutrophil (PMN), long arrow—fibroblast. The tissue is in the acute stage of wound healing. (b) Blank sponge (without curcumin): short arrow—eosinophil, long arrow—necrotic tissue. The tissue is under subacute stage of wound healing due to that there are many eosinophil and allergic reaction may be considered, and (c) curcumin sponge: arrow—lymphocyte, the tissue is under subacute stage of wound healing (400x).

Table 3: Wound closure of animal treated with blank sponge and curcumin sponge.

	Wound closure (%) (mean ± SD)			
Time	3rd day	12nd day	15th day	21st day
Control	15.36 ± 0.54	30.00 ± 1.05	48.80 ± 1.71	94.30 ± 1.93
SP3	14.79 ± 0.58	49.41 ± 1.93	77.96 ± 3.91	97.63 ± 4.28
Curcumin-SP3	26.53 ± 1.14	90.82 ± 2.11	95.41 ± 3.62	99.49 ± 3.81

wound is under subacute stage for curcumin-loaded sponge (Figure 6(c)). The granulation tissue and collagen alignment were more advanced in the sponge without curcurmin and curcumin-loaded sponge-treated wound as compared to the untreated wounds (control).

4. Conclusion

In this work, composite sponge of curcumin/chitosan/gelatin was prepared at the various ratios of chitosan and gelatin. The structure and morphology were characterized using FT-IR and SEM. The composite of curcumin, chitosan, and gelatin improved water uptake ability, antibacterial activity, and wound closure. Based on the results of drug release of curcumin, the higher content of gelatin in composite sponge exhibited a faster release behavior up to 240 min. These composite sponges were found to enhance the formation of collagen and wound closure *in vivo* and therefore improved the wound healing activity.

Acknowledgments

The authors would like to thank the Nafosted and Industrial University of Ho Chi Minh City for financial support. The authors thank Miss Tu and Miss Minh Nhat for their help on sample preparations.

References

[1] D. Gopinath, M. R. Ahmed, K. Gomathi, K. Chitra, P. K. Sehgal, and R. Jayakumar, "Dermal wound healing processes with curcumin incorporated collagen films," *Biomaterials*, vol. 25, no. 10, pp. 1911–1917, 2004.

[2] P. Basnet and N. Skalko-Basnet, "Curcumin: an anti-inflammatory molecule from a curry spice on the path to cancer treatment," *Molecules*, vol. 16, no. 6, pp. 4567–4598, 2011.

[3] A. Kunwar, A. Barik, R. Pandey, and K. I. Priyadarsini, "Transport of liposomal and albumin loaded curcumin to living cells: an absorption and fluorescence spectroscopic study," *Biochimica et Biophysica Acta*, vol. 1760, no. 10, pp. 1513–1520, 2006.

[4] A. Kumar, S. Dogra, and A. Prakash, "Protective effect of curcumin (Curcuma longa), against aluminium toxicity: possible behavioral and biochemical alterations in rats," *Behavioural Brain Research*, vol. 205, no. 2, pp. 384–390, 2009.

[5] B. T. Kurien and R. H. Scofield, "Increasing aqueous solubility of curcumin for improving bioavailability," *Trends in Pharmacological Sciences*, vol. 30, no. 7, pp. 334–335, 2009.

[6] C.-H. Chen, M.-F. Hsieh, Y.-N. Ho et al., "Enhancement of catechin skin permeation via a newly fabricated mPEG-PCL-graft-2-hydroxycellulose membrane," *Journal of Membrane Science*, vol. 371, no. 1-2, pp. 134–140, 2011.

[7] B. Wang, K. Chen, S. Jiang et al., "Chitosan-mediated synthesis of gold nanoparticles on patterned poly(dimethylsiloxane) surfaces," *Biomacromolecules*, vol. 7, no. 4, pp. 1203–1209, 2006.

[8] H. Yi, L.-Q. Wu, W. E. Bentley et al., "Biofabrication with chitosan," *Biomacromolecules*, vol. 6, no. 6, pp. 2881–2894, 2005.

[9] T. Dai, M. Tanaka, Y.-Y. Huang, and M. R. Hamblin, "Chitosan preparations for wounds and burns: antimicrobial and wound-healing effects," *Expert Review of Anti-Infective Therapy*, vol. 9, no. 7, pp. 857–879, 2011.

[10] R. Jayakumar, M. Prabaharan, P. T. Sudheesh Kumar, S. V. Nair, and H. Tamura, "Biomaterials based on chitin and chitosan in

wound dressing applications," *Biotechnology Advances*, vol. 29, no. 3, pp. 322–337, 2011.

[11] R. A. A. Muzzarelli, "Chitins and chitosans for the repair of wounded skin, nerve, cartilage and bone," *Carbohydrate Polymers*, vol. 76, no. 2, pp. 167–182, 2009.

[12] S.-J. Yang, F.-H. Lin, K.-C. Tsai et al., "Folic acid-conjugated chitosan nanoparticles enhanced protoporphyrin IX accumulation in colorectal cancer cells," *Bioconjugate Chemistry*, vol. 21, no. 4, pp. 679–689, 2010.

[13] Y.-Q. Ye, F.-Y. Chen, Q.-A. Wu et al., "Enhanced cytotoxicity of core modified chitosan based polymeric micelles for doxorubicin delivery," *Journal of Pharmaceutical Sciences*, vol. 98, no. 2, pp. 704–712, 2009.

[14] H. Zhou, W. Yu, X. Guo et al., "Synthesis and characterization of amphiphilic glycidol-chitosan-deoxycholic acid nanoparticles as a drug carrier for doxorubicin," *Biomacromolecules*, vol. 11, no. 12, pp. 3480–3486, 2010.

[15] A. Tanaka, T. Nagate, and H. Matsuda, "Acceleration of wound healing by gelatin film dressings with epidermal growth factor," *Journal of Veterinary Medical Science*, vol. 67, no. 9, pp. 909–913, 2005.

[16] E. J. Chong, T. T. Phan, I. J. Lim et al., "Evaluation of electrospun PCL/gelatin nanofibrous scaffold for wound healing and layered dermal reconstitution," *Acta Biomaterialia*, vol. 3, no. 3, pp. 321–330, 2007.

[17] K. Madhumathi, P. T. Sudheesh Kumar, S. Abhilash et al., "Development of novel chitin/nanosilver composite scaffolds for wound dressing applications," *Journal of Materials Science*, vol. 21, no. 2, pp. 807–813, 2010.

[18] M. Dai, X. Zheng, X. Xu et al., "Chitosan-alginate sponge: preparation and application in curcumin delivery for dermal wound healing in rat," *Journal of Biomedicine and Biotechnology*, vol. 2009, Article ID 595126, 8 pages, 2009.

[19] M. C. Silva and C. T. Andrade, "Evaluating conditions for the formation of chitosan/gelatin microparticles," *Polimeros*, vol. 19, no. 2, pp. 133–137, 2009.

[20] T. V. L. Hima Bindu, M. Vidyavathi, K. Kavitha, T. P. Sastry, and R. V. Suresh kumar, "Preparation and evaluation of ciprofloxacin loaded chitosan-gelatin composite films for wound healing activity," *International Journal of Drug Delivery*, vol. 2, no. 2, 2011.

Hindawi Publishing Corporation
International Journal of Polymer Science
Volume 2013, Article ID 760156, 10 pages
http://dx.doi.org/10.1155/2013/760156

Research Article

ZSM-5 Filled Polyether Block Amide Membranes for Separating EA from Aqueous Solution by Pervaporation

Jin Gu, Xinran Zhang, Yunxiang Bai, Le Yang, Chunfang Zhang, and Yuping Sun

The Key Laboratory of Food Colloids and Biotechnology, Ministry of Education, School of Chemical and Material Engineering, Jiangnan University, Wuxi 214122, China

Correspondence should be addressed to Yuping Sun; sunyp2003@yahoo.com.cn

Received 28 December 2012; Revised 25 March 2013; Accepted 9 April 2013

Academic Editor: Qian Yang

ZSM-5 filled polyether block amide membranes (PEBA), PEBA/ZSM-5, were prepared and used to recover aroma, ethyl acetate (EA), from aqueous solution by pervaporation (PV). The membranes demonstrated high EA permselectivity, and with the increase of ZSM-5 loading, the separation factor increased initially and then decreased, while the total flux demonstrated the similar variation until the ZSM-5 loading was 10 wt%, at which it reached the lowest value. After that, it began to increase again. On the other hand, the separation factor, and total flux of the PEBA/ZSM-5 membrane containing 10 wt% ZSM-5, PEBA/ZSM-5-10, increased with the increase of feed concentration and temperature. The best PV performance, separation factor and total flux of PEBA/ZSM-5-10 membrane were 185.5 and 199.5 $gm^{-2}h^{-1}$, respectively, with feed concentration of 5 wt% EA at 50°C.

1. Introduction

Ethyl acetate (EA) is a very important chemical raw material, which is widely used in producing perfumes, plasticizers, varnishes, synthetic resins, and adhesive agents [1]. EA is mainly synthesized via a classical esterification process of acetic acid with ethanol in conventional industry [2, 3]. Due to the fact that the process of esterification is a reversible one, the high concentration can inhibit the reaction, so the product of the low concentration should be separated from water in time [4, 5]. Distillation and pressure swing adsorption (PSA) were once the most common methods used to separate organic compounds from water. However, distillation is unsuitable for azeotropic mixtures, for separation of organic compounds in low concentration, or for thermally sensitive organic compounds [6]. PSA has the undesirable features of being energy intensive, with high investment cost and large installation area [7]. Compared with distillation and PSA, pervaporation (PV), as a new type of membrane separation technology, has obvious advantages in the field of gas separation and liquid separation in the separation of low concentration [8, 9]. In this area, most of the research has focused on the preparation and modification of the membrane due to the fact that membrane materials are the core components in the process of pervaporation. To date, the materials that have been used for pervaporative recovering organic compounds from water were mainly hydrophobic, such as polydimethylsiloxane (PDMS) [10–14], polyurethaneurea (PU) [15, 16], poly(vinylidene fluoride-co-hexafluoropropene) (P(VDF-co-HFP)) [17], ethylene-vinyl acetate (EVA) [18], and polyether block amide (PEBA) [19–21]. However, the trade off between permeability and selectivity is one of the biggest problems faced by pure polymer membranes, which greatly limits their further application in the chemical industries. In the past two decades, mixed matrix membranes started to emerge as an alternative approach in pervaporative membrane technology [22–25]. The PV performances as well as heat resistance were proved to be enhanced by incorporating inorganic fillers into polymer membranes. For the separation of organic compounds from aqueous solutions, hydrophobic inorganic fillers including zeolite [26–35], carbon black [36], carbon molecular sieve [37], and so on were adopted. Among them, zeolite with high Si/Al ratio (ZSM-5) and silicalite (Al-free zeolite) is intensely investigated to remove different organic compounds from water due to its high hydrophobicity, surface area, and void volume, and uniform pore size distribution. For example, Kittur and coworkers [26] prepared ZSM-5/PDMS blend

membranes for recovery of isopropanol from water. Their results showed that both permeation flux and selectivity increased simultaneously with the increase of zeolite content in the membrane matrix. The highest separation selectivity reached 80.84 and flux of 67.8 g/m^2 h at 30°C for 5 wt% of isopropanol in the feed when zeolite loading was 30 wt%. Vane et al. [27] prepared ZSM-5 filled PDMS membranes and showed that the separation factor of ethanol from water increased monotonously from 8.7 to 43.1 when ZSM-5 loading increased from 0 to 65 wt%, and the ethanol flux also increased from about 40 to 300 g/m^2 h. Jia et al. [28] found that the incorporation of silicalite into PDMS enhanced both the total flux and acetic acid/water separation factor which were from 57 to 150 g/m^2 h and from 1.35 to 2.75, respectively, with silicalite content of 49.9 wt%. Nevertheless, inevitably nonselective voids are generated near the interface of polymer and inorganic particles due to their incompatibility. Attempts were made to enhance the compatibility between the fillers and polymers by introducing silane coupling agent [38], but chemical modifying the fillers will partially block their pores. So, it is probably more reasonable and convenient to enhance physical affinity between polymer segments and the inorganic fillers by selecting or synthesizing suitable polymer materials. PEBA is a block copolymer material, which could provide hydrophobic and flexible soft segments (polyether) for facilitating organic compounds diffusion and rigid hard segments (polyamide) for mechanical strength. So inorganic fillers should have good affinity to PEBA segments and are prone to be dispersed well in PEBA membrane because the polymer segments are amphiphilic.

In the present study, to enhance the PV performance of PEBA membrane, ZSM-5 filled PEBA membranes, PEBA/ZSM-5, were prepared, and their PV performance with different ZSM-5 loading, feed concentration, and temperature for recovering EA from aqueous solution was investigated. Furthermore, the PV performances with the increase of ZSM-5 loading were discussed from the viewpoint of the chemical and physical structures of PEBA/ZSM-5 membranes.

2. Experimental

2.1. Materials. Polyether block amide (PEBA) 2533 was obtained from Arkema Co. Ltd. (France). ZSM-5 zeolite with the average pore size of 0.55 nm was purchased from the Catalyst Plant of Nankai University (Tianjin, China). *n*-Butanol and EA were bought from Sinopharm Chemical Reagent Co. Ltd. (Shanghai, China).

2.2. Membrane Preparation. PEBA and ZSM-5 were accurately weighed and then added to *n*-butanol and transferred to a flask at 80°C with mechanical stirring for 4 h until a homogeneous solution was formed. The obtained solution was cast on a tetrafluoroethylene plate with a dry scraper. The solutions with ZSM-5 loading of 0, 5, 10, 20, and 40 wt% (the weight ratio of ZSM-5 to PEBA) were evaporated at room temperature for 24 h in the air. The formed membranes were designated as PEBA, PEBA/ZSM-5-5, PEBA/ZSM-5-10, PEBA/ZSM-5-20, and PEBA/ZSM-5-40, respectively.

2.3. FT-IR Measurement. The samples of ZSM-5, PEBA, PEBA/ZSM-5-10, and PEBA/ZSM-5-40 for FT-IR measurement were prepared by painting a thin layer of casting solution on a potassium bromide flake and evaporated the solvent at room temperature. Then, the samples were characterized by a FTLA2000-type Fourier transform infrared (FT-IR) spectrometer.

2.4. TGA Measurement. Thermal stability of ZSM-5, PEBA, PEBA/ZSM-5-10, and PEBA/ZSM-5-40 was examined with a METTLER 1/1100SF Thermogravimetric Analyzer (TGA) from 30°C to 800°C with a heating rate of 10°C/min and a nitrogen flow of 50 mL/min.

2.5. Scanning Electron Microscopy. Scanning electron micrographs of ZSM-5, PEBA, PEBA/ZSM-5-10, and PEBA/ZSM-5-40 were performed on a Hitachi S4800 scanning electron microscope (SEM) instrument. All the samples were coated with a thin layer of gold to prevent charging.

2.6. Mechanical Properties Studies. Tensile tests on the membranes of PEBA, PEBA/ZSM-5-5, PEBA/ZSM-5-10, PEBA/ZSM-5-20, and PEBA/ZSM-5-40 were carried out at room temperature using an electronic universal testing machine (Shenzhen, China) with a crosshead speed of 30 mm/min. The width and length of the sample were 10 mm and 50 mm. The membranes were evaluated by two parameters as shown in the following equations:

$$\sigma = \frac{F}{bd}, \qquad E = \frac{\sigma}{\Delta L/L}, \tag{1}$$

where σ is the tensile stress, F is the maximum load, b, and d represent the width and thickness of the samples, respectively. E represents young's modulus, and ΔL and L are the extension and the original length.

2.7. Static Contact Angle Measurement. Static contact angles for water of PEBA/ZSM-5 membranes were measured by sessile drop method [39] using a contact angle meter (OCA 20, Dataphysics Instruments GmbH Germany) at 25°C and about 65% relative humidity. The volume of the water drop used was always 2 mL. All reported values were the average of at least eight measurements taken at different locations of the film surface and had a typical mean error of 1°.

2.8. Degree of Swelling Measurement. The dried PEBA/ZSM-5 membranes were immersed in different concentration of EA aqueous solution at 30°C at the same time, respectively. At regular intervals, the swollen membranes were wiped out carefully with tissue paper to remove superficial liquid and weighted in a tightly closed bottle. The degree of swelling (DS)

of the membrane was then determined from the following equation:

$$\mathrm{DS} = \frac{m_s - m_o}{m_o} \times 100\%, \quad (2)$$

where m_o and m_s are the weights of dry and swollen membranes, respectively.

2.9. Determination of Diffusion Coefficient. The diffusion coefficient was estimated to describe the diffusion behavior of the system. The diffusion coefficient of component i was calculated from (3) as previously reported by Ma et al. [40] and evolved from Fick's law of (4) when assuming that the concentration profile along the diffusion length x is linear:

$$D_i = \frac{J_i \delta}{C_i}, \quad (3)$$

$$J_i = -D_i \frac{dC_i}{dx}, \quad (4)$$

where D_i represents concentration-averaged diffusion coefficient of component i (m^2/s), J_i is the flux of component i, C_i is the concentration (kg/m^3), δ is the membrane thickness, and x is the diffusion length (m).

2.10. PV Experiments. The PV experiment setup and procedure were the same as those described previously [41]. The membrane was installed in the testing cell, and the effective area was 35.24 cm^2. The feed solution was continuously circulated from a feed tank to the upstream side of the membrane by a pump. The downstream pressure was kept at 200 ± 10 kPa, and the penetrant was collected in a cold trap. The compositions of the feed and the penetrant were measured using GC900 gas chromatography equipped with a thermal conductivity detector (TCD). The permeation flux (J) and the separation factor (α) for all membranes were calculated according to the following equation:

$$J = \frac{Q}{At},$$
$$\alpha_{\mathrm{EA/water}} = \frac{Y_{\mathrm{EA}}/Y_{\mathrm{water}}}{X_{\mathrm{EA}}/X_{\mathrm{water}}}, \quad (5)$$

where Q is the weight of permeate collected in time t, and A is the effective membrane area, and X and Y represent the mass fractions of the organic in the feed and permeate, respectively.

3. Results and Discussion

3.1. Membrane Characterization

3.1.1. FT-IR Analysis. Figure 1 shows the FT-IR spectra of ZSM-5, PEBA, PEBA/ZSM-5-10, and PEBA/ZSM-5-40. As shown from the spectra of ZSM-5 in Figure 1(a), a distinct absorption band appeared at around 1100 cm^{-1} assigning to Si–O. The peak at around 800 cm^{-1} represented the stretching vibrations of Al–O, which was weaker than that of Si–O due to the fact that the ratio of Si/Al was high. In Figure 1(b), the adsorptions observed at 3302 cm^{-1} and 1680 cm^{-1} correspond to the stretching vibration peak of NH, C=O indicating the presence of a polyamide group. The peak located at 1300 cm^{-1} was the stretching vibration of C–O corresponding to polyether groups. As can be seen from Figures 1(c) and 1(d), after the addition of ZSM-5 particles, no new absorption peak could be observed except for Si–O peak, suggesting that ZSM-5 particles were physically blended within the polymer matrix.

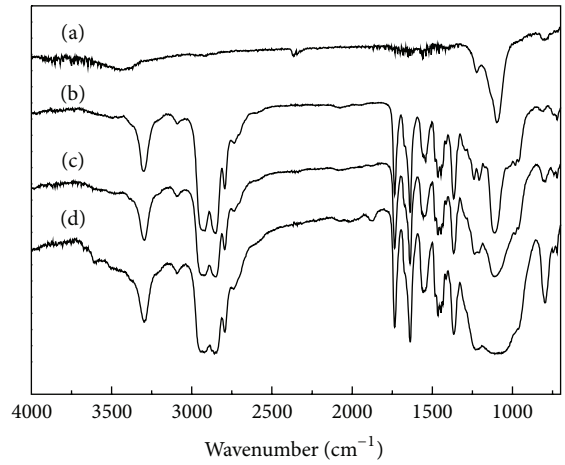

Figure 1: FT-IR spectra of (a) ZSM-5, (b) PEBA, (c) PEBA/ZSM-5-10, and (d) PEBA/ZSM-5-40.

3.1.2. TGA Analysis. The thermal decomposition curves of PEBA/ZSM-5 membranes were shown in Figure 2. In Figure 2(a), the ZSM-5 had an obvious thermal weight loss from 30°C to 200°C, mainly due to the loss of water molecules attached to the ZSM-5. Besides, the ZSM-5 presented a total weight loss about 3% from 30°C to 800°C, indicating that the ZSM-5 was stable at high temperature. It could be seen from Figure 2(b) that PEBA, PEBA/ZSM-5-10, and PEBA/ZSM-5-40 had an apparent thermogravimetric interval. Below 300°C, the sample presented a thermal weight loss at around 2%, mainly due to the loss of crystal water and solvent volatilization, while the membrane itself was stable without thermal decomposition. From 300°C to 500°C, the hot weight loss of the PEBA, PEBA/ZSM-5-10, and PEBA/ZSM-5-40 was 95.4%, 87.0%, and 67.9%, respectively. That means that the weight loss of PEBA, PEBA/ZSM-5-10, and PEBA/ZSM-5-40 membrane decreased and the decomposition temperature increased with the increasing loading of ZSM-5, indicating that the incorporation of ZSM-5 improved the thermal stability of PEBA/ZSM-5 membranes.

3.1.3. SEM Analysis. Figure 3 showed the scanning electron micrographs of ZSM-5 particles and the cross-section of PEBA, PEBA/ZSM-5-10, and PEBA/ZSM-5-40 membranes. As can be seen from Figure 3(a), ZSM-5 zeolite as a rectangular parallelepiped block particles was about 3~5 μm.

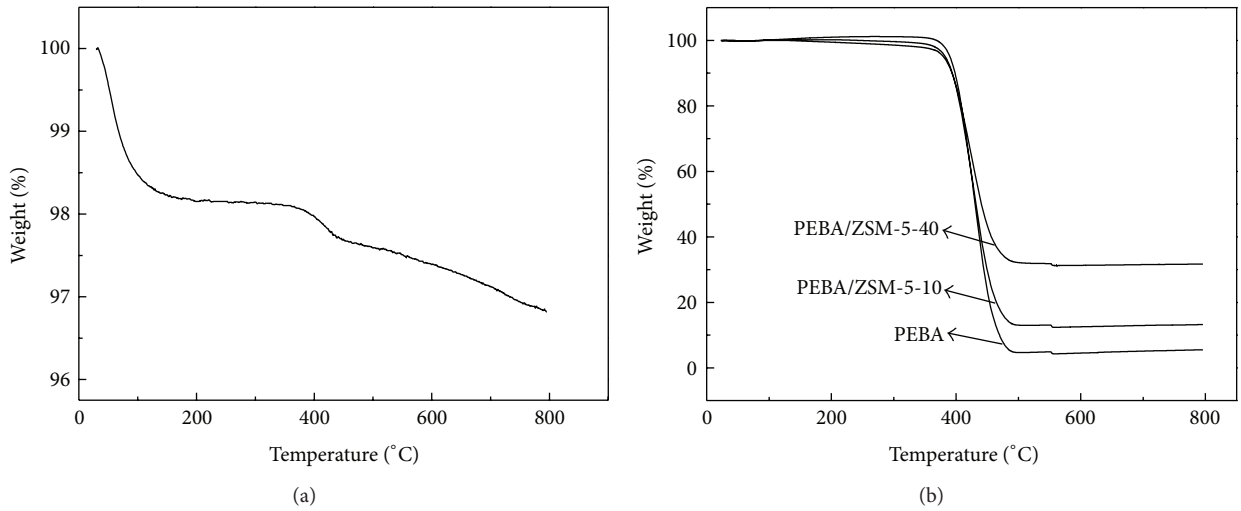

Figure 2: TGA plots of (a) ZSM-5 and (b) PEBA/ZSM-5.

From Figure 3(b) to Figure 3(f), no appreciable pore could be observed, indicating that defect-free dense membrane was synthesized. It could be seen from Figure 3(c) to Figure 3(f) that ZSM-5 particles were uniformly dispersed in the membrane matrix.

3.1.4. Mechanical Properties. Figure 4 described the effect of ZSM-5 content on the mechanical properties of PEBA/ZSM-5 membranes. From Figure 4, the tensile strength of PEBA/ZSM-5 membranes, which is the maximum stress value of uniform plastic deformation of material under tensile stress, decreased with the increase of ZSM-5 loading because the addition of inorganic particles reduced the elasticity of membrane. As shown in Figure 4, the Young's modulus of PEBA/ZSM-5 membranes, which is a physical quantity to describe the solid material to resist deformation, increased correspondingly with the increase of ZSM-5 loading due to the increased rigidity of PEBA/ZSM-5 chains.

3.1.5. Contact Angle. Figure 5 shows the effect of ZSM-5 loading on the contact angle for water of PEBA/ZSM-5 membranes. As can be seen from Figure 5, the contact angle for water of PEBA/ZSM-5 membranes increased with the increase of ZSM-5 loading. Obviously, the hydrophobicity of PEBA/ZSM-5 membranes was enhanced with the increase of ZSM-5 loading because that the zeolite ZSM-5 shows good hydrophobicity. But after the amount of ZSM-5 is up to 40%, the hydrophobicity of PEBA/ZSM-5 membranes substantially keeps constant with the increase of ZSM-5 loading, that means that the surface of PEBA membrane has a certain capacity of ZSM-5, and ZSM-5 will enter the interior of the membrane when the amount of ZSM-5 is increased to a certain degree.

3.2. Effect of ZSM-5 Loading on Membrane Swelling. The equilibrium DS values of PEBA/ZSM-5 membranes in pure water, pure EA, and EA/water mixtures with different EA concentration at 30°C were shown in Figure 6. It could be seen that the DS values of PEBA/ZSM-5 membranes decreased in pure EA and EA aqueous solutions, while nearly unchanged in pure water, with the increase of ZSM-5 loading. It may be explained that the incorporation of ZSM-5 decreased the mobility of the PEBA chains and blocked the free movement of EA and water molecular into PEBA/ZSM-5 membranes. From Figure 6, it could also be seen that the DS values of PEBA/ZSM-5 membranes increased with the increase of EA concentration, suggesting that the PEBA/ZSM-5 membranes had preferential selective adsorption for EA.

3.3. Effect of ZSM-5 Loading on PV Performance of PEBA/ZSM-5 Membranes. Figure 7 shows the variation of separation factor and permeation flux as a function of ZSM-5 loading in the PEBA/ZSM-5 membranes with 5 wt% of EA in feed at 30°C. As shown in Figure 7, the flux decreased initially and then increased with the increase of ZSM-5 loading, and when the ZSM-5 loading was 10 wt%, the flux reached the lowest value, while the separation factor increased initially and then decreased with the increase of ZSM-5 loading, and when the ZSM-5 loading was 10 wt%, the separation factor was the highest. The increase of separation factor of PEBA/ZSM-5 membranes with the increase of ZSM-5 loading from 0 to 10 wt% is mainly due to the increasing hydrophobicity of membrane after adding ZSM-5. But when ZSM-5 loading was more than 10 wt%, the separation factor began to decrease as it could be attributed to the aggregation of ZSM-5 particles and the increasing defect between polymer chains and ZSM-5 which allowed EA and water to permeate simultaneously.

3.4. Effect of Feed Concentration on PV Performance of PEBA/ZSM-5-10 Membrane. The effect of feed concentration on PV performance of PEBA/ZSM-5-10 membrane was studied at 30°C. The relationship among the permeation flux

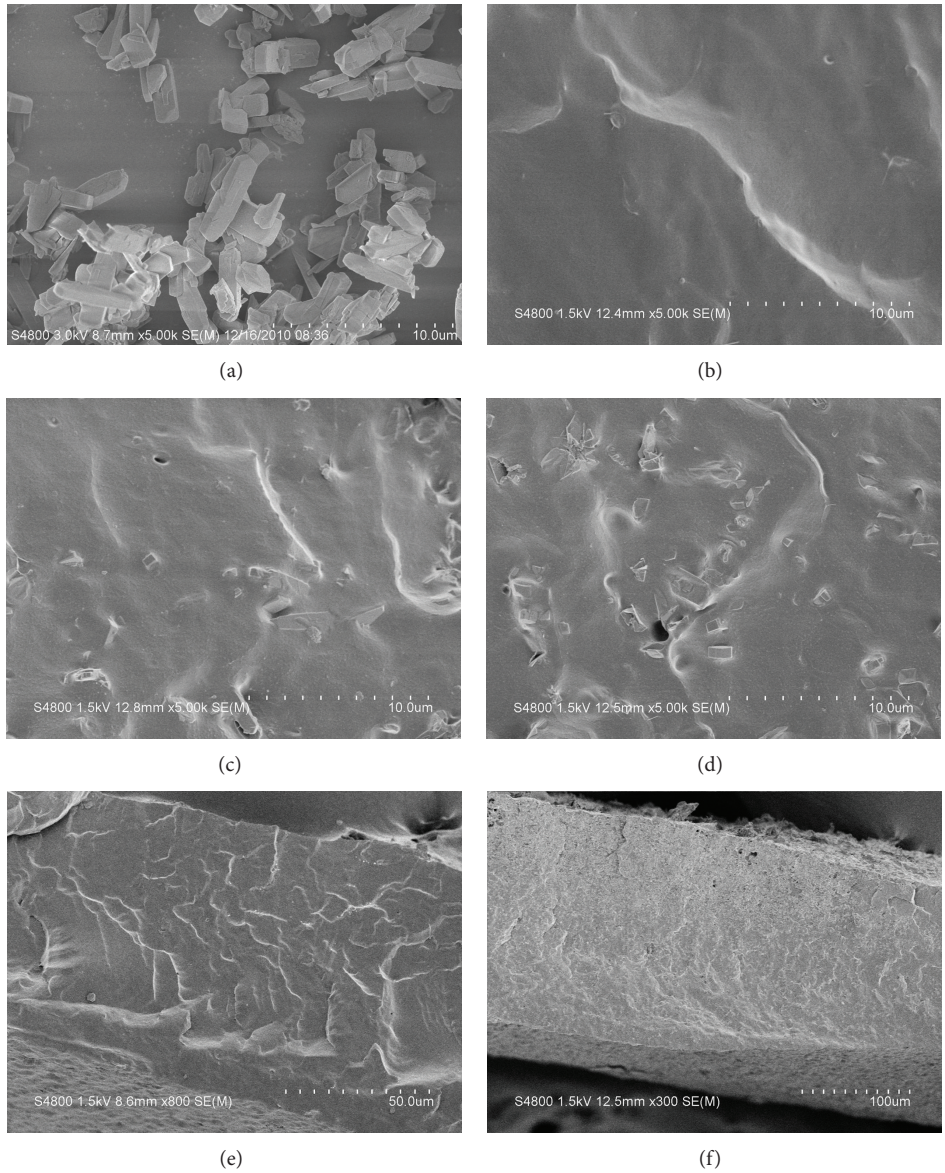

Figure 3: SEM images of ZSM-5 particles and the cross-section of membranes, (a) ZSM-5 particles, (b) pure PEBA, (c) PEBA/ZSM-5-10 (d) PEBA/ZSM-5-40, and (e) and (f) are the whole cross-sectional images of PEBA and PEBA/ZSM-5-40 membrane, respectively.

and liquid and vapor phase concentrations follows (6) for recovery of VOC from aqueous solution [42]:

$$J_i = K_i \rho \left[(C_i)^L - (C_i)^V \right], \quad (6)$$

where K_i (m/s), q (mol/m^3), $(C_i)^L$ (dimensionless), and $(C_i)^V$ (dimensionless) are the overall mass transfer rate coefficient, total molar density of feed, bulk liquid phase concentration (mole fraction), and bulk vapor phase concentration (mole fraction, reported as an equivalent liquid phase mole fraction), respectively, for component i. The increase of feed concentration is nearly equal to the increase of the driving force $(C_i)^L$ because $(C_i)^V$ is usually small and can be neglected. Therefore, the permeation flux increased usually with an increase of feed concentration. In this study, water flux decreased slightly from 59.58 to 26.26 g/m^2 h, and EA flux increased from 41.87 to 140.8 g/m^2 h when the feed concentration increased from 1 to 5 wt% as can be seen from Figure 8(b). This is because the driving force of EA was enhanced and that of water nearly depressed or unchanged with the increase of feed concentration. Uragami et al. [43] proved that organic molecules mainly permeated through the hydrophobic phase of a polymer membrane containing microphase structure, while water molecules mainly permeated through hydrophilic matrix. For PEBA membranes, the hydrophobic and prevalent polyether segments formed the main matrix of the whole membrane, and the low content of polar hard segments was dispersed evenly in the polyether matrix. The soft segments of polyether, which have the strong affinity to EA, provide a path for the permeation of EA.

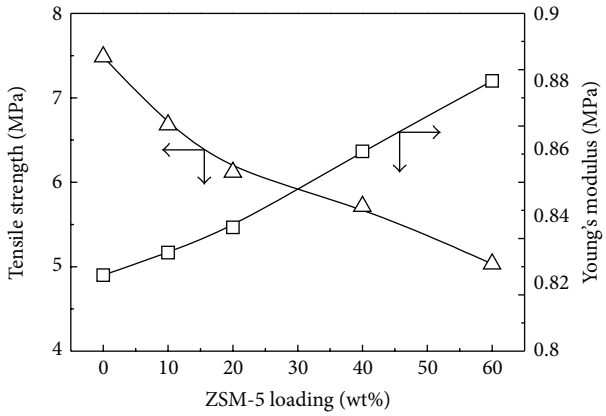

Figure 4: Tensile strength and Young's modulus of PEBA/ZSM-5 membranes with different ZSM-5 loading.

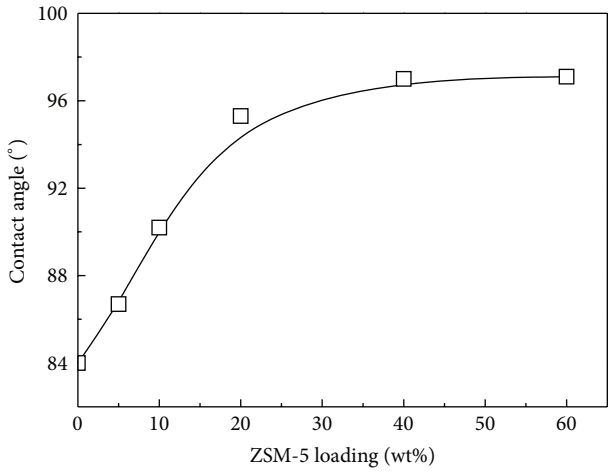

Figure 5: Effect of ZSM-5 loading on the contact angle of PEBA/ZSM-5 membranes.

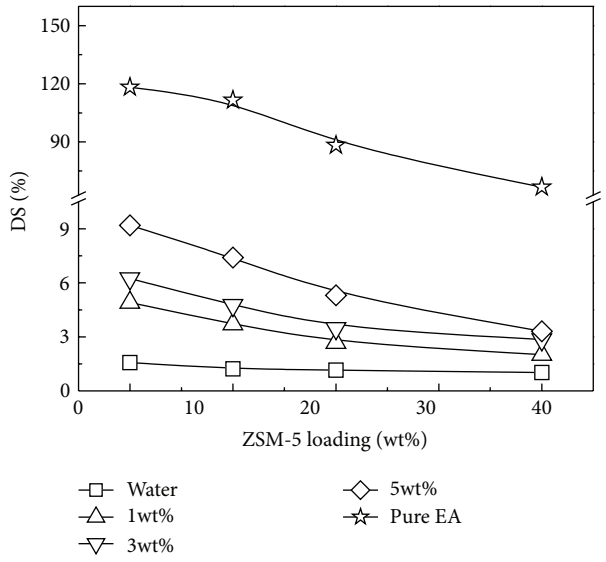

Figure 6: Effect of ZSM-5 loading and feed concentration on the equilibrium DS of PEBA/ZSM-5 membranes at 30°C.

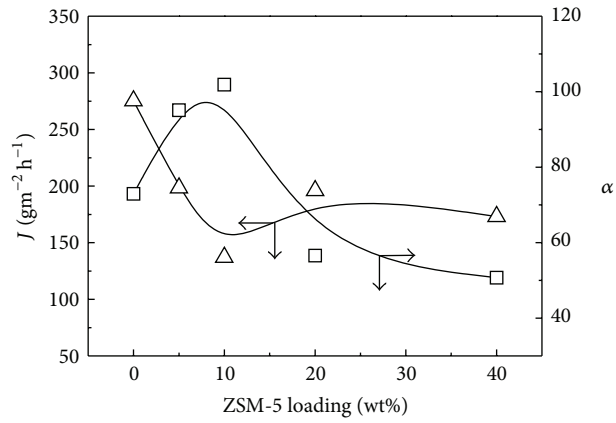

Figure 7: Effect of ZSM-5 loading on PV performance of PEBA/ZSM-5 membranes: separation factor and permeation flux (EA concentration in feed, 5 wt%, feed temperature, 30°C).

But the diffusion of water became very difficult because the low content of hard and polar segments of polyamide could not form a continuous phase in the PEBA membrane. In addition, in the studied feed concentration range, the mild DS of PEBA/ZSM-5-10 membrane, from 3.7% to 7.4% seen from Figure 6, will also be resistant to water permeation.

3.5. Effect of Operating Temperature on PV Performance of PEBA/ZSM-5-10 Membrane. Figure 9 shows the variation of the separation factor α and total flux of PEBA/ZSM-5-10 membrane with feed temperature. From Figure 9, it can be seen that both α and total flux increased with the increase of the feed temperature below 50°C. Commonly, the separation factor decreases with the increase of feed temperature in PV process. This anomalous phenomenon can be explained that the mass transfer driving force through the membrane increased at a higher temperature and the activity of the polymer chains increased, so the resistance of penetration component in the membrane was reduced. This could result in the increase of the total flux and the EA flux. Therefore, the separation factor increased. But when the temperature is higher than 50°C, the increasing swelling allowed EA and water to permeate simultaneously, resulting in the decrease of the separation factor. Generally, the relationship among the permeation flux and the operating temperature for recovery of VOC from aqueous solution follows the Arrhenius relationship, as shown in the following equation:

$$J_i = J_o \exp\left(\frac{-E_a}{\mathrm{RT}}\right), \tag{7}$$

where J_i is the flux ($\mathrm{gm^{-2}\,h^{-1}}$) of the component i, J_o is a constant ($\mathrm{gm^{-2}\,h^{-1}}$), E_a is the activation energy ($\mathrm{Jmol^{-1}}$), R is the gas constant ($\mathrm{Jmol^{-1}\,K^{-1}}$), and T is the absolute temperature (K).

Figure 10 shows the Arrhenius relationship between the flux and permeation activation energy. From Figure 10, the permeation activation energy of EA ($E_{a\mathrm{EA}}$ = 19.74 kJ/mol)

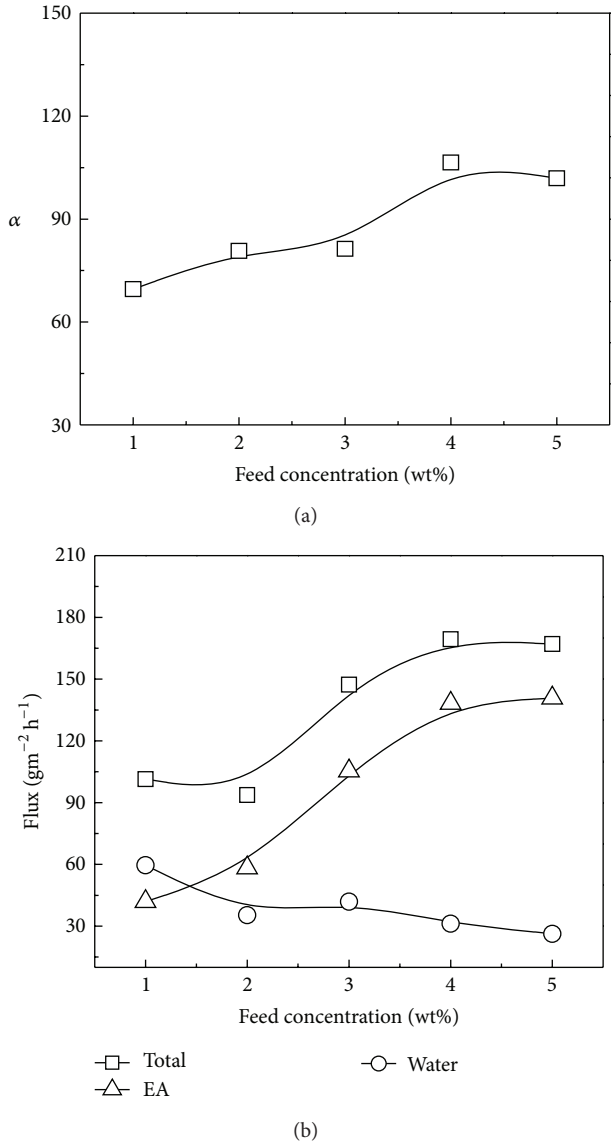

Figure 8: Effect of feed concentration on PV performance of PEBA/ZSM-5-10 membrane at 30°C: (a) separation factor and (b) permeation flux.

was higher than that of water ($E_{a\text{water}}$ = 7.62 kJ/mol) for the PEBA/ZSM-5-10 membrane. The value of the activation energy reflects the sensitivity of permeate flux to temperature. The larger permeation activation energy of EA implies that EA permeation flux is more sensitive to the increase of temperature compared to that of water. Consequently, the permeate flux of EA increased greater than the water molecules with the increase of temperature, which is corresponding to the increased separation factor. But when the temperature is higher than 50°C, EA and water pass through the membrane at the same time due to the intensification of the segment movement, so the separation factor decreased.

3.6. Diffusion Coefficient. The average diffusion coefficient of EA and water through the PEBA/ZSM-5-10 membrane in the feed concentration of 5 wt% at 30°C calculated by (3), the results are shown in Table 1. Overall, the diffusion coefficient of EA is 100 times higher than that of water molecules which implies that the membrane material is conducive to the diffusion of the EA.

Table 1: Diffusion coefficients of EA and water through PEBA/ZSM-5 membranes with different ZSM-5 loading.

	ZSM-5 loading (wt%)				
	0	5	10	20	40
D_{EA} (10^{10} m^2 s^{-1})	2.16	1.99	1.18	1.56	1.33
D_{water} (10^{12} m^2 s^{-1})	2.98	2.09	1.16	2.77	2.56

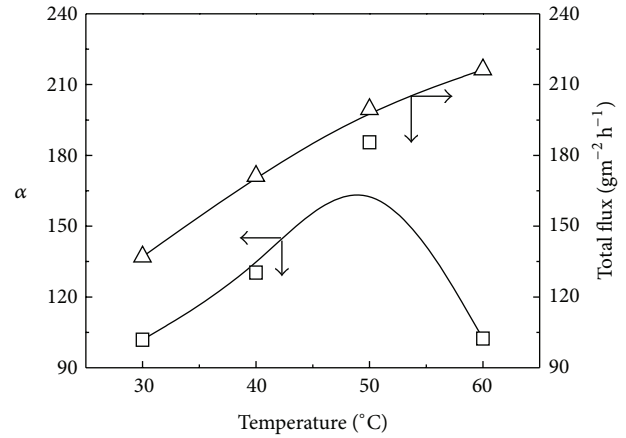

Figure 9: Effect of operating temperature on PV performance of PEBA-ZSM-5-10 membrane: separation factor and permeation flux (EA concentration in feed, 5 wt%).

3.7. PV Performance for Separating EA/Water Mixtures with the Literatures. Table 2 compares the PV performance for separating EA/water mixtures with the literatures. The PEBA/ZSM-5-10 membrane in this study exhibited the highest EA normalized flux (defined as the EA flux multiplied by the membrane thickness) though the separation factor is not outstanding enough compared to other membrane materials.

4. Conclusions

Defect-free ZSM-5 filled polyether block amide membranes, PEBA/ZSM-5, were prepared for the separation of EA from its aqueous solutions by pervaporation. The chemical structure, morphology, and thermal stability of these filled membranes were characterized. It could be seen that ZSM-5 dispersed uniformly in the membrane. With the incorporation of ZSM-5 in the membrane, the thermal stability of the membrane increased, while the swelling degree decreased. The separation factor increased first and then decreased with the increase of the ZSM-5 loading. The diffusion coefficient of EA was much larger than that of water for the PEBA/ZSM-5 membranes, indicating that the membranes were highly

Table 2: Comparison of PV results of PEBA/ZSM-5-10 membrane for EA/water mixture with the literatures.

Ref.	Membrane	W (EA)/%	T (°C)	J (kg μm/m^2·h)	α (EA/water)
[13]	PDMS-1070	0.05	50	3.5	524
[14]	PDMS/PTFE	0.99	30	6.7	95
[16]	Cross-linked polyurethaneurea	2.5	30	25	655
[17]	P(VDF-co-HFP)	5	30	28	175
[18]	EVA-38	2.5	30	11	118
[19]	PEBA	8.3	30	26	73
This work	PEBA/ZSM-5-10	5	30	40	102

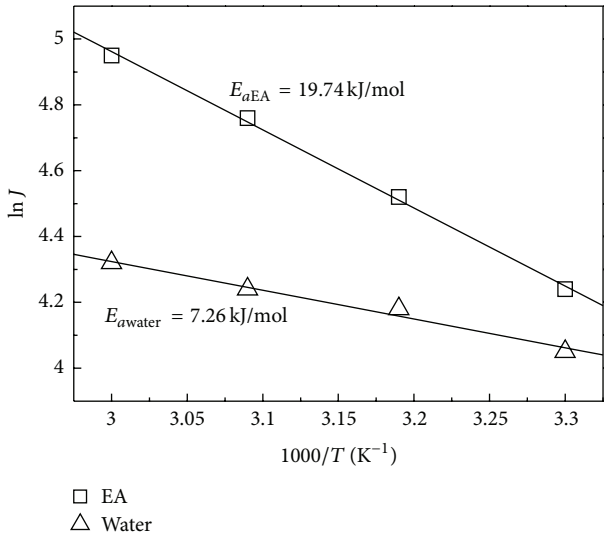

Figure 10: Arrhenius plots of PEBA/ZSM-5-10 membrane.

EA permselective. The PEBA/ZSM-5 membranes containing 10 wt% ZSM-5, that is, PEBA/ZSM-5-10, showed the highest separation factor at 30°C. With the increase of the operating temperature and feed concentration, both the permeation flux and separation factor increased except when the temperature exceeded 50°C. The best PV performance, separation factor, and total flux of the PEBA/ZSM-5 membranes containing 10 wt% ZSM-5 were 185.5 and 199.5 gm^{-2} h^{-1}, respectively, with feed concentration of 5 wt% EA at 50°C.

Conflict of Interests

"Arkema Co. Ltd." and "Sinopharm Chemical Reagent Co. Ltd." are two companies from wich the authors purchased chemical reagents. There is no conflict of interest in this paper.

Acknowledgments

This research was financially supported by the National Natural Science Foundation of China (Grant no. 21106053), the Fundamental Research Funds for the Central Universities (JUSRP3l1A01), and the Industry-Academia Cooperation Innovation Fund Projects of Jiangsu Province (BY2012058).

References

[1] H. K. Yuan, J. Ren, X. H. Ma, and Z. L. Xu, "Dehydration of ethyl acetate aqueous solution by pervaporation using PVA/PAN hollow fiber composite membrane," *Desalination*, vol. 280, no. 1–3, pp. 252–258, 2011.

[2] E. Y. Kenig, H. Bäder, A. Górak, B. Beßling, T. Adrian, and H. Schoenmakers, "Investigation of ethyl acetate reactive distillation process," *Chemical Engineering Science*, vol. 56, no. 21-22, pp. 6185–6193, 2001.

[3] Y. T. Tang, Y. W. Chen, H. P. Huang, C. C. Yu, S. B. Hung, and M. J. Lee, "Design of reactive distillations for acetic acid esterification," *AIChE Journal*, vol. 51, no. 6, pp. 1683–1699, 2005.

[4] S. G. Adoor, L. S. Manjeshwar, S. D. Bhat, and T. M. Aminabhavi, "Aluminum-rich zeolite beta incorporated sodium alginate mixed matrix membranes for pervaporation dehydration and esterification of ethanol and acetic acid," *Journal of Membrane Science*, vol. 318, no. 1-2, pp. 233–246, 2008.

[5] S. D. Bhat and T. M. Aminabhavi, "Pervaporation-aided dehydration and esterification of acetic acid with ethanol using 4A zeolite-filled cross-linked sodium alginate-mixed matrix membranes," *Journal of Applied Polymer Science*, vol. 113, no. 1, pp. 157–168, 2009.

[6] D. H. Park, N. Nishiyama, Y. Egashira, and K. Ueyama, "Separation of organic/water mixtures with silylated MCM-48 silica membranes," *Microporous and Mesoporous Materials*, vol. 66, no. 1, pp. 69–76, 2003.

[7] S. Araki, S. Imasaka, S. Tanaka, and Y. Miyake, "Pervaporation of organic/water mixtures with hydrophobic silica membranes functionalized by phenyl groups," *Journal of Membrane Science*, vol. 380, no. 1-2, pp. 41–47, 2011.

[8] P. Shao and R. Y. M. Huang, "Polymeric membrane pervaporation," *Journal of Membrane Science*, vol. 287, no. 2, pp. 162–179, 2007.

[9] D. Anjali Devi, K. V. S. N. Raju, and T. M. Aminabhavi, "Synthesis and characterization of moisture-cured polyurethane membranes and their applications in pervaporation separation of ethyl acetate/water azeotrope at 30°C," *Journal of Applied Polymer Science*, vol. 103, no. 5, pp. 3405–3414, 2007.

[10] A. Aroujalian and A. Raisi, "Recovery of volatile aroma components from orange juice by pervaporation," *Journal of Membrane Science*, vol. 303, no. 1-2, pp. 154–161, 2007.

[11] V. García, N. Diban, D. Gorri, R. Keiski, A. Urtiaga, and I. Ortiz, "Separation and concentration of bilberry impact aroma compound from dilute model solution by pervaporation," *Journal of Chemical Technology and Biotechnology*, vol. 83, no. 7, pp. 973–982, 2008.

[12] A. Isci, S. Sahin, and G. Sumnu, "Recovery of strawberry aroma compounds by pervaporation," *Journal of Food Engineering*, vol. 75, no. 1, pp. 36–42, 2006.

[13] A. Baudot and M. Marin, "Improved recovery of an ester flavor compound by pervaporation coupled with a flash condensation," *Industrial and Engineering Chemistry Research*, vol. 38, no. 11, pp. 4458–4469, 1999.

[14] W. D. Zhang, W. Sun, J. Yang, and Z. Q. Ren, "The study on pervaporation behaviors of dilute organic solution through PDMS/PTFE composite membrane," *Applied Biochemistry and Biotechnology*, vol. 160, no. 1, pp. 156–167, 2010.

[15] Y. X. Bai, J. W. Qian, J. Yin, Z. B. Zhai, and Y. Yang, "HTPB-based polyurethaneurea membranes for recovery of aroma compounds from aqueous solution by pervaporation," *Journal of Applied Polymer Science*, vol. 104, no. 1, pp. 552–559, 2007.

[16] Y. Bai, J. Qian, C. Zhang, L. Zhang, Q. An, and H. Chen, "Cross-linked HTPB-based polyurethaneurea membranes for recovery of ethyl acetate from aqueous solution by pervaporation," *Journal of Membrane Science*, vol. 325, no. 2, pp. 932–939, 2008.

[17] B. K. Zhu, X. Z. Tian, and Y. Y. Xu, "Recovering ethyl acetate from aqueous solution using P(VDF-co-HFP) membrane based pervaporation," *Desalination*, vol. 184, no. 1–3, pp. 71–78, 2005.

[18] Y. Bai, J. Qian, Q. An, Z. Zhu, and P. Zhang, "Pervaporation characteristics of ethylene-vinyl acetate copolymer membranes with different composition for recovery of ethyl acetate from aqueous solution," *Journal of Membrane Science*, vol. 305, no. 1-2, pp. 152–159, 2007.

[19] M. K. Djebbar, Q. T. Nguyen, R. Clément, and Y. Germain, "Pervaporation of aqueous ester solutions through hydrophobic poly(ether-block-amide) copolymer membranes," *Journal of Membrane Science*, vol. 146, no. 1, pp. 125–133, 1998.

[20] R. Jiraratananon, P. Sampranpiboon, D. Uttapap, and R. Y. M. Huang, "Pervaporation separation and mass transport of ethylbutanoate solution by polyether block amide (PEBA) membranes," *Journal of Membrane Science*, vol. 210, no. 2, pp. 389–409, 2002.

[21] P. Sampranpiboon, R. Jiraratananon, D. Uttapap, X. Feng, and R. Y. M. Huang, "Pervaporation separation of ethyl butyrate and isopropanol with polyether block amide (PEBA) membranes," *Journal of Membrane Science*, vol. 173, no. 1, pp. 53–59, 2000.

[22] S. D. Bhat and T. M. Aminabhavi, "Novel sodium alginate composite membranes incorporated with SBA-15 molecular sieves for the pervaporation dehydration of aqueous mixtures of isopropanol and 1,4-dioxane at 30°C," *Microporous and Mesoporous Materials*, vol. 91, no. 1–3, pp. 206–214, 2006.

[23] S. D. Bhat, B. V. K. Naidu, G. V. Shanbhag, S. B. Halligudi, M. Sairam, and T. M. Aminabhavi, "Mesoporous molecular sieve (MCM-41)-filled sodium alginate hybrid nanocomposite membranes for pervaporation separation of water-isopropanol mixtures," *Separation and Purification Technology*, vol. 49, no. 1, pp. 56–63, 2006.

[24] B. V. K. Naidu, S. D. Bhat, M. Sairam et al., "Comparison of the pervaporation separation of a water-acetonitrile mixture with zeolite-filled sodium alginate and poly(vinyl alcohol)-polyaniline semi-interpenetrating polymer network membranes," *Journal of Applied Polymer Science*, vol. 96, no. 5, pp. 1968–1978, 2005.

[25] S. D. Bhat and T. M. Aminabhavi, "Zeolite K-LTL-loaded sodium alginate mixed matrix membranes for pervaporation dehydration of aqueous-organic mixtures," *Journal of Membrane Science*, vol. 306, no. 1-2, pp. 173–185, 2007.

[26] A. A. Kittur, S. K. Choudhari, and M. Y. Kariduraganavar, "Preparation of zeolite-incorporated PDMS membranes for pervaporation separation of isopropanol-water mixtures," *Composite Interfaces*, vol. 13, no. 4-6, pp. 507–521, 2006.

[27] L. M. Vane, V. V. Namboodiri, and T. C. Bowen, "Hydrophobic zeolite-silicone rubber mixed matrix membranes for ethanol-water separation: effect of zeolite and silicone component selection on pervaporation performance," *Journal of Membrane Science*, vol. 308, no. 1-2, pp. 230–241, 2008.

[28] M. D. Jia, K. V. Peinemann, and R. D. Behling, "Preparation and characterization of thin-film zeolite-PDMS composite membranes," *Journal of Membrane Science*, vol. 73, no. 2-3, pp. 119–128, 1992.

[29] I. F. J. Vankelecom, D. Depre, S. De Beukelaer, and J. B. Uytterhoeven, "Influence of zeolites in PDMS membranes. Pervaporation of water/alcohol mixtures," *The Journal of Physical Chemistry*, vol. 99, no. 35, pp. 13193–13197, 1995.

[30] H. Yang, Q. T. Nguyen, Z. Ping, Y. Long, and Y. Hirata, "Desorption and pervaporation properties of zeolite-filled poly(dimethylsiloxane) membranes," *Materials Research Innovations*, vol. 5, no. 2, pp. 101–106, 2001.

[31] S. Y. Lu, C. P. Chiu, and H. Y. Huang, "Pervaporation of acetic acid/water mixtures through silicalite filled polydimethylsiloxane membranes," *Journal of Membrane Science*, vol. 176, no. 2, pp. 159–167, 2000.

[32] C. Dotremont, B. Brabants, K. Geeroms, J. Mewis, and C. Vandecasteele, "Sorption and diffusion of chlorinated hydrocarbons in silicalite-filled PDMS membranes," *Journal of Membrane Science*, vol. 104, no. 1-2, pp. 109–117, 1995.

[33] M. V. Chandak, Y. S. Lin, W. Ji, and R. J. Higgins, "Sorption and diffusion of VOCs in DAY zeolite and silicalite-filled PDMS membranes," *Journal of Membrane Science*, vol. 133, no. 2, pp. 231–243, 1997.

[34] E. A. Fouad and X. Feng, "Pervaporative separation of n-butanol from dilute aqueous solutions using silicalite-filled poly (dimethyl siloxane) membranes," *Journal of Membrane Science*, vol. 339, no. 1-2, pp. 120–125, 2009.

[35] A. Dobrak, A. Figoli, S. Chovau et al., "Performance of PDMS membranes in pervaporation: effect of silicalite fillers and comparison with SBS membranes," *Journal of Colloid and Interface Science*, vol. 346, no. 1, pp. 254–264, 2010.

[36] D. Panek and K. Konieczny, "Preparation and applying the membranes with carbon black to pervaporation of toluene from the diluted aqueous solutions," *Separation and Purification Technology*, vol. 57, no. 3, pp. 507–512, 2007.

[37] F. Peng, Z. Jiang, C. Hu, Y. Wang, H. Xu, and J. Liu, "Removing benzene from aqueous solution using CMS-filled PDMS pervaporation membranes," *Separation and Purification Technology*, vol. 48, no. 3, pp. 229–234, 2006.

[38] S. Yi, Y. Su, and Y. Wan, "Preparation and characterization of vinyltriethoxysilane (VTES) modified silicalite-1/PDMS hybrid pervaporation membrane and its application in ethanol separation from dilute aqueous solution," *Journal of Membrane Science*, vol. 360, no. 1-2, pp. 341–351, 2010.

[39] O. N. Tretinnikov, "Selective accumulation of functional groups at the film surfaces of stereoregular poly(methyl methacrylate)s," *Langmuir*, vol. 13, no. 11, pp. 2988–2992, 1997.

[40] X. Ma, C. Hu, R. Guo, X. Fang, H. Wu, and Z. Jiang, "HZSM5-filled cellulose acetate membranes for pervaporation separation of methanol/MTBE mixtures," *Separation and Purification Technology*, vol. 59, no. 1, pp. 34–42, 2008.

[41] C. F. Zhang, L. Yang, Y. X. Bai, J. Gu, and Y. P. Sun, "ZSM-5 filled polyurethaneurea membranes for pervaporation separation isopropyl acetate from aqueous solution," *Separation and Purification Technology*, vol. 85, pp. 8–16, 2012.

[42] G. A. Polotskaya, A. V. Penkova, A. M. Toikka, Z. Pientka, L. Brozova, and M. Bleha, "Transport of small molecules through polyphenylene oxide membranes modified by fullerene," *Separation Science and Technology*, vol. 42, no. 2, pp. 333–347, 2007.

[43] T. Uragami, T. Meotoiwa, and T. Miyata, "Effects of the addition of calixarene to microphase-separated membranes for the removal of volatile organic compounds from dilute aqueous solutions," *Macromolecules*, vol. 34, no. 19, pp. 6806–6811, 2001.

Hindawi Publishing Corporation
International Journal of Polymer Science
Volume 2013, Article ID 529474, 7 pages
http://dx.doi.org/10.1155/2013/529474

Research Article

VTOS Cross-Linked PDMS Membranes for Recovery of Ethanol from Aqueous Solution by Pervaporation

Jin Gu,[1] Yunxiang Bai,[1] Lin Zhang,[2] Lirong Deng,[1] Chunfang Zhang,[1] Yuping Sun,[1] and Huanlin Chen[2]

[1] *The Key Laboratory of Food Colloids and Biotechnology, Ministry of Education, School of Chemical and Material Engineering, Jiangnan University, Wuxi 214122, China*
[2] *Department of Chemical and Biochemical Engineering, Zhejiang University, Hangzhou 310027, China*

Correspondence should be addressed to Yuping Sun; sunyp2003@yahoo.com.cn

Received 25 March 2013; Accepted 7 May 2013

Academic Editor: Hai-Yin Yu

PDMS membranes were prepared by cross-linking with vinyltriethoxysilane (VTOS) on polyacrylonitrile (PAN) substrate to increase hydrophobicity and improve pervaporation (PV) performance. It was shown that the membranes had high ethanol permselectivity and flux. The effects of cross-linking temperature, the content of cross-linking agent, and feed temperature on PV performance of VTOS cross-linked PDMS membranes were investigated. For 6 wt% ethanol aqueous solution, the PDMS membrane had the high separation factor of 15.5 and total flux 573.3 $g \cdot m^{-2} \cdot h^{-1}$, respectively, when the feed temperature was 40°C, H-PDMS : VTOS : DBTDL = 1 : 0.2 : 0.02 and cross-linking temperature was 80°C.

1. Introduction

The production of ethanol as an alternative fossil fuel energy resource has been a subject of great interest so far, because of the uncertainty of petroleum supplies and the finite nature of fossil fuels. Moreover, from the viewpoint of global environmental protection, since the industrial uses of fossil resources go on releasing a large quantity of CO_2 on earth which leads to increasing atmospheric temperature, the production of liquid fuel ethanol by fermentation from renewable biomass as a carbon source has been focused on. For removal of ethanol from water, other separation technologies such as distillation, liquid-liquid extraction, carbon adsorption, and air stripping are not applicable because of feed condition limitations, large volume of byproducts, or high cost of posttreatments. However, pervaporation can be applied without these limitations [1–4]. Pervaporation is a promising separation technique and is becoming recognized as an energy-efficient alternative to distillation and other separating methods for liquid mixtures, especially in cases that the traditional separation techniques are not efficient, such as separating of azeotropic mixtures [5, 6], isomeric components [7], and close-boiling point systems [8]. In addition, it can also offer advantages in energy savings. The success of PV for ethanol-water separation depends on the development of a membrane material that has high permeability, high permselectivity, and good film-forming properties. The polymers that have been used for ethanol permselective membranes include polydimethylsiloxane (PDMS) [9, 10], poly[1-(trimethylsilyl)-1-propyne] (PTMSP) [11, 12], in which PTMSP suffers from unstable PV performance with time. So, PDMS membrane is the most important and promising polymer membrane at present, which has the highest permeability for gas or vapors [13] and a high separation performance for organic chemicals in water [14, 15] among all the industrialized polymers. However, PDMS membrane has an intrinsic disadvantage. PDMS has the properties of poor film-forming and the low selectivity. These disadvantages have been overcome by using cross-linked PDMS [9]. But the preparation of PDMS using tetraethylorthosilicate (TEOS) [16] as a cross-linking agent has insufficient hydrophobicity in traditional methods resulted in poor permeability. In this paper, PDMS membranes were prepared using the cross-linking agent vinyltriethoxysilane (VTOS) and used for separation of

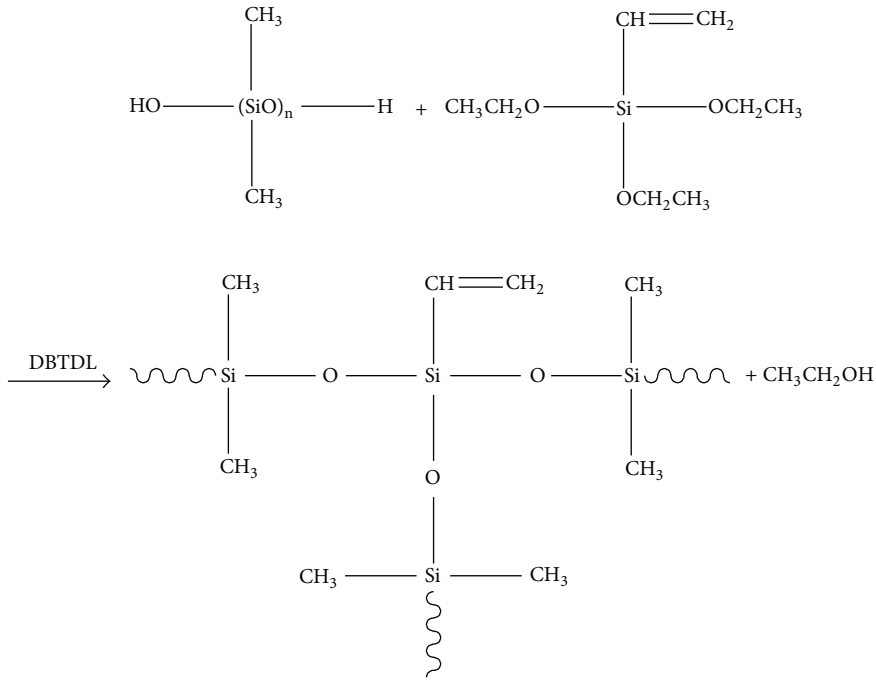

Figure 1: Preparation route of PDMS-VTOS.

ethanol/water mixtures. Due to the introduction of vinyl group, the hydrophobicity and the permeability of the PDMS membranes were increased.

The main objective of this study was to determine the effect of cross-linking temperature on the performance of PDMS membranes. Additionally, several of the parameters listed above were studied to assess their importance for the system.

2. Experimental

2.1. Materials. α,ω,-Dihydroxypolydimethylsiloxane (H-PDMS) with an average molecular weight of 5000 was purchased from Chenguang Research Institute of Chemical Industry, Chengdu, China. Tetraethylorthosilicate (TEOS), triethoxyvinylsilane (VTOS), dibutyltin dilaurate (DBTDL), *n*-hexane, and ethanol were obtained as analytical reagents from Shanghai Chemical Reagent Company, China. Polyacrylonitrile (PAN) ultrafiltration support membrane was purchased from Research and Development Center of Water Treatment Technology, Hangzhou, China.

2.2. Preparation of PDMS-VTOS/PAN Composite Membranes. H-PDMS, cross-linking agent VTOS, and catalyst DBTDL were mixed according to a 10/1/0.2 weight ratio in *n*-hexane. Prior to coating, PAN support was laid and spread out on the surface of water in a basin. Excess water on the PAN support surface was wiped off quickly with a filter paper. Directly afterwards, the PDMS solution was poured on the surface of support and the basin was put under a hood. The membrane system containing some cross-linked PDMS, after kept under ambient temperature for 2 h, was introduced into a vacuum oven at 60°C for 4 h to complete the cross-linking. The chemical scheme was shown in Figure 1.

2.3. FTIR Measurement of PDMS-VTOS Membranes. The chemical structures of H-PDMS, PDMS-VTOS samples were confirmed by Fourier transform infrared (FTIR) using a VECTOR-22 type spectrometer. Samples for FTIR measurements were obtained by spreading a thin film of their solutions in *n*-hexane on a potassium bromide flake and evaporating the solvent under vacuum at room temperature.

2.4. Differential Scanning Calorimetry Measurements. DSC analyses over the temperature range from −150°C to 25°C were conducted on a Perkin-Elmer DSC7 under nitrogen purge at a heating rate of 10°C/min. The DSC curves were obtained from a second heating cycle in order to remove heat history.

2.5. Static Contact Angle Measurement. Static contact angles for water of PDMS-VTOS/PAN composite membranes were measured by the sessile drop method using a Contact Angle Meter (OCA 20, Dataphysics, Germany) at 25°C and about 65% relative humidity. The volume of the water drop used was always 2 μL. All reported values were the average of at least eight measurements taken at different locations of the film surface and had a typical mean error of ±1°.

2.6. Degree of Swelling Measurement. Dried PDMS-VTOS membranes without substrate were weighed and then immersed into an aqueous solution of 6 wt% ethanol in a sealed vessel at 30°C until equilibrium was reached. The membranes were carefully wiped by tissue papers to remove

surface solvent and then weighted to measure the weight of the swollen membrane obtained. The equilibrium degree of swelling (DS) of the membranes was then determined from the following:

$$\mathrm{DS} = \frac{m_S - m_0}{m_0} \times 100\%, \quad (1)$$

where m_0 and m_S are the weights of dry and swollen membranes, respectively.

2.7. Pervaporation Measurement. PV experiments were conducted as previously reported [20]. The vacuum system of the downstream side was maintained at about 180 Pa. The experiments were carried out in a continuous steady state, operated at constant temperature for ethanol/water mixtures. The flow rate was maintained at 2 m/s. Re number is about 10000. The permeation solution was collected in cold traps by condensation with liquid nitrogen. The composition of the permeation solution was determined using gas chromatography. The permeation flux (J) and the separation factor ($\alpha_{\mathrm{sep,ethanol/water}}$) for all membranes were calculated according to the following equations:

$$J = \frac{\Delta g}{A \times \Delta t}, \quad (2)$$

$$\alpha_{\mathrm{sep,ethanol/water}} = \frac{\left(P_{\mathrm{ethanol}}/P_{\mathrm{water}}\right)}{\left(F_{\mathrm{ethanol}}/F_{\mathrm{water}}\right)}, \quad (3)$$

where Δg is the permeation weight collected in cold traps during the operation time Δt, A is the membrane area (18.1 cm^2), F_{ethanol} and F_{water} are the weight fractions of ethanol and water in the feed side, and P_{ethanol} and P_{water} are the weight fractions in the permeate side, respectively.

2.8. Determination of Sorption Selectivity and Diffusion Selectivity. The sorption experiments were carried out as follows. A piece of dried PDMS-VTOS membrane without substrate with determined weight was immersed in anethanol/water mixture with 6 wt% ethanol in a sealed vessel at 30°C until equilibrium was reached. The swollen PDMS-VTOS membrane was wiped with a tissue paper quickly and placed into another container. The solution adsorbed in the swollen membrane was desorbed under reduced pressure and collected in a cold trap. The composition of the solution in the swollen membrane was obtained by measuring the ethanol concentration by gas chromatography in the collected solution. The sorption selectivity, $\alpha_{\mathrm{sorp,ethanol/water}}$, was determined by the ethanol composition in the membrane and the feed solution as expressed as follows:

$$\alpha_{\mathrm{sorp,ethanol/water}} = \frac{\left(M_{\mathrm{ethanol}}/M_{\mathrm{water}}\right)}{\left(F_{\mathrm{ethanol}}/F_{\mathrm{water}}\right)}, \quad (4)$$

where F_{ethanol} and F_{water} are the weight fractions of ethanol and water in the feed and M_{ethanol} and M_{water} are the weight fractions of ethanol and water in the swollen membrane, respectively. According to the solution-diffusion mechanism, separation and permeation characteristics for organic liquid mixtures through polymeric dense membranes by PV are based on the solubility of the permeants into the polymer membrane (sorption process) and the diffusivity of the permeants in the polymer membrane (diffusion process). In general, the relation between them for ethanol/water mixture can be written as follows:

$$\alpha_{\mathrm{diff,ethanol/water}} = \frac{\alpha_{\mathrm{sep,ethanol/water}}}{\alpha_{\mathrm{sorp,ethanol/water}}}. \quad (5)$$

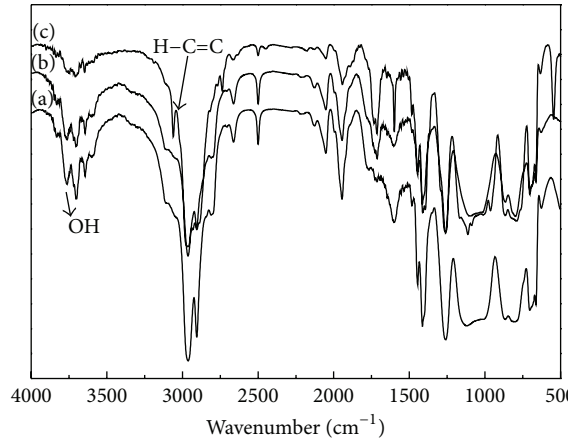

(a) H-PDMS
(b) 20°C PDMS-VTOS
(c) 80°C PDMS-VTOS

Figure 2: FTIR spectra of H-PDMS are 20°C PDMS-VTOS, 80°C PDMS-VTOS; H-PDMS is PDMS with terminal OH groups, 20°C PDMS-VTOS is PDMS membrane prepared at 20°C; 80°C PDMS-VTOS is PDMS membrane prepared at 80°C.

3. Results and Discussion

3.1. Characterization of Membranes

3.1.1. FT-IR Spectra of Different Polymers. The hydrophobicity of H-PDMS and cross-linked PDMS membrane at 80°C and 20°C are characterized by FTIR as shown in Figure 2. The peaks that occur at about 3100 cm^{-1} and 3744 cm^{-1} are assigned to the stretching vibrations of unsaturated carbon-hydrogen bond and Si–OH. As can be seen in Figure 2, the intensities of peaks at 3744 cm^{-1} of 80°C PDMS samples are lower than those of H-PDMS and 20°C PDMS. Meanwhile, unsaturated carbon-hydrogen bond peak appears at 3100 cm^{-1} of cross-linked PDMS. The intensity of the peak from 80°C PDMS is larger than that from 20°C PDMS. These results may confirm that H-PDMS cross-linked with VTOS at 80°C becomes more hydrophobic.

3.1.2. Contact Angle of PDMS-VTOS Membranes. The membrane surface properties are also affected by cross-linking temperature and VTOS content. Table 1 and Figure 3 display the change of contact angle on the respective surfaces. The contact angle (CA) of PDMS-VTOS membranes

Table 1: Contact angle for water of PDMS-VTOS membranes synthesized at different temperatures.

Cross-linking temperature (°C)	20	40	50	60	80
Contact angle (°)	64.5	101.9	106.2	107.7	108.3

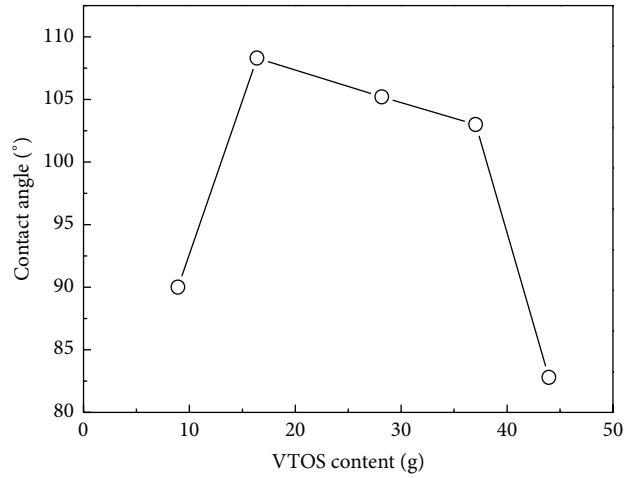

Figure 3: The effect of content of VTOS on contact angle of PDMS-VTOS membranes (the cross-linking temperature: 80°C).

Table 2: Cross-linking effect on the glass transition temperatures (T_g) of PDMS-VTOS membranes (the weight ratio of H-PDMS : VTES : DBTDL is 1 : 0.2 : 0.02).

Cross-linking temperature (°C)	40	50	60	80
T_g (°C)	−119.3	−123.9	−118.7	−118.2

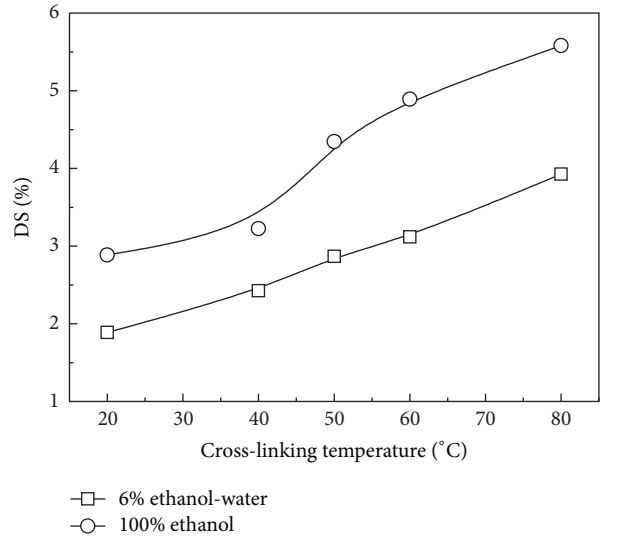

Figure 4: Effect of cross-linking temperature on the degree of swelling (DS) of PDMS-VTOS membrane immersed in aqueous solution of ethanol 6 wt% and 100 wt% ethanol content in the feed (temperature, 40°C).

increased with increasing cross-linking temperature. After cross-linking at 60°C, the CA was 107.7°, and further increase of cross-linking temperature did not bring significant change in CA. This phenomenon is attributed to the fact that more hydroxyl groups were left in the membranes cross-linked under 60°C than those in the membranes cross-linked over 60°C, as can be confirmed by the FT-IR spectra results.

However, the effects of VTOS content on surface properties show parabola tendency. As shown in Figure 3, the highest contact angle was achieved with 16.39 wt% of VTOS, which was the optimal content of the cross-linking agent. Too low VTOS content cross-linking is not enough to be preparation dense membrane which affects hydrophobicity of the membrane surface. Too much VTOS leads to some unreacted hydrophilic ethoxy group left in the membrane after the reaction of hydrolysis and condensation of VTOS, which made the hydrophobicity of PDMS-VTOS membrane decrease.

3.1.3. Measurements of Differential Scanning Calorimetry. Table 2 shows the DSC data of PDMS-VTOS cross-linked membranes with different cross-linking temperature. The T_g has an insignificant fluctuation (from −123.9°C to −118.2°C) with increasing cross-linking temperature. This result indicates that cross-linking temperature has no obvious effect on thermal property of the membrane. Meanwhile, it shows that membrane will not transform during pervaporation.

3.1.4. Swelling of PDMS Membrane in Alcohol/Water Mixtures. The results of swelling measurements of PDMS-VTOS in 6 wt% and 100 wt% ethanol/water binary mixtures at 40°C are presented in Figure 4. As can be seen, the DS of PDMS-VTOS for mixtures increases separately with increasing cross-linking temperature. In addition, DS of PDMS in 100 wt% ethanol is higher than that of PDMS in 6 wt%. These results indicate that VTOS cross-linked PDMS was swelling more in ethanol than in water.

3.2. Pervaporation Performance

3.2.1. Effect of Cross-Linking Temperature. Figure 5 shows the effects of cross-linking temperature on (a) ethanol in permeate and (b) the normalized permeation flux for an aqueous solution of 6 wt% ethanol through PDMS-VTOS membrane during PV with VTOS content of 16.39 wt%. From Figure 5(a), the ethanol concentration in permeate through the PDMS-VTOS membranes was much higher than that in the feed in the studied cross-linking temperature range. These results suggest that PDMS-VTOS membranes have high ethanol permselectivity for an aqueous solution of 6 wt% ethanol. Meanwhile, both the separation factor and the ethanol concentration in permeate increased with increasing cross-linking temperature. From Figure 5(b), the ethanol and water flux through PDMS-VTOS membranes decreased with increasing cross-linking temperature.

In general, the PV performance for recovery of organic from its aqueous solution is based on the solubility of permeants into the polymer membrane (sorption process)

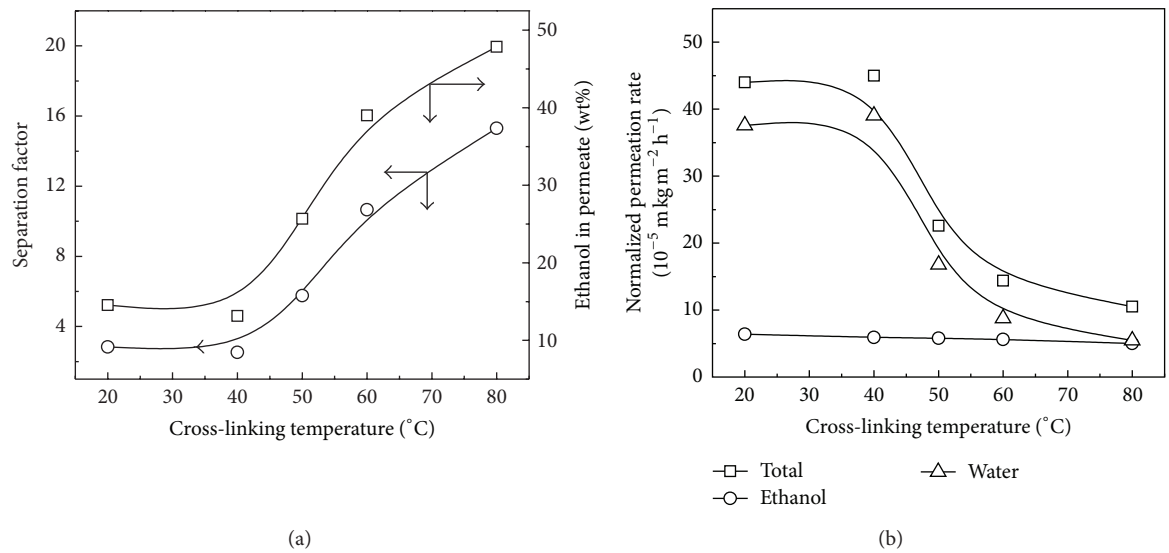

Figure 5: Effect of cross-linking temperature on (a) ethanol in permeate and (b) the normalized permeation flux for an aqueous solution of 6 wt% ethanol through PDMS-VTOS membrane during PV (operating temperature: 40°C, the weight ratio of H-PDMS : VTOS : DBTDL is 1 : 0.2 : 0.02).

and the diffusivity of the permeants in the polymer membrane (diffusion process). The solubility and diffusivity of the permeants are significantly influenced by the chemical and physical structures of the polymer membranes. After cross-linked by VTOS, the PDMS-VTOS has better ethanol sorption selectivity with increasing cross-linking temperature. This result in Figure 6 is compared with those of the contact angle for water in Table 1; it is noted that the ethanol permselectivity strongly depends on the contact angle for water on the cross-linked membrane surface. Namely, the ethanol permselectivity of the cross-linked PDMS-VTOS membrane increased with an increase of the contact angle of water. The above results suggest that the ethanol permselectivity for an aqueous ethanol solution of the cross-linked PDMS-VTOS membranes is more significantly governed by the solubility of the permeants into the membrane than the diffusivity of the permeants in the membrane.

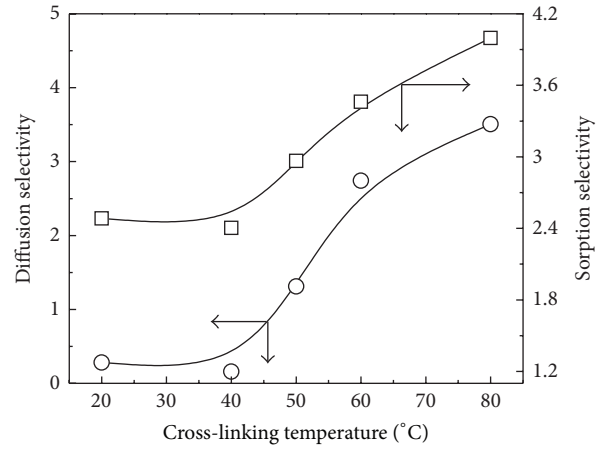

Figure 6: Effects of cross-linking temperature on the diffusion selectivity and sorption selectivity.

3.2.2. Effect of Cross-Linker VTOS Content. Curves of the pervaporation flux and the separation factor of PDMS-VTOS cross-linked membranes versus VTOS contents are presented in Figure 7. As it can be seen, when VTOS content is from 8.93 wt% to 16.39 wt%, the separation factor (a) upgrades but the pervaporation flux (J) reduces with the increase of VTOS content. Obviously, the increase of VTOS content makes the structures of PDMS-VTOS cross-linked membranes compact and prevents the large ethanol molecules from passing the membrane. As it also can be seen, when VTOS content is from 16.39 wt% to 43.96 wt%, the increase of VTOS content improves the pervaporation flux (J) but decreases the separation factor (α). This phenomenon demonstrates that membranes with high VTOS content become more hydrophilic and relatively incompact structures. In this situation, both water and ethanol molecules can easily transmit the membranes, so the exaltation of the pervaporation flux (J) is accompanied by the decrease of the separation factor (α). Experimental data verify that when VTOS content is 16.39 wt%, the separating properties of the cross-linked membranes are better; the separation factor (α) and the pervaporation flux (J) of membranes can reach 15.3 and 573.3 g·m^{-2}·h^{-1}, respectively.

3.2.3. Effect of Feed Temperature. Figure 8 presents the effect of temperature on pervaporation total flux of ethanol/water mixtures through cross-linked PDMS-VTOS membranes; the feed concentration is 6 wt% and VTOS content is 16.39 wt%. An increase in feed temperature from 40°C to 80°C results in the increase in the total fluxes for the membranes. This is due to the fact that, during pervaporation, permeating

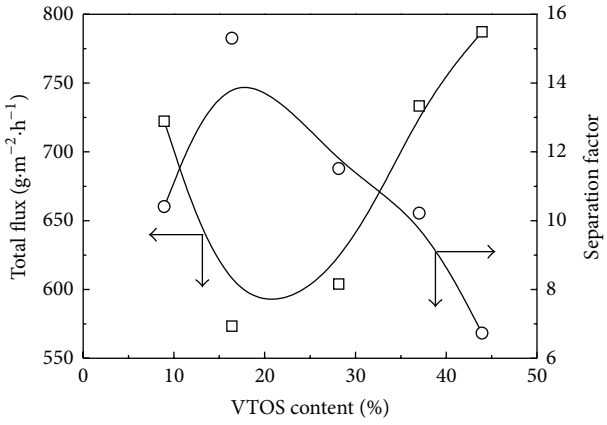

Figure 7: The effect of VTOS content on pervaporation properties of PDMS-VTOS membrane (feed concentration is 6 wt%, the cross-linking temperature is 80°C, and the PV temperature is 60°C).

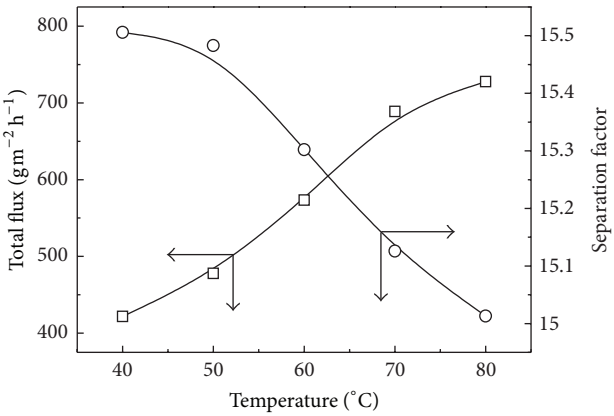

Figure 8: Feed temperature effect on PV performance of PDMS-VTOS membrane feed concentration, 6 wt%, the weight ratio of H-PDMS : VTOS : DBTDL is 1 : 0.2 : 0.02, the cross-linking temperature is 80°C.

molecules diffuse easily through free volumes of the membrane which is produced by thermal motions of polymer chains. Frequency and amplitude of polymer jumping chains increase as temperature increases. Thus, diffusion rate of individual permeating molecules increases leading to high permeation fluxes at higher temperatures. The separation factor for ethanol decreases with increasing temperature. This is a common phenomenon in a pervaporation process and can be explained by two theories. One claimed that a water molecular is much smaller than an ethanol molecular, so with the increase of operating temperature, the more flexible of polymer chains allow more water permeate through the membrane than ethanol, which leads to the reduction of separation factor. The other theory says that water cluster come into being on the feed side of a hydrophobic membrane. And the size of water cluster becomes more dominant at a lower temperature than at a higher temperature [21]. Therefore, the diffusivity of water will be restraint in a membrane at a lower temperature.

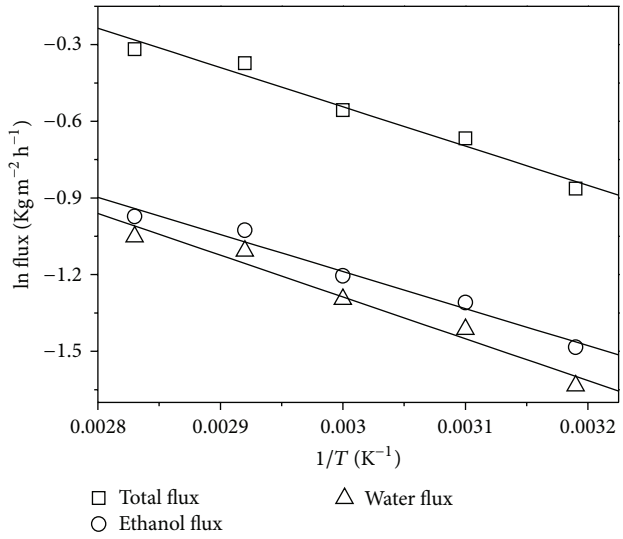

Figure 9: Arrhenius plots of the PDMS-VTOS membrane.

To get a deeper view of the relationships between temperature and permeation flux, the Arrhenius type equation was applied by $J = J_0 \exp(-E_p/RT)$. E_p is apparent activation energy for permeation, J_0 the permeation rate constant, R the molar gas constant, and T is the temperature in Kelvin. The E_p values are 12.060 kJ/mol and 13.596 kJ/mol for ethanol and water, respectively, which are determined from the $\ln J$ versus $1/T$ plots (Figure 9). The larger permeation activation energy of water implies that water permeation flux is more sensitive to increased temperature compared to that of ethanol permeation flux.

3.2.4. Comparing of Pervaporation Performance. Pervaporation performance in some previous studies and our study is listed in Table 3. As can be seen, the PDMS-VTOS membrane prepared in this research showed higher separation and lower permeation flux than those PDMS membranes cross-linked with TAOS reported for pervaporation removal of ethanol from dilute aqueous solution. The higher separation factor of PDMS-VTOS membranes can be attributed to two factors. One is a more hydrophobic nature of VTOS than TAOS and the other is that PDMS-VTOS membranes possess a higher cross-linking density than PDMS-TAOS membranes, because PDMS-VTOS membranes with a high separation factor were cross-linked at a higher temperature of 80°C, which was usually performed at 60°C. However, a higher cross-linking density is not favored for a permeation flux. That is why the total flux of PDMS-VTOS membranes is relatively lower than that of PDMS-TAOS membranes.

4. Conclusions

Cross-linked PDMS-PAN membranes using VTOS were prepared. The effects of parameters on the preparation and pervaporation performance were investigated. It was found that cross-linked PDMS-VTOS membranes had better hydrophobic when H-PDMS : VTOS : DBTDL = 1 : 0.2 : 0.02,

Table 3: Pervaporation performance of different PDMS-VTOS using cross-linking agent.

Cross-linking agent	Total flux ($g \cdot m^{-2} \cdot h^{-1}$)	Separation factor	Reference
TAOS	1140	9.3	[17]
TAOS	1300	8.3	[18]
TAOS	750	2.7	[19]
VTOS	573	15.3	This work

cross-linking temperature is 80°C. Meanwhile, PDMS-VTOS membranes have much higher separation factor than PDMS-TAOS membranes reported in the literatures. Though the ethanol flux of PDMS-VTOS membranes are not so remarkable, it is also acceptable.

Disclosure

Shanghai Chemical Reagent Company and Research and Development Center of Water Treatment Technology are two companies from which we purchased chemical reagents.

Conflict of Interests

The authors declare that they have no conflict of interests.

Acknowledgments

The authors acknowledge the financial supports for this work from Natural Science Foundation of China (21106053), the Fundamental Research Funds for the Central Universities (JUSRP311A01), and the Industry-Academia Cooperation Innovation Fund Projects of Jiangsu Province (BY2012058).

References

[1] H. J. Kim, S. S. Nah, and B. R. Min, "A new technique for preparation of PDMS pervaporation membrane for VOC removal," *Advances in Environmental Research*, vol. 6, no. 3, pp. 255–264, 2002.

[2] D. J. O'Brien, L. H. Roth, and A. J. McAloon, "Ethanol production by continuous fermentation-pervaporation: a preliminary economic analysis," *Journal of Membrane Science*, vol. 166, no. 1-2, pp. 105–111, 2000.

[3] M. Di Luccio, C. P. Borges, and T. L. M. Alves, "Economic analysis of ethanol fructose production by selective fermentation coupled to pervaporation: effect of membrane costs on process economics," *Desalination*, vol. 147, no. 1–3, pp. 161–166, 2002.

[4] L. M. Vane, "A review of pervaporation for product recovery from biomass fermentation processes," *Journal of Chemical Technology and Biotechnology*, vol. 80, no. 6, pp. 603–629, 2005.

[5] M. Peng, L. M. Vane, and S. X. Liu, "Recent advances in VOCs removal from water by pervaporation," *Journal of Hazardous Materials*, vol. 98, no. 1–3, pp. 69–90, 2003.

[6] R. Psaume, P. Aptel, Y. Aurelle, J. C. Mora, and J. L. Bersillon, "Pervaporation: importance of concentration polarization in the extraction of trace organics from water," *Journal of Membrane Science*, vol. 36, pp. 373–384, 1988.

[7] H. L. Chen, L. G. Wu, J. Tan, and C. L. Zhu, "PVA membrane filled β-cyclodextrin for separation of isomeric xylenes by pervaporation," *Chemical Engineering Journal*, vol. 78, no. 2-3, pp. 159–164, 2000.

[8] I. Blume, J. G. Wijmans, and R. W. Baker, "The separation of dissolved organics from water by pervaporation," *Journal of Membrane Science*, vol. 49, no. 3, pp. 253–286, 1990.

[9] S. Takegami, H. Yamada, and S. Tsujii, "Pervaporation of ethanol/water mixtures using novel hydrophobic membranes containing polydimethylsiloxane," *Journal of Membrane Science*, vol. 75, no. 1-2, pp. 93–105, 1992.

[10] J. M. Molina, G. Vatai, and E. Bekassy-Molnar, "Comparison of pervaporation of different alcohols from water on CMG-OM-010 and 1060-SULZER membranes," *Desalination*, vol. 149, no. 1–3, pp. 89–94, 2002.

[11] J. A. González-Marcos, C. López-Dehesa, and J. R. González-Velasco, "Effect of operation conditions in the pervaporation of ethanol-water mixtures with poly(l-trimethylsilyl-1-propyne) membranes," *Journal of Applied Polymer Science*, vol. 94, no. 4, pp. 1395–1403, 2004.

[12] T. Masuda, M. Takatsuka, B. Z. Tang, and T. Higashimura, "Pervaporation of organic liquid-water mixtures through substituted polyacetylene membranes," *Journal of Membrane Science*, vol. 49, no. 1, pp. 69–83, 1990.

[13] S. A. Stern, Y. Mi, H. Yamamoto, and A. K. S. Clair, "Structure/permeability relationships of polyimide membranes. Applications to the separation of gas mixtures," *Journal of Polymer Science B*, vol. 27, no. 9, pp. 1887–1909, 1989.

[14] T. Miyata, Y. Nakanishi, and T. Uragami, "Ethanol permselectivity of poly(dimethylsiloxane) membranes controlled by simple surface modifications using polymer additives," *Macromolecules*, vol. 30, no. 18, pp. 5563–5565, 1997.

[15] T. Miyata, J. I. Higuchi, H. Okuno, and T. Uragami, "Preparation of polydimethylsiloxane/polystyrene interpenetrating polymer network membranes and permeation of aqueous ethanol solutions through the membranes by pervaporation," *Journal of Applied Polymer Science*, vol. 61, no. 8, pp. 1315–1324, 1996.

[16] F. J. Xiangli, W. Wei, Y. W. Chen, W. Q. Jin, and N. P. Xu, "Optimization of preparation conditions for polydimethylsiloxane (PDMS)/ceramic composite pervaporation membranes using response surface methodology," *Journal of Membrane Science*, vol. 311, no. 1-2, pp. 23–33, 2008.

[17] Y. Luo, S. J. Tan, H. Wang et al., "PPMS composite membranes for the concentration of organics from aqueous solutions by pervaporation," *Chemical Engineering Journal*, vol. 137, no. 3, pp. 496–502, 2008.

[18] L. Li, S. J. Tan, Z. Xiao, L. Pu, and Z. Zhang, "Composite PDMS membrane with high flux for the separation of organics from water by pervaporation," *Journal of Membrane Science*, vol. 243, no. 1-2, pp. 177–187, 2004.

[19] T. Mohammadi, A. Aroujalian, and A. Bakhshi, "Pervaporation of dilute alcoholic mixtures using PDMS membrane," *Chemical Engineering Science*, vol. 60, no. 7, pp. 1875–1880, 2005.

[20] J. Gu, X. Shi, Y. X. Bai, H. M. Zhang, L. Zhang, and H. Huang, "Silicalite-filled polyether-block-amides membranes for recovering ethanol from aqueous solution by pervaporation," *Chemical Engineering and Technology*, vol. 32, no. 1, pp. 155–160, 2009.

[21] Y. W. Huang, J. W. Fu, Y. Pan, X. B. Huang, and X. Z. Tang, "Pervaporation of ethanol aqueous solution by polyphosphazene membranes: effect of pendant groups," *Separation and Purification Technology*, vol. 66, no. 3, pp. 504–509, 2009.

Hindawi Publishing Corporation
International Journal of Polymer Science
Volume 2013, Article ID 451398, 8 pages
http://dx.doi.org/10.1155/2013/451398

Research Article

Decoloring Methyl Orange under Sunlight by a Photocatalytic Membrane Reactor Based on ZnO Nanoparticles and Polypropylene Macroporous Membrane

Bing Hu,[1,2] Jin Zhou,[1,2] and Xiu-Min Wu[2]

[1] *Department of Material and Chemistry Engineering, Chizhou University, Chizhou, Anhui 247000, China*
[2] *Laboratory of Functional Molecular Solids, Ministry of Education, Anhui Key Laboratory of Molecular-Based Materials, College of Chemistry and Materials Science, Anhui Normal University, 1 East Beijing Road, Wuhu, Anhui 241000, China*

Correspondence should be addressed to Jin Zhou; zhoujin_ah@163.com

Received 2 February 2013; Accepted 10 March 2013

Academic Editor: Hai-Yin Yu

Decoloring methyl orange (MeOr) under sunlight was conducted in a photocatalytic membrane reactor (PMR). Zinc oxide nanoparticles (ZnO NPs) were suspended in the solution or immobilized on the membrane. The membrane was modified by grafting 2-hydroxyethyl methacrylate (HEMA) to enhance the adsorption of ZnO NPs on the hydrophobic membrane surface and improve the membrane permeability. The results show that the water fluxes through the modified membranes are higher than that through the unmodified membrane. After introducing ZnO NPs to the membrane, the water fluxes still rise with the immobilization degree of ZnO NPs. For the PMR with ZnO NPs in suspension, the photocatalytic decoloration percent (PDP) was over 98.2% after 40 min under sunlight. For the PMR with ZnO NPs immobilized on the membrane, the max of PDP was 74.3% after 6 h under sunlight, and maintained at 72% after repeated uses for five times. These results demonstrate that photocatalytic membrane reactor (PMR) based on ZnO NPs and polypropylene macroporous membrane(PPMM) could be applied in decoloring dyes.

1. Introduction

Dyes, widely used in industries, like textiles, paper, rubber, and plastics, have led to severe environmental contamination due to the toxic and colored wastewater poured into water bodies, which seriously worsens the quality of water, inhibiting sunlight penetration and reducing photosynthetic reaction.

Conventional treatment methods for dye removal, such as ozonation, bleaching, hydrogen peroxide/UV, and electrochemical techniques, were found to be nondestructive and inefficient, because most dyes have complex aromatic molecular structures that resist degradation [1]. They are stable to light, oxidizing agents, and aerobic digestion. The motivation for more efficient treatment processes has inspired environmental scientists and engineers to explore the technique of combing pressure-driven membrane filtration and heterogeneous photocatalysis [2–6].

Recently, heterogeneous photocatalysis employing semiconductor photocatalysts (TiO_2, ZnO, and adulterate or complex semiconductor) has demonstrated their efficiencies in degrading a wide range of toxic organic compounds into relatively innocuous end products, such as carbon dioxide and water [5]. Photocatalytic oxidation of various harmful organic dyes and inorganic pollutants in industrial wastewater has been carried out by nanosemiconductors under UV light due to their high photosensitivity and nontoxicity [7, 8].

ZnO NPs have great photocatalytic activity under sunlight, which can effectively absorb photons in the UV region from the sunlight [9] and have shown higher photocatalytic efficiencies for the degradation of several organic pollutants [10, 11]. It is known that many adulterate or complex semiconductors have shown great photocatalytic activity under solar light [12, 13]. Compared with these semiconductors, the advantages of ZnO NPs are simple synthesis process (only one step by chemical depositing method) and low cost.

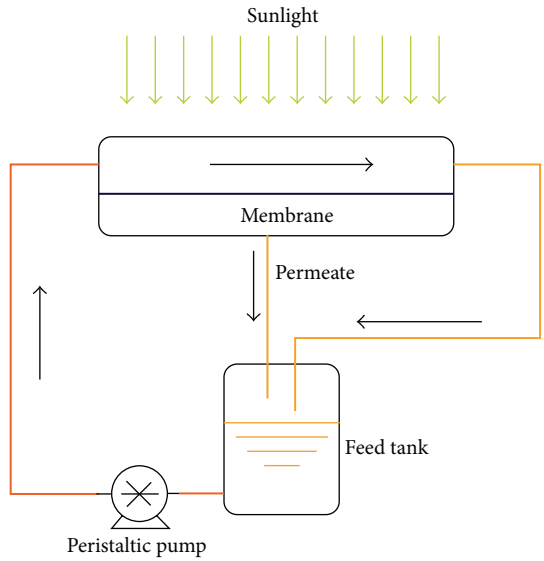

Figure 1: A schematic diagram of the photocatalytic membrane reactor (active membrane area is 2700 mm^2).

On the other hand, membrane process is widely applied in many industries. The process has several main advantages, such as low energy consumption, low chemicals consumption, low maintenance costs, and easy scale up [14].

Photocatalytic membrane reactors (PMRs) are of hybrid processes in which photocatalysis is coupled with a membrane process, and the permeation of solutes through the membrane and photocatalytic reaction occurs simultaneously. As a low-cost, environmentally friendly, and sustainable treatment technology, the PMRs for wastewater treatment using semiconductors have shown a great potential [15, 16]. Although UV light has been commonly employed in the photocatalytic studies, worldwide efforts are underway to make use of sunlight for environmental protection and water purification [17], because sunlight consists of about 5–7% UV light, 46% visible light, and 47% other irradiation [18], and additionally it is inexhaustible (Figure 1).

In the present work, to improve the membrane permeability and to enhance the adsorption of the semiconductors, hydrophilic surface modification of polypropylene macroporous membrane was carried out. Grafting 2-hydroxyethyl methacrylate (HEMA) onto the membrane surface was performed according to previous work [19, 20]. ZnO NPs were one pot fabricated by direct precipitation; their photocatalytic activity for environmental application was carefully investigated by using decoloring methyl orange (MeOr) under sunlight.

2. Materials and Methods

2.1. Materials. Benzophenone (BP), 2-hydroxyethyl methacrylate (HEMA), methyl orange (MeOr), $Zn(NO_3)_2$, and oxalic acid were used as purchased from Lingfeng Shanghai Reagent Co. Ltd. Polypropylene macroporous membranes (PPMMs) with a porosity of 45–50% and an average pore diameter of 0.10 μm were prepared [21], and benzyl dithiobenzoate (BDTB) was synthesized according to the literature [22].

2.2. Synthesis of ZnO NPs. ZnO NPs were synthesized by direct precipitation with oxalic acid as the precipitator [23] with minor modification. 12.7 g $Zn(NO_3)_2$ and 10.0 g oxalic acid were dissolved in 50 mL distilled water separately. Then the two solutions were mixed slowly under stirring during which the white precipitate produced immediately. After this, the precipitate was washed with distilled water and ethanol for three or four times, dried at 90–100°C, and finally calcined at 450°C for 3 h to achieve ZnO NPs.

2.3. Surface Modification of Membrane. The used method and experimental setup for the membrane surface modification were described in [19].

2.4. Photocatalytic Membrane Reactor. The permeation properties of the unmodified and modified PPMMs were examined in a stirred dead-ended ultrafiltration test cell connected to a 2 L feed tank [24]. The volumetric flux was determined through the timed collection of permeate, and the relative flux was described by the following equation:

$$\text{Relative flux} = \frac{J_{0,m}}{J_{0,u}} \times 100\%, \quad (1)$$

where $J_{0,u}$ and $J_{0,m}$ are the pure water fluxes through the unmodified and modified membranes. $J_{0,u}$ varied from 250 to 450 $Lm^{-2}\,h^{-1}$, and as a result, the relative flux was adopted to eliminate the differences between the unmodified membranes.

The PHEMA grafted PPMMs were submerged in the ZnO NPs ethanol dispersion for 24 h; ZnO NPs were physically adsorbed on the membrane surface [24]. The immobilization degree (ID) of the ZnO NPs on the membrane is calculated by the following equation:

$$\mathrm{ID} = \frac{(W_2 - W_1)}{W_1} \times 100\%, \quad (2)$$

where ID refers to the immobilization degree of ZnO NPs on the membrane surface, % (wt), and W_1 and W_2 the respective weights of PHEMA grafted membranes before and after the immobilization of the ZnO NPs. All the results are the average values of three parallel experiments.

The photocatalytic decoloring MeOr with ZnO NPs suspended is investigated. 0.05 g ZnO NPs were added to 200 mL 10 mg/L MeOr aqueous solution, stirred for 30 min in the dark to achieve the adsorption—desorption equilibrium, and then exposed to the sunlight with stirring (Wuhu, Anhui Province, China, July 2010) (the light intensity was determined by a UV power meter, LS123, Shenzhen Linshang Technology Co. Ltd.); the photocatalytic reaction was conducted within the light intensity of 90 ± 15 mW/cm^2; then pure water was added to the reacting solution to compensate the evaporation during its exposition to sunlight. The solution was sampled at intervals of 5 min, and the samples were centrifuged for 10 min.

The PMR with ZnO NPs immobilized on the membrane surface is similar to [24]. The membrane (GD = 36.0%, ID = 6.2%) was sandwiched in the cross flow PMMA reactor (each of the PMMA plate is 20 mm in thickness), the total weight of the immobilized ZnO NPs is about 0.05 g; 200 mL 10 mg/L MeOr aqueous solution was pumped into the reactor circularly by a peristaltic pump with the reactor exposed to the sunlight, and the cross flow velocity was kept at 0.15 m/s [25]. At the end of each run, the membrane was taken out, flushed with pure water for three times, then dried and stored in air for a period of time (as shown in Figure 6). After that the next run started.

The supernatant of the effluent was measured by the UV-Vis spectrophotometer (UV-2450, Shimadzu, Japan) at 464 nm (the maximal adsorption wavelength of MeOr). The photocatalytic decoloration percentage (PDP) is calculated by the following equation:

$$\mathrm{PDP} = \frac{A_0 - A}{A_0} \times 100\%, \quad (3)$$

where A and A_0 correspond to the UV absorbance of the feed and the filtrate, respectively.

2.5. Characterization. The crystalline structures of ZnO NPs were examined by X-ray powder diffraction on an X-ray diffractometer (XRD) (XRD-6000, Japan) with CuKα radiation (λ = 0.154056 nm) at a scanning rate of 0.05 °/s. Surface morphology of the membranes was observed by field emission scanning electron microscopy (FESEM) (Hitachi 4800, Japan), and the surface hydrophilicity was determined by water contact angle measurements (OCA20, Germany) [26].

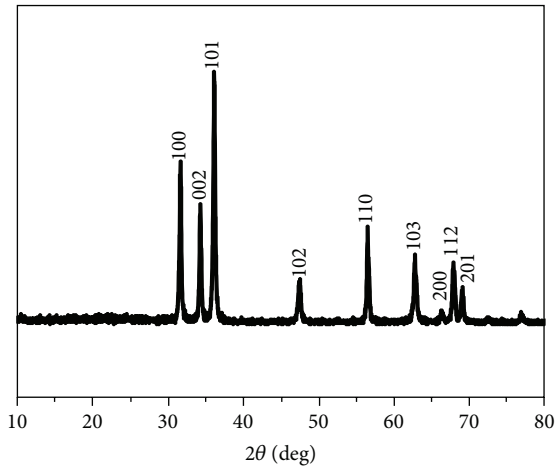

Figure 2: XRD pattern of ZnO NPs.

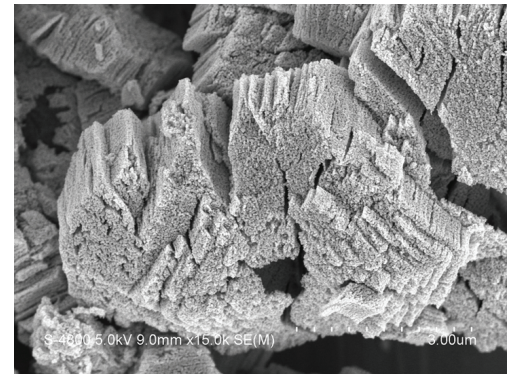

Figure 3: FESEM image of the ZnO NPs (×15000).

3. Results and Discussion

3.1. Characterization and Permeation of the Membranes. XRD is used to investigate the changes of crystalline nature of the prepared ZnO NPs (Figure 2). Most of the diffraction peaks could be attributed to the hexagonal wurtzite structure of ZnO (JCPDS card 36-1451) [27]. It can be observed that no diffraction peaks from other phases of ZnO or impurities, suggesting that the obtained ZnO is of high purity. The average crystallite size for ZnO NPs calcined at 450°C was calculated at 26.6 ± 4.8 nm according to the Scherrer formula [28].

Figure 3 presents the FESEM images of the ZnO NPs, which reveal that the surfaces are rough and porous, indicating that the ZnO NPs aggregate due to large specific surface area and high surface energy.

The surface morphologies of the unmodified, the PHEMA grafted, and the ZnO NPs immobilized membranes were observed by FESEM (Figure 4). Compared with the unmodified PPMM with high porosity (Figure 4(a)), the surfaces of the PHEMA grafted PPMMs are gradually covered with polymers; as the grafting degree increases (Figures 4(b) and 4(c)), the membrane pores are plugged and the surface porosity reduces with GD increasing. It can be clearly observed that ZnO NPs have been introduced to the

Table 1: Relative water flux (%) through PHEMA grafted and ZnO NPs immobilized PPMMs with different GD. The average water flux for the membranes is 400 ± 25 Lm^{-2} h^{-1}.

GD, % (wt)	Water contact angle on PHEMA grafted PPMMs,°	Relative water flux, %	
		PHEMA grafted PPMM	ZnO NPs immobilized PPMM
0.00	90	100	113
1.00	72	120	124
4.48	54	118	143
6.89	43	115	—
8.21	35	116	136

—: The membrane was broken after ZnO NPs immobilization. The error margin is within ±10%.

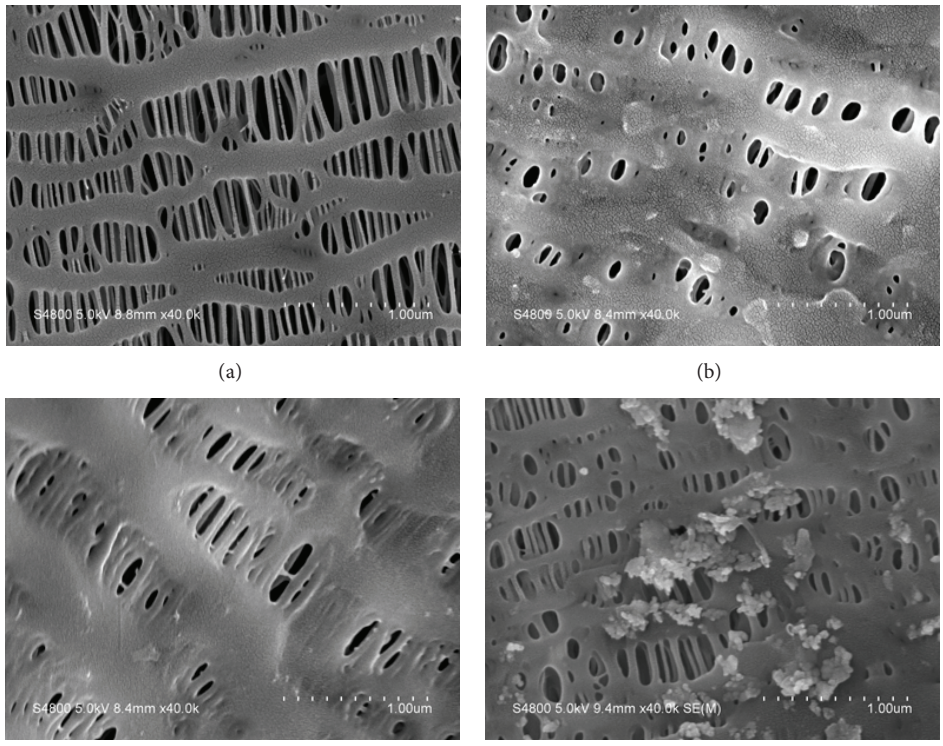

(a) (b) (c) (d)

Figure 4: FESEM images (×40000) of (a) the unmodified, and (b)-(c) PHEMA grafted PPMMs with GD = 2.40 and 4.05% (wt), respectively; (d) ZnO NPs immobilized PPMMs with GD = 36.0% (wt), ID = 6.2% (wt).

membrane surface from Figure 4(d). The ZnO NPs appear in large clusters, instead of being evenly distributed. The immobilization degree of ZnO NPs immobilized PPMMs with different GD of PHEMA was shown in Supplementary Material (See Supplementary Material available online at http://dx.doi.org/10.1155/2013/451398). The result verified that the grafting of polyHEMA can enhance the adsorption of ZnO NPs on the hydrophobic membrane surface.

Variation of the relative water fluxes through PHEMA grafted and ZnO NPs immobilized PPMMs was investigated (Table 1). The relative water flux goes up after PHEMA grafted on the PPMMs due to the membrane surface hydrophilicity increasing (Table 1) [29]. For the PHEMA grafted membrane with a GD of 4.48% (wt), the relative water flux reaches the maximum value of 118%; after that, the relative water flux decreases slowly.

Membrane permeability in the filtration of aqueous solution is mainly determined by two factors: one is the membrane structure, such as membrane thickness, pore size, and porosity; the other is the membrane surface hydrophilicity. When DG is low, the hydration of PHEMA chains results in a decreased resistance to water permeation and thus improves the water fluxes. For the membranes with a high DG, the graft layer is thick and the expanded PHEMA conformation in aqueous circumstance tends to cover the membrane pores, and consequently the water fluxes decrease [30, 31].

It can also be found in Table 1 that after the immobilization of ZnO NPs on the membrane surface, the membrane permeability continues to increase and the relative water flux rises to 143%. The coating of ZnO NPs on the membrane causes the decrease of water contact angle, because hydrophilic ZnO NPs anchored to the membrane [32, 33],

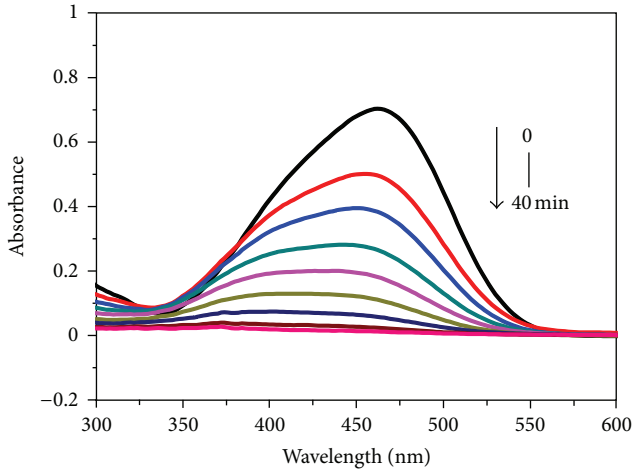

Figure 5: UV-Vis spectrum of MeOr under sunlight, using the photocatalytic membrane reactor with the ZnO NPs in suspension.

leading to the increase of the membrane surface hydrophilicity and hence increases the membrane permeability.

For the filtration of the dye solution, it was observed that the relative water fluxes were similar to those of the pure water fluxes, that is, the dyes could not be rejected by the membranes, and as a result, the filtrate was returned to the feed tank for the improvement of dyes decoloration. Membranes just acted as barriers for the ZnO NPs.

3.2. Photocatalytic Decoloring MeOr under Sunlight. In order to examine the performance of ZnO NPs in decoloring dyes in wastewater, photocatalytically decoloring MeOr was carried out in a photocatalytic membrane reactor under sunlight. The catalysts were suspended in the solution or immobilized on the membrane.

Figure 5 shows that MeOr is nearly completely decolored after 40 min sunlight (ZnO NPs were suspended in the solution). The result shows that ZnO NPs prepared in the present work are highly effective in decoloring dyes in water and wastewater. The mechanism of ZnO NPs catalyzed decoloring reaction is as follows. ZnO NPs are excited by absorbing the photon with more energy than the band gap, resulting to the photoinduced electron-hole pairs. The peroxy radical anions are reacted by the electron and oxygen, and the hydroxyl radical is reacted by the hole and water. Hydroxyl radical can further decompose and remove organic molecules, namely, organic photodegradation [34]. Figure 5 also shows that the peak position is blue-shifted along with reaction time, which may be attributed to the deamination products of MeOr [35, 36].

The photostability of ZnO NPs photocatalysts is an essential factor to promote heterogeneous photocatalysis technology for practical applications. In this research, hybrid membrane is derived from coating ZnO NPs on the PHEMA grafted membrane. The photocatalytic reaction was conducted within the light intensity of $90 \pm 15\ \text{mW/cm}^2$ for each run to eliminate the differences in light intensity. After each run, the membrane was taken out of the reaction chamber,

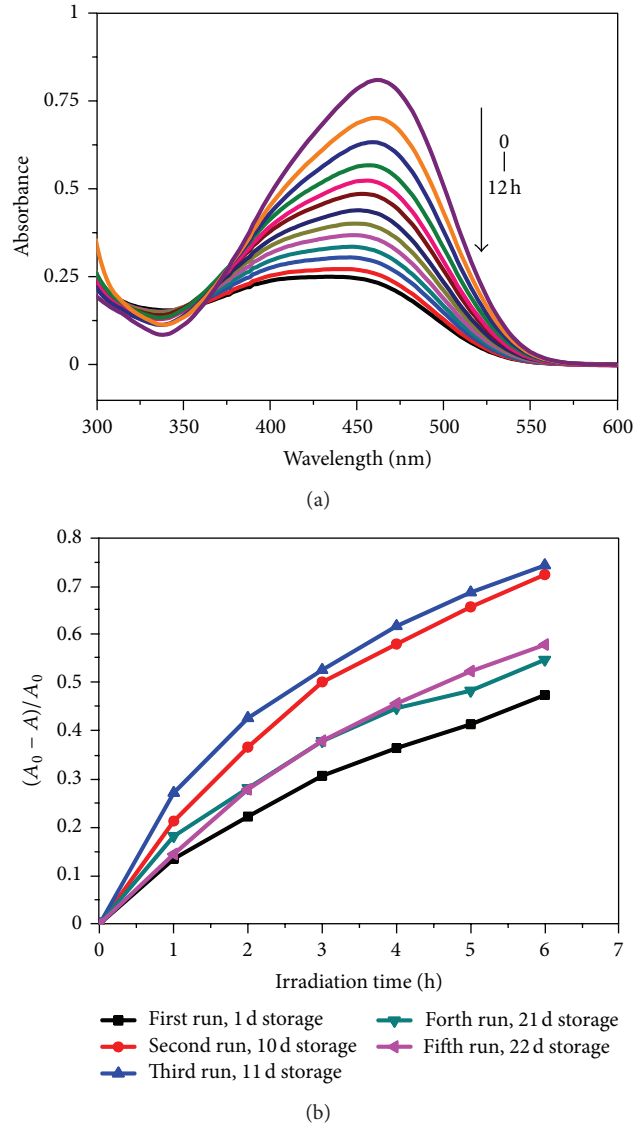

Figure 6: Decoloring MeOr in the PMR with the ZnO NPs immobilized on the membrane surface. (a) UV-Vis spectrum of MeOr at 1 h intervals (1–12 h) for the first cycle; (b) photocatalytic experiments for 5 cycles.

flushed with pure water and dried in air. UV-Vis spectrum of MeOr at 1 h intervals (1–12 h) for the first cycle is depicted in Figure 6(a), which shows that MeOr was decolored slowly. The photostability of ZnO NPs immobilized membrane for the decoloring MeOr is shown in Figure 6(b), which indicates that the ZnO NPs immobilized on polypropylene membrane can photocatalytically decolor MeOr by 47.4%, 72.4%, 74.3%, 54.7%, and 57.8% after 6 h sunlight irradiation from the first to the fifth run, respectively. The PDP of the first run is the lowest, but those of the second and the third run reach the highest.

The reason may be that the active point of ZnO NPs was covered because of the agglomeration. After the first run, the agglomeration configuration of ZnO NPs became

a little dispersive and the MeOr can enter into the interstice between ZnO NPs. In addition, the transparence of membrane increased after the first run, and the loosely adsorbed ZnO NPs were washed off (however, this could not be determined due to the trivial gravity changes), causing an increase in sunlight penetrating, hence the PDP ascends.

PDPs of the fourth and fifth run are between those of the first and the second run, showing that PDPs of the two runs slightly decrease, compared with those of the second and the third run. This phenomenon may be resulted from the deactivation of the photocatalysts, which is due to that many MeOr molecules were adsorbed on the membrane surface after being used for three times [37]. The PDP maintains at a very high level of about 55% in the fifth run, which means that after being used for five cycles, the PDP is still 8% higher than that of the first run. This result confirms that the catalysts were not photocorroded during the photocatalytic decoloration of the pollutant molecules under sunlight. After being used for five times, a lot of ZnO NPs were also visibly adsorbed on the membrane surface, suggesting that they are not easy to wash off.

These results demonstrate that PMR with ZnO NPs immobilized on the polypropylene macroporous membrane surface can be reused for several times without weakening the photocatalytic activity, exhibiting potential application for continual and long-time reactions [38]. Generally, the immobilized ZnO NPs are stable for repeated uses [34]. Therefore, the ZnO NPs can be regarded as ideal photocatalysts for environmental friendly purification on industrial scale under sunlight.

Figure 6 shows that the PDPs are much lower than those of the PMR with ZnO NPs in suspension (Figure 5), which may be attributed to the following reasons: (1) the active area of ZnO NPs decreased; (2) 3/4 of the sunlight was absorbed by the PMMA reactor, which was characterized by a UV power meter; consequently, a more effective reactor with little absorption of the sunlight should be adopted.

It is well known that the polymeric membranes are not promising materials for application in the PMRs due to their susceptibility to damage by irradiation and hydroxyl radicals [24]. However, in the present work, sunlight was employed to decompose the dye; the damage effect was infinitesimal, and as a result, the mechanical properties were not presented.

4. Conclusions

Decoloring methyl orange in a photocatalytic membrane reactor was conducted via coupling zinc oxide nanoparticles and polypropylene macroporous membrane under sunlight. Poly(2-hydroxyethyl methacrylate) was grafted on the membrane surface to enhance the physical adsorption of zinc oxide nanoparticles on the membrane and to improve the membrane permeability.

The poly(2-hydroxyethyl methacrylate) modified membrane with a grafting degree of 4.48% (wt) has the maximum value, the relative flux is 118%; after the immobilization of zinc oxide nanoparticles on this membrane surface, it reaches 143%, improved by 25%.

The photocatalytic decoloration percent of methyl orange is 98.2% under 40 min sunlight irradiation in the photocatalytic membrane reactor with the ZnO NPs in suspension; and in the photocatalytic membrane reactor with the ZnO NPs immobilized on the membrane, the photocatalytic decoloration percent of methyl orange decreases greatly; it reaches 74.3% under 6 h sunlight irradiation. Overall, after repeated uses for five times, it is still 8% higher than that of the first run. These results demonstrate that the immobilized ZnO NPs are stable for repeated uses.

Nomenclature

BDTB: Benzyl dithiobenzoate
BP: Benzophenone
GD: Grafting degree
ID: Immobilization degree
FESEM: Field emission scanning electron microscopy
HEMA: 2-hydroxyethyl methacrylate
PHEMA: Poly-2-hydroxyethyl methacrylate
MeOr: Methyl orange
PDPs: Photocatalytic decoloration percents
PMR: Photocatalytic membrane reactor
PPMM: Polypropylene macroporous membrane
RAFT: Reversible addition-fragmentation chain transfer
ZnO NPs: Zinc oxide nanoparticles.

Authors' Contribution

B. Hu contributed to the preparation and characterization of ZnO NPs and membrane surface modification. X.-M. Wu contributed to the synthesis of the chain transfer agent. J. Zhou, corresponding author, contributed to the conducting photocatalytic membrane reactor and photocatalytic decoloring of dye.

Acknowledgments

We gratefully acknowledge the financial support from the National Natural Science Foundation of China (No. 20871003) and the instruction of professor Hai-Yin Yu.

References

[1] A. Akbari, J. C. Remigy, and P. Aptel, "Treatment of textile dye effluent using a polyamide-based nanofiltration membrane," *Chemical Engineering and Processing*, vol. 41, no. 7, pp. 601–609, 2002.

[2] V. K. Gupta, R. Jain, A. Mittal, M. Mathur, and S. Sikarwar, "Photochemical degradation of the hazardous dye Safranin-T using TiO_2 catalyst," *Journal of Colloid and Interface Science*, vol. 309, no. 2, pp. 464–469, 2007.

[3] V. K. Gupta, R. Jain, A. Nayak, S. Agarwal, and M. Shrivastava, "Removal of the hazardous dye-Tartrazine by photodegradation on titanium dioxide surface," *Materials Science and Engineering C*, vol. 31, no. 5, pp. 1062–1067, 2011.

[4] V. K. Gupta, R. Jain, A. Mittal et al., "Photo-catalytic degradation of toxic dye amaranth on TiO(2)/UV in aqueous suspensions," *Materials Science and Engineering C*, vol. 32, no. 1, pp. 12–17, 2012.

[5] V. K. Gupta, R. Jain, S. Agarwal, A. Nayak, and M. Shrivastava, "Photodegradation of haz- ardous dye quinoline yellow catalyzed by TiO_2 ," *Journal of Colloid and Interface Sciences*, vol. 366, no. 1, pp. 135–140, 2012.

[6] V. K. Gupta, R. Jain, S. Agarwal, and M. Shrivastava, "Kinetics of photo-catalytic degradation of hazardous dye Tropaeoline 000 using UV/TiO_2 in a UV reactor," *Colloids and Surfaces A*, vol. 378, no. 1–3, pp. 22–26, 2011.

[7] A. Lei, B. Qu, W. Zhou, Y. Wang, Q. Zhang, and B. Zou, "Facile synthesis and enhanced photocatalytic activity of hierarchical porous ZnO microspheres," *Materals Letters*, vol. 66, no. 1, pp. 72–75, 2012.

[8] R. Mohan, K. Krishnamoorthy, and S. J. Kim, "Enhanced photocatalytic activity of Cu-doped ZnO nanorods," *Solid State Communications*, vol. 152, no. 5, pp. 375–380, 2012.

[9] R. Selvin, H. L. Hsu, N. S. Arul, and S. Mathew, "Comparison of photo-catalytic efficiency of various metal oxide photo-catalysts for the degradation of methyl orange," *Science of Advanced Materials*, vol. 2, no. 1, pp. 58–63, 2010.

[10] Y. Abdollahi, A. H. Abdullah, Z. Zainal, and N. A. Yusof, "Photodegradation of m-cresol by zinc oxide under visible-light irradiation," *International Journal of Chemistry*, vol. 3, no. 3, pp. 31–43, 2011.

[11] Y. Abdollahi, A. H. Abdullah, Z. Zainal, and N. A. Yusof, "Photocatalytic Degradation of p-Cresol by Zinc Oxide under UV Irradiation," *International Journal of Molecular Sciences*, vol. 13, no. 1, pp. 302–315, 2012.

[12] Y. Gou, D. Chen, and Z. Su, "Photocatalyst of nanometer TiO_2/conjugated polymer complex employed for depigmentation of methyl orange," *Applied Catalysis A*, vol. 261, no. 1, pp. 15–18, 2004.

[13] H. R. Pouretedal and M. H. Keshavarz, "Synthesis and characterization of $Zn_{1-X}Cu_XS$ and Zn1-XNiXS nanoparticles and their applications as photocatalyst in Congo red degradation," *Journal of Alloys and Compounds*, vol. 501, no. 1, pp. 130–135, 2010.

[14] M. Zhang, L. Zhang, L. H. Cheng et al., "Extracorporeal endotoxin removal by novel l-serine grafted PVDF membrane modules," *Journal of Membrane Science*, vol. 405, no. 1, pp. 104–112, 2012.

[15] R. A. Damodar, S. J. You, and G. W. Chiou, "Investigation on the conditions mitigating membrane fouling caused by TiO_2 deposition in a membrane photocatalytic reactor (MPR) used for dye wastewater treatment," *Journal of Hazardous Materals*, vol. 203, no. 15, pp. 348–356, 2013.

[16] G. Zhang, J. Zhang, L. Wang, Q. Meng, and J. Wang, "Fouling mechanism of low-pressure hollow fiber membranes used in separating nanosized photocatalysts," *Journal of Membrane Science*, vol. 389, no. 1, pp. 532–543, 2012.

[17] J. Marto, P. S. Marcos, T. Trindade, and J. A. Labrincha, "Photocatalytic decolouration of Orange II by ZnO active layers screen-printed on ceramic tiles," *Journal of Hazardous Materials*, vol. 163, no. 1, pp. 36–42, 2009.

[18] S. Rehman, R. Ullah, A. M. Butt, and N. D. Gohar, "Strategies of making TiO_2 and ZnO visible light active," *Journal of Hazardous Materials*, vol. 170, no. 2-3, pp. 560–569, 2009.

[19] H. Y. Yu, J. Zhou, J. S. Gu, and S. Yang, "Manipulating membrane permeability and protein rejection of UV-modified polypropylene macroporous membrane," *Journal of Membrane Science*, vol. 364, no. 1-2, pp. 203–210, 2010.

[20] B. Hu, L. Wang, X. M. Wu, S. Yang, J. S. Gu, and H. Y. Yu, "Low protein fouling polypropylene membrane prepared by photoinduced reversible addition-fragmentation chain transfer polymerization," *Journal of Applied Polymer Science*, vol. 123, no. 6, pp. 3668–3674, 2011.

[21] H. Y. Yu, Z. K. Xu, Q. Yang, M. X. Hu, and S. Y. Wang, "Improvement of the antifouling characteristics for polypropylene microporous membranes by the sequential photoinduced graft polymerization of acrylic acid," *Journal of Membrane Science*, vol. 281, no. 1-2, pp. 658–665, 2006.

[22] J. Chiefari, Y. K. Chong, F. Ercole et al., "Living free-radical polymerization by reversible addition-fragmentation chain transfer: the RAFT process," *Macromolecules*, vol. 31, no. 16, pp. 5559–5562, 1998.

[23] D. Zhang, H. Xu, M. Xue, W. Xu, and V. Tarasov, "Preparation and photocatalytic kinetics of nano-ZnO powders by precipitation stripping process," *Frontiers of Chemical Engineering in China*, vol. 2, no. 3, pp. 319–324, 2008.

[24] S. Yang, J. S. Gu, H. Y. Yu et al., "Polypropylene membrane surface modification by RAFT grafting polymerization and TiO_2 photocatalysts immobilization for phenol decomposition in a photocatalytic membrane reactor," *Separation and Purification Technology*, vol. 83, no. 15, pp. 157–165, 2011.

[25] T. Toshinori, K. Takehiro, Y. Tomohisa, and A. Masashi, "A photocatalytic membrane reactor for VOC decomposition using Pt-modified titanium oxide porous membranes," *Journal of Membrane Science*, vol. 280, no. 1-2, pp. 156–162, 2006.

[26] J. S. Gu, H. Y. Yu, L. Huang et al., "Chain-length dependence of the antifouling characteristics of the glycopolymer-modified polypropylene membrane in an SMBR," *Journal of Membrane Science*, vol. 326, no. 1, pp. 145–152, 2009.

[27] R. Brayner, S. A. Dahoumane, C. Yéprémian et al., "ZnO nanoparticles: synthesis, characterization, and ecotoxicological studies," *Langmuir*, vol. 26, no. 9, pp. 6522–6528, 2010.

[28] R. Hong, T. Pan, J. Qian, and H. Li, "Synthesis and surface modification of ZnO nanoparticles," *Chemical Engineering Journal*, vol. 119, no. 2-3, pp. 71–81, 2006.

[29] M. X. Hu, Q. Yang, and Z.-K. Xu, "Enhancing the hydrophilicity of polypropylene microporous membranes by the grafting of 2-hydroxyethyl methacrylate via a synergistic effect of photoinitiators," *Journal of Membrane Science*, vol. 285, no. 1-2, pp. 196–205, 2006.

[30] D. S. Wavhal and E. R. Fisher, "Membrane surface modification by plasma-induced polymerization of acrylamide for improved surface properties and reduced protein fouling," *Langmuir*, vol. 19, no. 1, pp. 79–85, 2003.

[31] Q. Yang, Z. K. Xu, Z. W. Dai, J. L. Wang, and M. Ulbricht, "Surface modification of polypropylene microporous membranes with a novel glycopolymer," *Chemistry of Materials*, vol. 17, no. 11, pp. 3050–3058, 2005.

[32] C. Y. Kuan, M. H. Hon, J. M. Chou, and I. C. Leu, "Wetting characteristics on micro/nanostructured zinc oxide coatings," *Journal of the Electrochemical Society*, vol. 156, no. 2, pp. J32–J36, 2009.

[33] O. Akhavan, M. Mehrabian, K. Mirabbaszadeh, and R. Azimirad, "Hydrothermal synthesis of ZnO nanorod arrays for photocatalytic inactivation of bacteria," *Journal of Physics D*, vol. 42, no. 22, Article ID 225305, 2009.

[34] G. Wang, D. Chen, H. Zhang, J. Z. Zhang, and J. Li, "Tunable photocurrent spectrum in well-oriented zinc oxide nanorod arrays with enhanced photocatalytic activity," *Journal of Physical Chemistry C*, vol. 112, no. 24, pp. 8850–8855, 2008.

[35] R. Y. Hong, J. H. Li, L. L. Chen et al., "Synthesis, surface modification and photocatalytic property of ZnO nanoparticles," *Powder Technology*, vol. 189, no. 3, pp. 426–432, 2009.

[36] F. B. Li, G. B. Gu, G. F. Huang, Y. L. Gu, and H. F. Wan, "TiO_2-assisted photo-catalysis degradation process of dye chemicals," *Journal of Environmental Sciences*, vol. 13, no. 1, pp. 64–68, 2001.

[37] J. Liqiang, X. Baifu, Y. Fulong et al., "Deactivation and regeneration of ZnO and TiO_2 nanoparticles in the gas phase photocatalytic oxidation of n-C_7H_{16} or SO_2 ," *Applied Catalysis A*, vol. 275, no. 1-2, pp. 49–54, 2004.

[38] J. Xu, Y. Ao, D. Fu, and C. Yuan, "Low-temperature preparation of F-doped TiO_2 film and its photocatalytic activity under solar light," *Applied Surface Science*, vol. 254, no. 10, pp. 3033–3038, 2008.